ATTACHMENT B

NATIONAL AERONAUTICS AND SPACE ADMINISTRATION
PHASE II PROJECT SUMMARY
CONTRACT NO. NAS7-993
FINAL REPORT

SBIR – 08.10-2753
release date 3/14/91

POLATOMIC, INC.
2201 Waterview Parkway
Richardson, TX 75080

PRINCIPAL INVESTIGATOR: Dr. Robert E. Slocum

TITLE OF PROJECT: Advanced Helium Magnetometer for Space Applications

TECHNICAL SUMMARY

The goal of this effort was demonstration of the concepts for an advanced helium magnetometer which meets the demands of future NASA earth orbiting, interplanetary, solar and interstellar missions. The technical effort focused on optical pumping of helium with tunable solid state lasers. We were able to demonstrate the concept of a laser pumped helium magnetometer with improved accuracy, low power, and sensitivity of the order of 1 pT.

A number of technical approaches were investigated for building a solid state laser tunable to the helium absorption line at 1083 nm. The laser selected was an Nd-doped LNA crystal pumped by a diode laser. Two laboratory versions of the LNA laser were fabricated and used to conduct optical pumping experiments in helium and demonstrate laser pumped magnetometer concepts for both the low field vector mode and the scalar mode of operation. A digital resonance spectrometer was designed and built in order to evaluate the helium resonance signals and observe scalar magnetometer operation.

The results indicate that the laser pumped sensor in the VHM mode is 45 times more sensitive than a lamp pumped sensor for identical system noise levels. A study was made of typical laser pumped resonance signals in the conventional magnetic resonance mode. The laser pumped sensor was operated as a scalar magnetometer, and it is concluded that magnetometers with 1 pT sensitivity can be achieved with the use of laser pumping and stable laser pump sources.

POTENTIAL COMMERCIAL APPLICATIONS

This new generation of laser pumped helium magnetometers and gradiometers will find use in: 1) geophysical exploration, 2) naval warfare (submarine and surface ship detection, localization and tracking), 3) biomagnetics, 4) mine warfare (mine activation and mine countermeasures).

TABLE OF CONTENTS

LIST OF ILLUSTRATIONS

INTRODUCTION - BACKGROUND AND PURPOSE OF THE PHASE II PROJECT

Magnetic field measurements are frequently a primary objective for NASA planetary missions, earth orbiting missions and comet encounters. A family of space magnetometers has been developed over the years to meet the requirements of these missions. It is now anticipated that NASA missions to be launched over the next three decades will challenge the capabilities of present day space magnetometers.

Currently, the most advanced space magnetometers are optically pumped sensors which derive magnetic field information from perturbations of optically pumped Zeeman states of gases and vapors. The vector helium magnetometer (VHM) provides 3-axis vector field information, and it was originally designed to operate in interplanetary magnetic fields which are far less than the earth's field at the surface (25,000 nT to 75,000 nT). The interplanetary field is of the order of 10 nT. For measurements of the earth's field, optically pumped magnetic resonance magnetometers employing helium or alkali vapors as the resonance element are often used. Historically, rubidium and cesium vapor have been the resonance element of choice for orbiting space instruments but reliability problems are sometimes encountered because of the requirement to control the temperature of the alkali vapor. These magnetic resonance devices are scalar instruments and provide only the magnitude, not the direction, of the ambient field.

In preparing for future NASA missions carrying magnetometers in earth's orbit, approaching the sun, or orbiting the neighboring or outer planets, a number of new requirements can be anticipated for magnetometer systems which must measure planetary or interplanetary fields. One requirement may be for the measurement of both vector and absolute scalar measurements with the same sensor. A second requirement may call for the ability to make measurements over the range from 10^5 nT to 10^{-3} nT with sample rates of 1 to 100 Hz using a single sensor. A third requirement may call for magnetometers which maintain long-term stability of 10^{-3} nT during missions with duration greater than 10 years. A fourth requirement may call for gradiometer arrays of

ultra-low noise optically pumped sensors to investigate planets, moons, and asteroids. A final requirement could be for instruments which have high reliability and very low mass and power requirements in comparison with today's instruments. The purpose of the Phase II Project was to investigate proposed technical advances in optically pumped helium magnetometry in order to establish the feasibility of designing and fabricating advanced helium magnetometers for future space applications. Such an instrument must meet the performance requirements for range, sensitivity, and accuracy described above. It must also satisfy, if possible, the requirement for reduced power, mass and size.

The Phase II Project was limited to optically pumped helium magnetometers. The helium magnetometer is the most widely utilized optically pumped magnetometer in the world. It is also one with which NASA has extensive in-house experience. The vector helium magnetometer (VHM) has been used for interplanetary missions since the early 1960's. Although NASA has not used a scalar helium magnetometer (SHM) for space missions, this has been the instrument of choice for the U.S. Navy. Over 1,000 SHM systems have been built and installed in Naval aircraft for use in detecting perturbations in the earth's magnetic field caused by submarines. The SHM and the VHM use essentially the same sensor components with different electronics and techniques extracting magnetic field information from the sensor. A third version of an optically pumped helium magnetometer is the nuclear free precession helium magnetometer which utilizes optically pumped helium 3 nuclei (FPHM). Both the SHM and the VHM use the isotope helium 4, which has no nuclear magnetic moment.

During the Phase I Project we identified potential innovations for space magnetometers in the area of laser pumping. The laser would replace the rf electrodeless discharge helium lamp shown in the schematic diagram of a helium optical-pumping apparatus shown in Figure 1. Conceptually, laser pumping offers a number of advantages over the helium lamp. The most important advantage comes from the ability of the laser to emit a narrow line which can be used to achieve single-line pumping. Single-line

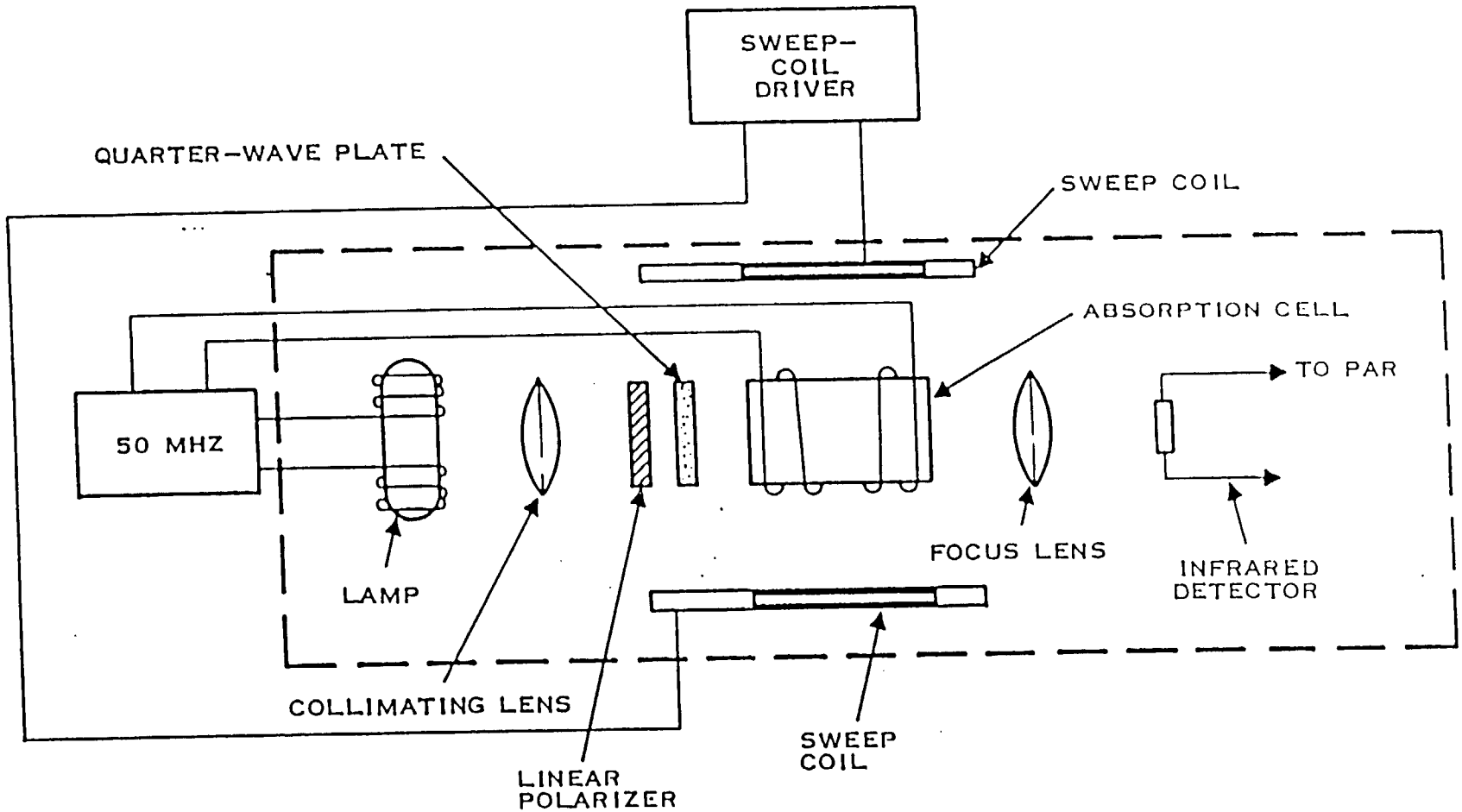

FIGURE 1 - OPTICAL PUMPING APPARATUS FOR HELIUM 3 AND HELIUM 4

pumping, in theory, offers two orders of magnitude improvement in sensitivity over conventional lamp pumped magnetometers.[1] A second important advantage is the elimination of offsets in the magnetic field reading caused by the pumping light.

Laser pumping offers indirect benefits as well. Because a laser converts electrical energy into light at the desired wavelength more efficiently than the rf discharge lamp, a laser-pumping source would be expected to use less power than a lamp in order to achieve the same signal-to-noise ratio in the sensor output. If lasers can be pulsed on and off at high frequencies, pulsed resonance operation (light pulsed at the magnetic resonance frequency of 28 Hz per nT) can be used to produce magnetic resonance transitions without applying an rf drive field through a coil system. The pulsed light mode eliminates the need for an rf drive coil. Finally, if the laser can be made to emit light with all energy in a single linearly polarized state, half the light will not be used in circularly polarizing the beam to prepare it for optical pumping as is the case for unpolarized helium lamp light. It has become apparent that the availability of a laser for optical pumping in a magnetometer would constitute a major technological breakthrough in the field of magnetometry.

A major task of the Phase II Project was identification of lasers which had been used or could be considered for use in helium optical-pumping experiments. For efficient optical pumping, the laser output wavelength must be locked to the wavelength of a helium resonance line at 1083 nm. Since every solid-state crystal laser must be pumped, the survey of available laser pumping light sources must lead to an efficient source for use in a portable magnetometer.

The overall purpose of the Phase II Project was met with the demonstration of a laser-pumped helium magnetometer concept. The feasibility of designing and fabricating a laser-pumped helium magnetometer for use in space was determined using a tunable solid laser for 1083 nm radiation which was developed during the Phase II Project (Nd-doped LNA crystal). LNA is available in limited quantities and was pumped

with a thermoelectrically cooled diode laser to construct a laboratory laser for optical pumping experiments and a laser-pumped helium magnetometer demonstration and evaluation.

The second issue to be resolved was the effectiveness of laser pumping of helium 4. For the laser-pumped magnetometer to be feasible, laser pumping of the optimum individual helium spectral line must be considerably more effective than optical pumping with a conventional rf electrodeless discharge helium lamp. Schearer and Leduc[2] have demonstrated laser pumping of helium 3 and polarizations as large as 70% have been reported using tunable lasers for pumping the helium 3 sample. Reports from the Rice University group have investigated optical pumping of helium 4 in an atomic beam and reported that 10 mW of laser power achieves polarizations equivalent to that obtained with a 400 W of excited helium lamp.

We were able to demonstrate a magnetic resonance signal which was 45 times stronger than that produced by a helium lamp. It had been predicted that single line laser pumping has a theoretical sensitivity improvement of 100 over conventional helium rf lamp pumped VHM and SHM instruments. Analysis of the projected wall plug efficiencies for laser diodes as a pump source for the tunable solid-state laser indicates that the laser pumping should also be more efficient. Finally, it appears that pumping line selection and wavelength tuning can greatly reduce offsets produced by light shifts in the SHM instrument.

In summary, we have achieved our purpose in demonstrating that the concept of a laser-pumped helium magnetometer offers improved sensitivity and accuracy and reduced power consumption for the SHM and VHM modes of operation. The successful bringing together of two mainstream quantum electronic technologies (optically pumped magnetometers and lasers) should prove to be a major technical breakthrough in the arena of high performance magnetometry and gradiometry for space, military and geophysical applications.

PHASE II APPROACH

The Phase II Project has as primary technical tasks demonstration and characterization of laser pumping and monitoring of resonance signals in helium magnetometers. The Phase II Project was divided into two parts. In Part 1, we fabricated an LNA laser for demonstration of laser pumping of helium 4 and investigated the parameters which impact the design and performance of a laser-pumped helium magnetometer. The LNA tunable solid-state laser was selected for laboratory use after evaluation of competing lasers. The LNA laser was used to investigate the optically observed parametric resonance signal, linewidth, and relative sensitivity of the helium resonance curves for a single axis VHM sensor.

Part 2 of the Phase II Project consisted of assembly and evaluation of a laboratory laser-pumped helium magnetometer operating in the scalar (magnetic resonance) mode. The LNA laser was again selected for the scalar magnetometer evaluation. We obtained from Part 1 the operating parameters and design information for fabrication of a laser-pumped helium magnetometer sensor which was evaluated in the SHM mode in Part 2. The data from Part 1 was used to design a tunable solid-state laser optimized for optically pumping and monitoring the magnetic resonance signal in a magnetometer.

The optical pumping apparatus, tunable solid-state laser and magnetometers electronics were fabricated at Polatomic, Inc. The design, fabrication and evaluation of the initial LNA laboratory laser was carried out by Dr. L. D. Schearer at the University of Missouri-Rolla. The laser-pumping experiments and VHM magnetometer sensor evaluation was conducted at the magnetics test facility of the Jet Propulsion Laboratory (Pasadena, CA). Laser pumping experiments in the SHM (scalar) mode were conducted at the Polatomic Magnetics Laboratory (Richardson, Texas). Consulting services on the selection of tunable solid-state laser materials were supplied by Dr. Richard Powell of the Department of Physics at Oklahoma State University.

PART 1 TECHNICAL OBJECTIVES - LASER OPTICAL PUMPING AND MONITORING

The objective of Part 1 was design and fabrication of a tunable laser and optical-pumping apparatus and demonstration of the concept of a laser-pumped magnetometer sensor for the VHM mode of operation. A tunable solid-state LNA laser was selected which can be tuned to the appropriate helium resonance line at 1083 nm. This laboratory LNA laser was used with a helium optical pumping apparatus to investigate the laser monitored parametric resonance parameters and demonstrate magnetometer performance. The task included analysis and evaluation of a number of tunable solid-state laser materials. The optically pumping apparatus was basically a VHM space magnetometer pumped by a laboratory LNA laser. A series of experiments were conducted to correlate laser characteristics with laser pumped and monitored resonance signals in helium 4.

1. LASER PUMPED AND MONITORED RESONANCE SIGNALS

The technical objective was to monitor laser pumping in helium. The optical-pumping process in helium 4 was monitored for the three cases of single-line pumping. The optical pumping efficiency and strength of the optically-observed resonances was observed for pumping on each of the helium 4 resonance lines (D_0, D_1 and D_2). The effect of discharge conditions was taken into account when optimizing the resonance signal. The effect of laser mode structure and laser light characteristics was also taken into account. These observations were used to select the laser design and optical pumping apparatus with which to investigate the scalar magnetometer performance in Part 2.

2. LASER OPTICAL PUMPING APPARATUS

The technical objective was assembling an apparatus for comparison of laser pumping with pumping by a typical rf helium lamp. A typical VHM optical pumping apparatus which includes collimating and polarizing optics, a helium 4 cell, drive coils and infrared detector was modified for operation with either rf helium lamp or laser. A

standard VHM rf electrodeless discharge helium 4 lamp was used for comparison with the laser-pumping source. The apparatus was suitable for observing the linewidth, amplitude, noise and line slope of the laser or lamp monitored resonance curve. The electronic test and support equipment required to operate this apparatus and conduct the experiments consisted of standard laboratory test equipment. The apparatus could also be pumped using a laboratory version of a tunable diode laser pumped LNA laser.

3. SOLID-STATE LASER MATERIAL

The technical objective was selection of a solid-state laser material tunable to 1083 nm for use in the laboratory tunable laser. Based on information available from Phase I research, LNA was the first choice followed by YAP, Nd-doped lithium niobate and Nd-doped glass fibers. Although LNA was not expected to be available until the end of 1986 by J. J. Aubert of the Commissariat a l'Energie Atomic (Grenoble, France), samples were available from Prof. Schearer for use in a laboratory laser for concept evaluation. The Nd-doped lithium niobate available from Crystal Technology is not found to be suitable for laser operation. YAP is commercially available but the efficiency is low at 1083 nm in low power level operations.

Each laser crystal sample to be used in a solid-state laser had its spectroscopic properties measured, and the merits of material samples to be used in the laser were measured. The measured parameters include gain, threshold, tunability and coupling. The material characteristics and sample selection were determined by Prof. Schearer at his laboratory. Confirming measurements were made in the laser materials laboratory of Dr. Richard Powell at Oklahoma State University.

4. OPTICAL RESONATOR AND CAVITY

The technical objective was selection of the optical elements and mechanical mounting mechanisms for the laboratory laser cavity, and a selection of a mechanical design. Several different tuning elements were investigated, including Lyot filters, prisms, and solid etalons. These elements were used to select the appropriate laser

transition, to tune across the selected laser line, and to achieve the desired mode structure, gain, threshold, and laser stability.

5. PUMP SOURCE

The technical objective was selection of a pump source for the crystal laser. The laboratory laser performance was evaluated to determine the effect of wavelength and type of pump source. Ion lasers are selected initially for the Part 1 experiments but the lasers are bulky and the radiation would have to be coupled to the helium cell with an optical fiber. In fact, semiconductor laser diodes became available and proved very effective. A compact optical pumping apparatus was designed using a thermoelectrically cooled diode laser. The goal of using diode lasers to pump the tunable laser crystal was met. Spectroscopic analysis of the diode laser radiation was conducted in Dr. Schearer's laboratory.

6. LASER PUMPING AND MONITORING EXPERIMENTS

The technical objective was to use parametric resonance techniques to monitor parametric resonances in laser pumped helium 4. We observed signal strength, linewidth and noise level for laser-pumped and monitored resonance signals. The effect of laser light characteristics and helium discharge characteristics on the laser pumping signal were investigated. Since parametric resonance requires low magnetic field for observation, the low-field magnetic shield facility at the JPL magnetic test facility was used for these experiments. The resonance line strengths for laser-pumping and pumping with a conventional helium lamp were compared. For equivalent noise levels the laser would result in a factor of 45 improvement in sensitivity.

7. ADVANCED PUMPING AND RESONANCE TECHNIQUES

The technical objective was examination of new and novel techniques made possible by laser pumping of helium. Several advance concepts in optical pumping and magnetic resonance were considered for incorporation in the laser pumped helium magnetometer. Pumping via fiber-optic coupling was examined and found effective.

Optical fiber coupling for pumping hybrid (VHM and SHM) sensors appears feasible. The technique of driving the optically pumped atoms into forced precession using a laser beam pulsed at the resonance frequency was investigated in the laboratory in order to eliminate drive coils from the SHM sensor. However, the LNA crystal has limited response frequency. The optogalvanic effect was examined for the first time in helium and used to observe amplitude modulated optical pumping.

PART 2 TECHNICAL OBJECTIVES

The technical objective of Part 2 was construction, evaluation of a demonstration of the laser pumped scalar helium magnetometer concept. The data taken during the Part 1 investigation of tunable laser design and laser pumping and monitoring in helium 4 was used to construct a laboratory scalar magnetometer during Part 2. The following objectives were met during Part 2 of the Phase II project.

1. LASER-PUMPED HELIUM MAGNETOMETER DEMONSTRATION

The technical objective was use of data and technology from the Phase II Project (Part 1) to design, fabricate and evaluate a laser-pumped helium magnetometer in the scalar (SHM) mode. A portable solid-state LNA laser was fabricated which can be wavelength tuned to 1083 nm for a scalar laser-pumped magnetometer. An optical-pumping apparatus was fabricated so the sensor can be operated in the laser pumping mode. The magnetometer was evaluated in the scalar mode using a digital resonance spectrometer consisting of a tracking digital oscillator designed especially for evaluation of laser pumped sensors. The performance of the laser-pumped magnetometer was demonstrated at the Polatomic Magnetics Laboratory at the University of Texas at Dallas industrial park. The vector mode of operation was not included because of time limitations imposed by unexpected technical delays in the development of the LNA laser.

2. SOLID-STATE LASER MATERIAL

The technical objective of selection of a tunable solid-state laser based on results from Part 1. Prior to the start of Part 2 of the Phase II Project, the state-of-the-art in solid-state lasers tunable to 1083 nm was reviewed with Prof. Schearer and Prof. Richard Powell of OSU. Prof. Powell is beginning a three-year effort to identify and develop tunable solid-state laser materials for the 1000 nm to 2000 nm wavelength band. Although diode lasers would appear to be suitable for laser pumping the helium magnetometer, this technology was found to be too immature for use in the Part II laser pumped magnetometer experiments. Other emerging candidates were evaluated in order to select the material which best meets the magnetometer laser specification prior to the selection of diode laser pumped LNA as the Part 2 laser.

3. OPTICAL RESONATOR

The technical objective was use of information gathered in Part 1 on cavity design, tuning elements, coupling optics, pump sources and desirable laser output characteristics to design an optical resonator for the LNA laser. The coupling of the LNA laser radiation into an optical fiber was demonstrated but was not used for magnetometer tests. Eventually, fiber optics must be used to remove the laser from the neighborhood of the helium cell and minimize the requirement for non-magnetic components in the laser. The resonator must be designed to achieve the desired mode structure, tuning accuracy and output power as determined by the magnetometer performance. Additional design improvements will be required in order to incorporate the tuning elements into a servo-control system. The optical resonator for the laser-pumped helium magnetometer was fabricated at Polatomic, Inc.

4. PUMP SOURCE

The technical objective was selection of a laser diode pump for the laser-pumped magnetometer experiments and demonstration. After evaluation of possible laser diodes, a portable 0.5 watt high-brightness diode laser was selected which had built

in thermoelectric cooling. The laser diode wavelength was temperature tuned to couple into the laser crystal. The laser diode pump, including power supply, coupling optics, and mounts, was assembled at Polatomic, Inc. using laser diode and material spectral data collected during Part 1.

5. WAVELENGTH STABILIZATION AND CONTROL

The technical objective was use of Part 1 data to specify the accuracy and stability requirements for laser tuning. Techniques for generating feedback error signals were investigated analytically and experimentally. Both the strength of the laser-pumped resonance signal and the desired magnetometer accuracy and stability were taken into account in specifying the control system performance. The prototype wavelength control system using conventional optical components proved more difficult to stabilize than anticipated. The magnetometer data was collected using manual tuning. Additional R & D effort will be required to design a wavelength locking servo.

6. LASER-PUMPED MAGNETOMETER EVALUATION

The technical objective was evaluation of the laser-pumped scalar magnetometer in actual field tests conducted at the Polatomic Magnetics Laboratory. A test plan was prepared and laser-pumped resonance signals were investigated to characterize signal strength, line strength, noise and sensitivity. The test program demonstrated the laser-pumped magnetometer concept and defined the key parameters needed to construct a final design version of the laser pumping source and laser-pumped magnetometer. A key parameter for achieving 1 pT operation is stabilization of the laser source to reduce system noise.

PHASE II TECHNICAL EFFORT

The Phase II Project consisted of seven technical tasks which provide technical insight for design and fabrication of a prototype laser-pumped VHM and SHM. The results of the Phase II Project technical effort will be summarized in the following seven sections which correspond to the seven tasks of the original Statement of Work:

PART 1

Section 1 - Conduct research, design and development on tunable laser for 1083 nm.

Section 2 - Design and fabricate laser pumping apparatus and experiment for helium optical pumping demonstration.

Section 3 - Conduct laser pumping experiments, analyze data, and formulate conclusions.

PART 2

Section 4 - Design and fabricate stabilized solid-state laser for laser-pumped magnetometer.

Section 5 - Design and fabricate prototype laser-pumped magnetometer sensor.

Section 6 - Evaluate laser-pumped magnetometer sensor in VHM and SHM modes.

Section 7 - Conduct experimental evaluation of diode laser-pumping designs and AMPO effects in laser-pumped helium 4.

REFERENCES - INTRODUCTION

1 D. D. McGregor, Rev. Sci. Instrum. 58, 1067 (1987).

2 L. D. Schearer and M. Leduc, Presented at the First International Laser Science Conference, Dallas, Texas, 18 November 1985.

1.0 RESEARCH AND DESIGN OF TUNABLE LASER FOR 1083 nm

We have investigated the tuning characteristics of several Nd-doped lasers for use as cw sources to optically pump helium metastable atoms at 1083 nm, replacing the conventional discharge lamp. We report the gain and tuning curves obtained for $LaMgAl_{11}O_{19}$, $YAlO_3$, $LiNbO_3$. The materials are pumped with a variety of laser sources including Ar^+ and Kr^+ ion lasers, Kr arc lamps, and GaAlAs diodes. Single-mode laser power at the helium resonance wavelength is greater than 15 mw when LNA is pumped with a 450 mw diode. Tunable power up to 1 w is obtained with Nd:$YAlO_3$ in a cw, arc-lamp pumped cavity. Applications for laser-pumped, spin-polarized ensembles of ^3He and metastable ^4He range from magnetometers to nuclear targets. Optical pumping signals derived from the laser-pumped systems for several different operating modes are described in the report following this section.

1.1 BACKGROUND

Neodymium-doped materials have elicited considerable interest as efficient laser systems in the infrared region of the spectrum. The Nd^{3+}:Yttrium Aluminium Garnet laser is a commercially successful device having a wide variety of uses and offering unique advantages. The most recent innovation with this system has resulted from the availability of high power, cW GaAlAs diodes which can be used to efficiently pump small Nd:YAG crystals. A hand-held, efficient laser is now available at moderate cost.

Where a variable frequency (tunable) output is desired however, the Nd:YAG system cannot be utilized. The spectral output of a Nd:YAG laser cannot be continuously tuned over a significant wavelength range although a number of discrete wavelengths can be obtained. Additionally, when the Nd:YAG laser is diode pumped, the diode temperature, hence wavelength, must be controlled and stabilized. While this stabilization can be performed without much difficulty, it does require that the diode

wavelength be carefully selected, adding to unit costs since the wavelength cannot be controlled significantly during the manufacturing process.

In those applications for which a broadly tunable, near infrared laser radiation is required, the Nd:YAG laser loses some of its appeal. It thus becomes necessary to find other host materials for the neodymium ion which retain the advantages of YAG but offer the potential for broad tunability in a region of the spectrum which is generally devoid of tunable laser sources.

The necessity for finding other host materials for the Nd^{3+} ions is illustrated in Figure 1.1(b) which shows the fluorescence spectrum of Nd:YAG. The spectrum is seen to consist of a number of relatively narrow spectral lines. By contrast, in Figure 1.1(a), the fluorescence spectrum of Nd-doped Lanthanum Hexaluminate is shown. In addition to the expected shift in the peak emission of the Nd fluorescence, a singularly notable difference is the substantially broader emission spectrum. Now, instead of a series of discrete lines, one sees a broad, continuous emission. One also observes a broader absorption spectrum which suggests that the diode temperature control and wavelength selection are less vexing problems.

We have indeed found several Nd hosts which have the desired spectral properties while also having adequately large emission cross-sections. We describe several such host materials which offer desirable lasing properties. We have identified potential tunable laser systems and delineated their operating parameters in order to provide a basis for assessing potential applications, especially as related to helium optical pumping experiments.

Our goal was to identify host materials and lasing ions to be incorporated into the host material which could yield efficient, tunable, cw laser sources at 1083 nm, the wavelength of the optical pumping radiation in helium. All the lasers which we have investigated use the neodymium ion as the lasing species and all the laser systems involve optical excitation for the inversion mechanism.

FIGURE 1.1 - (a) Fluorescence Spectrum of Nd-doped Lanthanum-Magnesium Hexaluminate Excited by a Kr^+ Laser at 752 nm. (b) Similar Fluorescence Spectrum Obtained with an Nd-doped YAG Crystal.

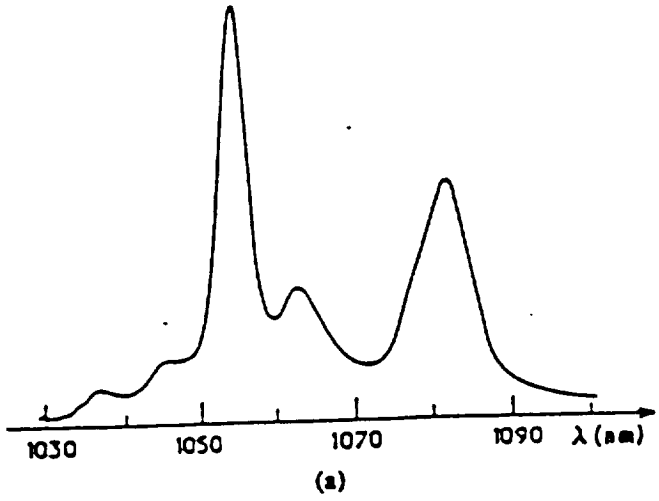

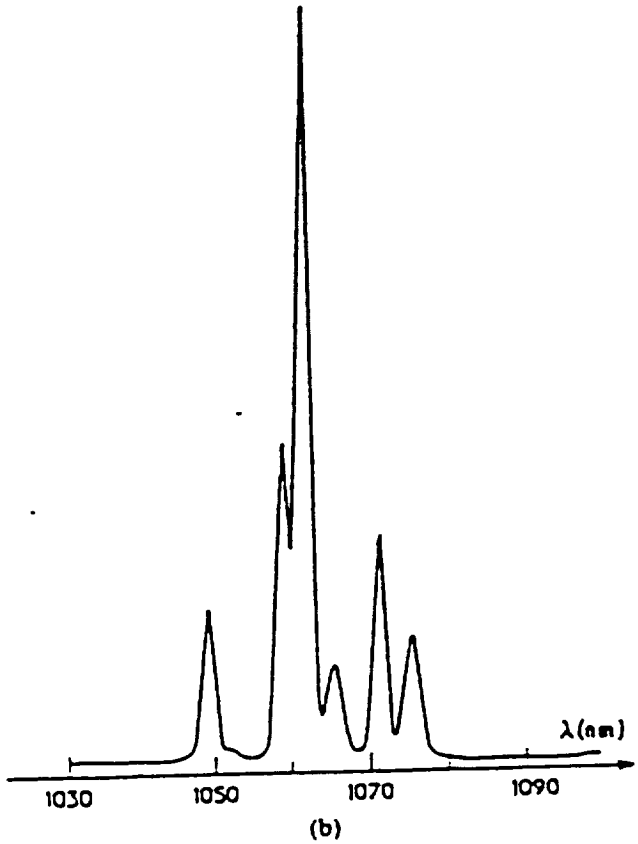

We have used the Ar^+ and Kr+ laser, the Kr arc lamp, and also GaAlAs diodes as optical excitation sources for the tunable laser systems. The host materials we have investigated include Lanthanum-Magnesium-Hexaluminate, Lithium niobate, Yttrium Aluminate, and non-crystalline SiO_2. We have also identified three other materials which might deserve further consideration after some additional materials development. These are Nd-doped B- aluminate, Chromium-doped zinc tungstate, and Nd-doped Lutecium Aluminate. Fluorescence studies clearly label these materials as potential laser systems of interest to the applications discussed herein.

Neodymium-doped hard glass fibers also represent very interesting possibilities for low-power, low cost applications. We have investigated briefly the lasing properties of such devices but the constraints of time prevented an adequate, systematic evaluation. But they clearly deserve additional study. Thresholds below 200 μwatts have been reported for short, monomode fibers, and sufficient gain exists that they can be tuned over a large fraction of the fluorescence bandwidth.

We have investigated the gain, threshold, and tuning characteristics of the LNA, YAP, and $LiNbO_3$ when optically excited with the pump sources mentioned above. The LNA and YAP systems especially, have been explored and their utilization in helium optical pumping experiments evaluated. Several modes of helium optical pumping have also been explored. These include the conventional, transmitted signal mode, scattered light mode, parametric detection mode, transverse pumping mode, and optogalvanic detection mode. Each of these modes is discussed in the sections following.

We have also developed a single, generic laser cavity which can be used for all the materials investigated. It is only necessary to change the laser host material within the cavity to select a particular set of operating values. A simple solid etalon and/or a Lyot filter of appropriate thickness is then used to tune the laser to the desired wavelength.

Of particular interest is the use of GaAlAs diodes as optical excitation sources for the lasers described herein. Enormous strides have been made recently in the development of high-power, cw diode lasers. Presently, devices to 2 watts are available commercially from several manufacturers which have active junction sizes smaller than 1μ x 200μ. These diodes are ideal sources for end-pumping a number of neodymium based materials. The diodes themselves are compact, very efficient sources which can efficiently pump a number of neodymium laser systems. In addition, lower power (<50 mw) single-element diodes are commercially available with junction sizes of less than 1μ x 4μ. These diodes are very low cost since they are also used in the CD player market. For lower power laser applications where small size and low cost are prime considerations, these devices are ideal pump sources.

Diode-pumped solid-state laser materials provide efficient as well as compact and relatively low cost laser devices leading to a wide range of applications. End pumping of Nd:YAG crystals with the laser diodes can deliver 100's of milliwatts of continuous power at 1064 nm with overall wallplug efficiencies as large as 8%.[1] Transverse pumping of a 1.3 cm YAG rod with an 8 w array has yielded 1.8 w of cw output power.[2] There is now a rapidly increasing number of Nd-doped materials which have been shown to lase under diode pump excitation, including $LiNbO_3$, LNA, YAG, YAP, and glass fibers.[3]

Our motivation in this work is to obtain tunable cm laser radiation at 1083 nm which can be used in helium optical pumping experiments. The interaction of an appropriately prepared source of radiation with metastable $He(2^3S_1)$ atoms can produce spin-polarized ensembles of metastable ^4He atoms and ground state ^3He nuclei.[4,5] The pumping process requires cw laser powers from several milliwatts single mode to 1 watt or more in bandwidths ranging from 10 MHz (the natural linewidth) to 1.8 GHz (the Doppler broadened width), depending on the particular application. In the sections below, we describe the results we have obtained for three Nd hosts when pumped with

several different types of laser sources. The final sections are devoted to several interesting applications which are currently being explored.

1.2 LNA (Nd:LaMgAl_{11}O1_{19} LASER

1.2.1 LASER CRYSTAL

Initial results obtained with LNA utilized material obtained from the LETI corporation in Grenoble, France. However, we were informed that as a result of competitive pressures they would not market this material in the United States. Consequently, our first task was to identify other potential sources. There are now two U.S. firms which are growing this material commercially: Airtron, NJ and Union Carbide. We obtained material from all three sources. At the present time, and based on limited data, the Union carbide material is consistently good. Airtron crystals show a large variation in quality. The results reported herein are for the best Airtron crystals. Comparable results are obtained with all Union Carbide crystals.

The crystals typically are 3-4 mm in diameter and 7-10 mm in length. The long axis is the crystalline 'c' axis and coincides with the laser axis. In this orientation pump light absorbed by the crystal is independent of its polarization. In general, the laser output in this orientation is also unpolarized unless polarizing elements are included in the cavity.

The LNA material has strong absorption peaks at 514.5, 590, 752, and 800 nm: consequently, it may be conveniently pumped with Ar+ and Kr+ ion lasers, Ar+ pumped dye lasers, and GaA*l*As diode lasers. The characteristics of this laser pumped with sources other than GaA*l*As diodes have been reported earlier.[6] We restrict our discussion here to the diode laser pumped LNA laser.

1.2.2 DIODE LASER PUMP SOURCE AND OPTICS

The high power GaA*l*As diodes used in this research are gain-guided devices having rated cw power outputs of 0.5 to 1 w. The active, emitting facet is a stripe or a multi-element array of dimensions typically 1 x 200μ and having emission linewidths on

the order of 2 mm. This geometry produces an asymmetric radiation pattern caused by diffraction at the aperture. If a spherical lens is used to collimate the diode output, a beam with an elliptical cross-section results since the beam divergence is different in the direction parallel and perpendicular to the diode output. In order to compensate for this, an anamorphic prism pair is used. The prism pair provides a magnification in only one direction.

The collimating optics is a single, best form spherical, AR coated lens with a numerical aperture of about 0.5. The anamorphic magnification is 3x or 4x. The collimated diode light is then focussed on the LNA crystal at a point just inside the dichroic coated surface with a lens of focal length, f=20cm.

The diode emission wavelength must be selected to coincide with the peak absorption of the LNA crystal which is near 797 mm. The diode laser emission is temperature dependent with a coefficient of about 0.3 mm per degree centigrade. In general it is necessary to cool the diode. This has the added benefit in that the diode lifetime increases substantially as the diode temperature is lowered. Cooling is provided by thermoelectric coolers mounted either internally or externally. Waste heat is removed by an air or water bath.

1.2.3 LASER CAVITY

Cavity design requires that there be a maximum overlap of the volume excited by the pump source within the LNA crystal and the laser mode volume within the cavity. This volume matching was achieved using a computer program written at the Ecole Normale Supericure, Paris which calculates the beam diameters within the laser cavity including the thermal effects within the crystal. The program also calculates the mode volume within the crystal. The final choice of cavity elements was determined with the help of this program. Figure 1.2 for example, is a computer plot of the beam size within the cavity showing the divergence and beam dimensions at the cavity ends calculated using this program.

FIGURE 1.2 - Computer Calculation of Beam Diameter Inside Cavity

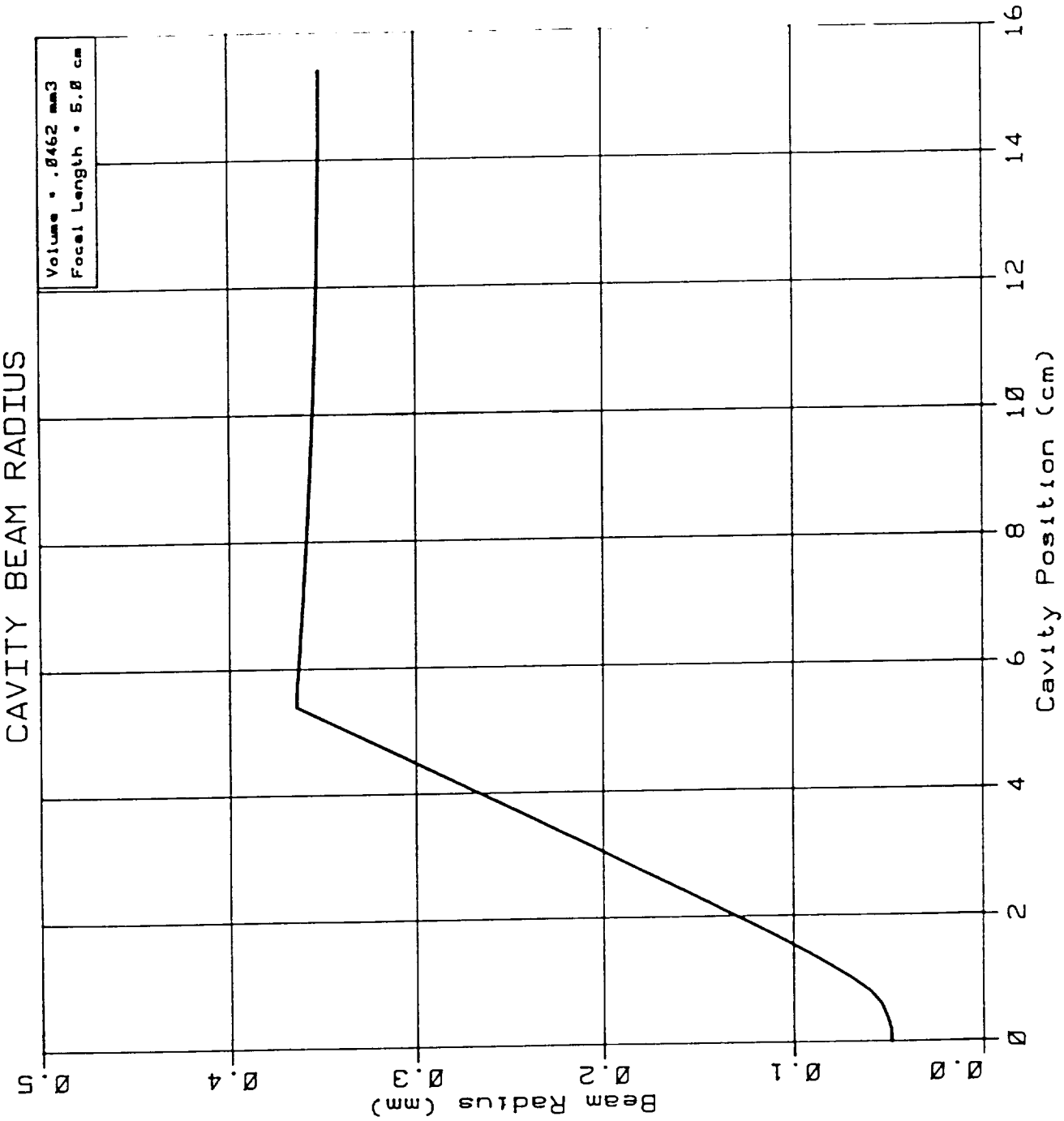

As described above, the LNA material used in this project was obtained from 3 different suppliers: LETI, Grenoble, AIRTRON, and Union Carbide. Of the three sources, the Union Carbide material yielded the most uniform results, i.e. all material was good. Some AIRTRON samples were of poor quality. Two different laser diodes used as the pump source were a 1 w SONY, single-element diode, and the 500 mw Spectra Diodes Lab array. Comparable results were obtained with both diodes. However, the SONY diode deteriorated after 3 months operation and was replaced with the Spectra Diodes high-brightness diode, model SL\DL 2430. This diode has a 1 x 100 μm aperture. The diode is thermoelectrically cooled. The output wavelength is about 797 nm at operating temperature which corresponds to the peak absorption of the Nd^{3+} in LNA. When the LNA is excited with the diode emission, we obtain the fluorescence spectrum shown in Figure 1.3. The arrow indicates the helium resonance wavelength.

The cavity used for the LNA laser is shown in Figure 1.4. The diode light is collimated with a 6 mm focal length lens (Melles Griot 06GLC 002). An anamorphic 4x prism pair (3x for the SONY diode) is used to compensate for the astigmatism of the diode emission. A 25 mm focal length lens (Melles Griot 06GLC 004) focuses the diode light onto the front surface of the LNA crystal (Airtron). The front surface fo the crystal was coated with a high reflectance coating at 1083 nm: thus, forming one end of the cavity. The front surface was also AR coated at 800 nm to permit entrance of the pump light. The second surface of the crystal was AR coated at 1083 nm. The laser output wavelength. The coatings were done by either AIRTRON or Virgo Optics. The interior lens of focal length 25 mm, collimates the laser light. A Lyot filter of thickness 0.76 mm, an etalon with 50% reflective coatings of thickness 0.5 mm, and a 95-98% partially reflecting output mirror complete the cavity. The total cavity length is approximately 30 cm.

The Lyot filter is used to isolate one of the three bands shown in Figure 1.3. The etalon narrows the emission line and permits the laser output to be 'fine' tuned over

FIGURE 1.3 - Fluorescence spectra of Nd in LNA excited by the infrared line of a Kr^+ laser at 752 nm. (Schearer and Leduc 1986)

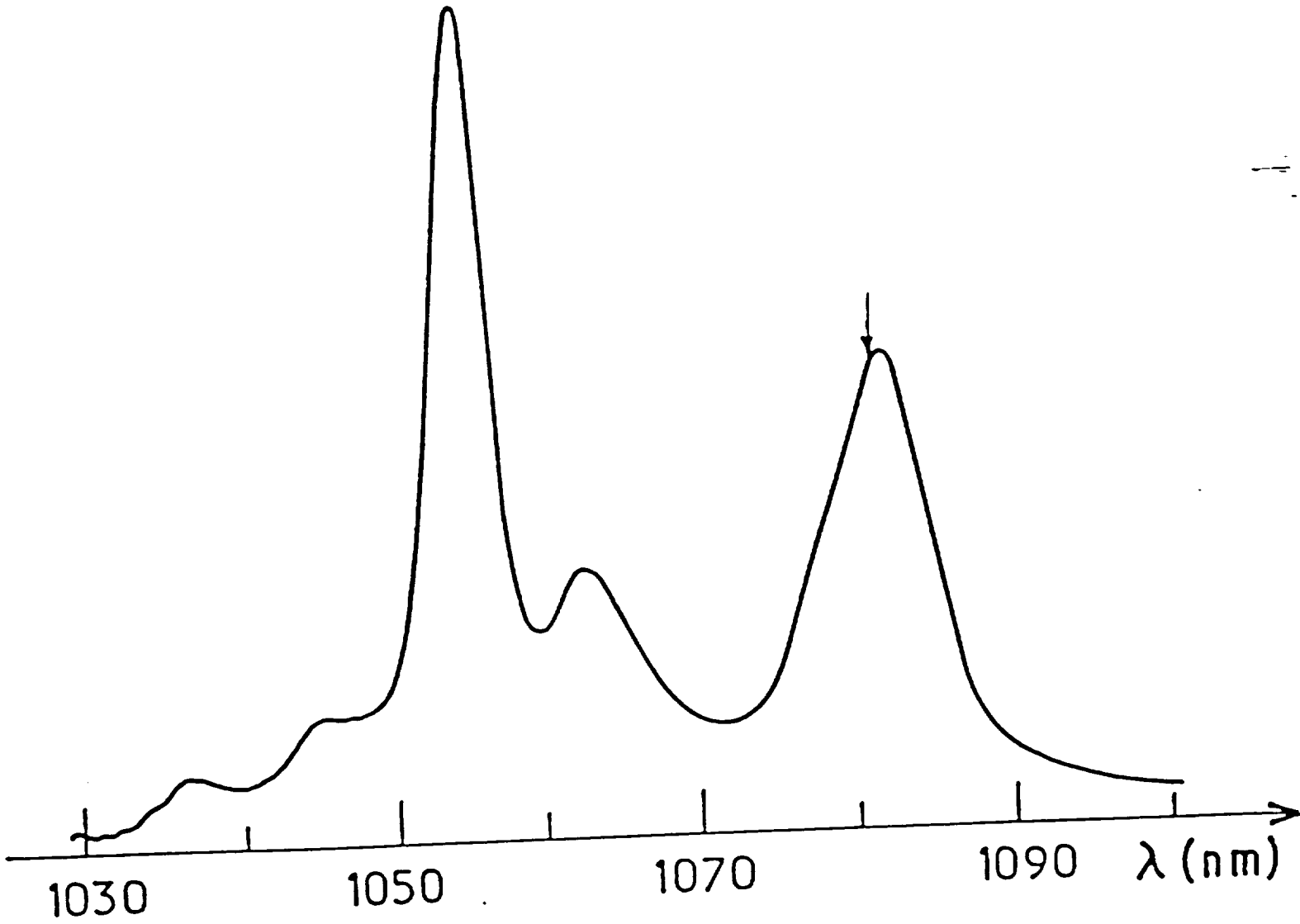

FIGURE 1.4 - Laser Cavity Showing Major Elements

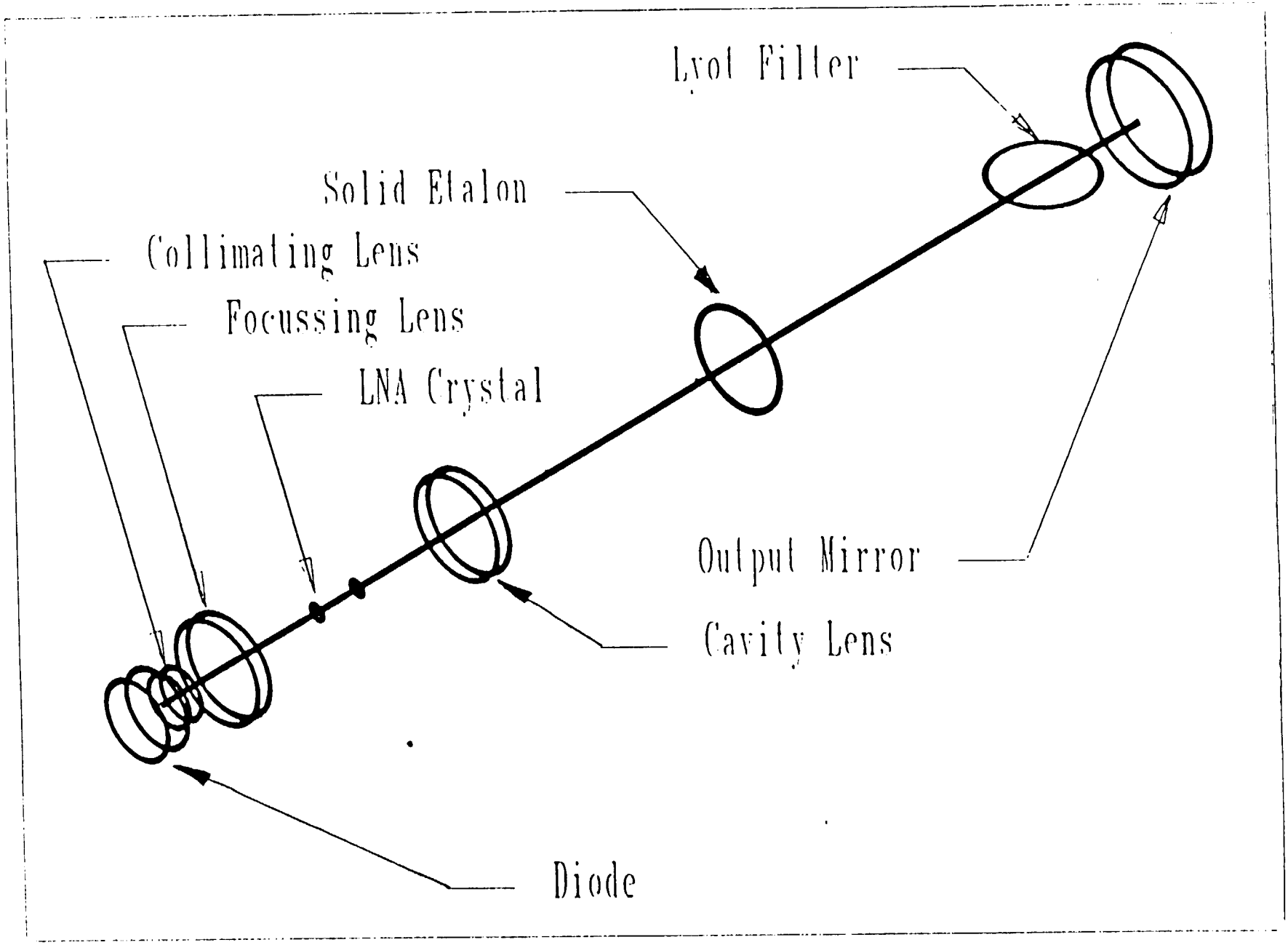

the Lyot filter-selected band by tilt-tuning. When the laser is 'free-running', i.e. with no frequency selective elements within the cavity, the laser oscillates at the peak of the fluorescence near 1054 nm. The LNA laser output at 1054 nm as a function of the diode pump power is shown in Figure 1.5. The slope efficiency is approximately 20%. In Figure 1.6 is a spectral scan obtained with a 1 meter Jarrell-Ash monochromator of the laser output at the free-running wavelength ~ 1054 nm. The output consists of a series of relatively narrow laser emission lines separated by approximately .05 nm. This wavelength separation corresponds to modes selected by the length of the LNA crystal, i.e. $\Delta\lambda = \lambda^2/2nL$ where n is the index of refraction of the LNA at 1054 nm and L is the crystal length. The power output in the free-running mode is about 50 mw. The effective laser bandwidth is 0.6 nm.

Upon insertion of the Lyot filter, the laser output wavelength can be continuously scanned from 1087 nm to 1052 nm. The tuning curves obtained with the Lyot filter is shown in Figure 1.7. The peak power output is about 40 mw. With the Lyot filter in place the laser emission bandwidth is substantially reduced as shown in Figure 1.8. The emission linewidth is now determined by the transmission bandwidth of the Lyot filter. Insertion of the Lyot filter introduces only small losses when the filter is adjusted for peak transmission of the laser radiation.

Since the two main fluorescence bands are separated by almost 30 nm, the dichroic coating on the output mirror can be specified so that transmission loss at 1054 nm exceeds system gain while still retaining 98+% reflectivity at 1083 nm. With this mirror in place it is unnecessary to use the Lyot filter to tune to the 1083 nm band, thus simplifying the tuning sequence. However, unless other effects are present, the laser emission is now unpolarized.

1.2.4 ETALON TUNING

With a single, uncoated 0.25 mm etalon in the cavity the laser output may be tuned by tilting the solid etalon within the cavity. The spectral output of the laser now

FIGURE 1.5 - LNA Laser Power Output as a Function of Diode Pump Power

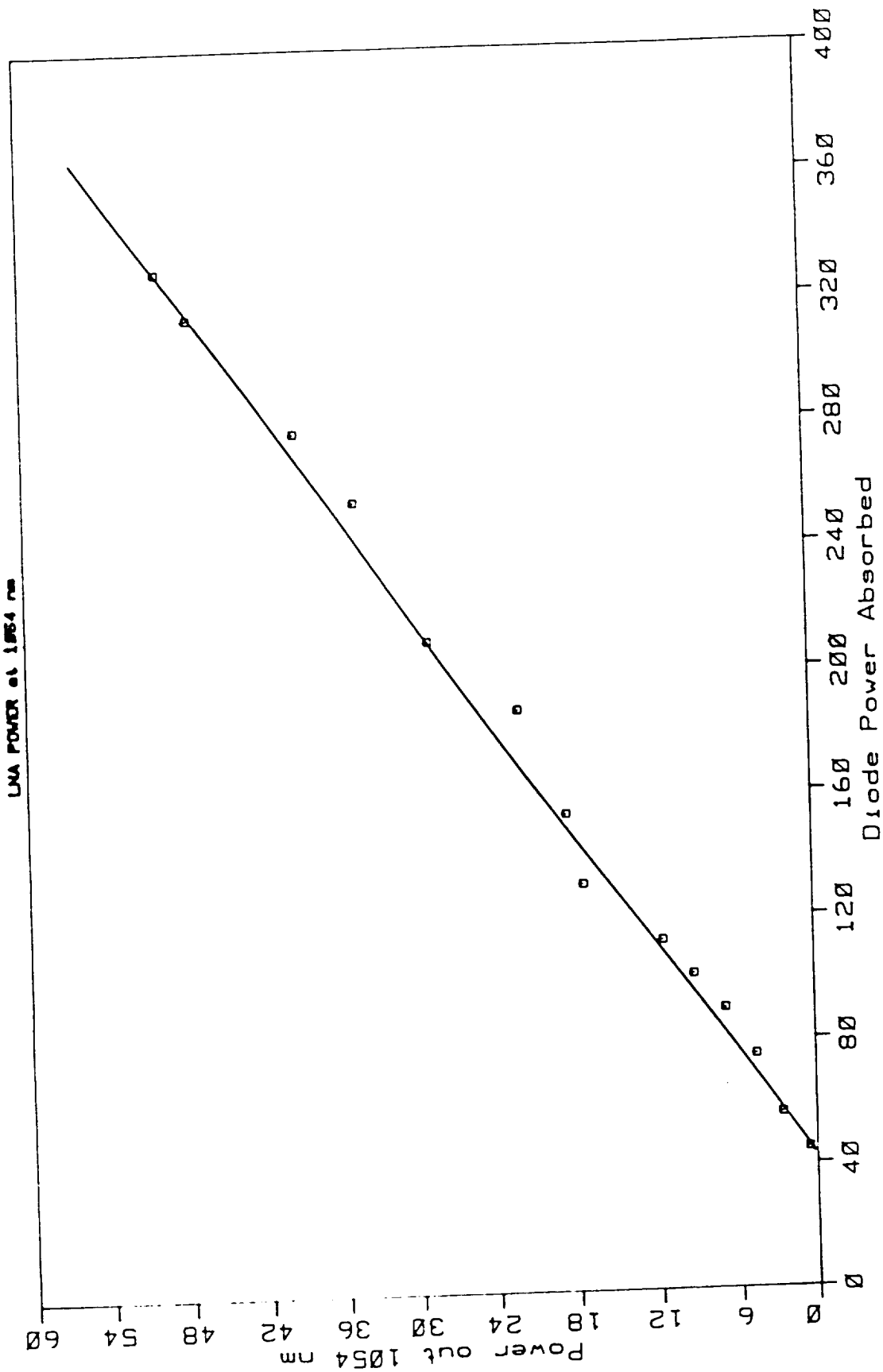

FIGURE 1.6 - Monochromator Scan of Free-Running LNA Laser

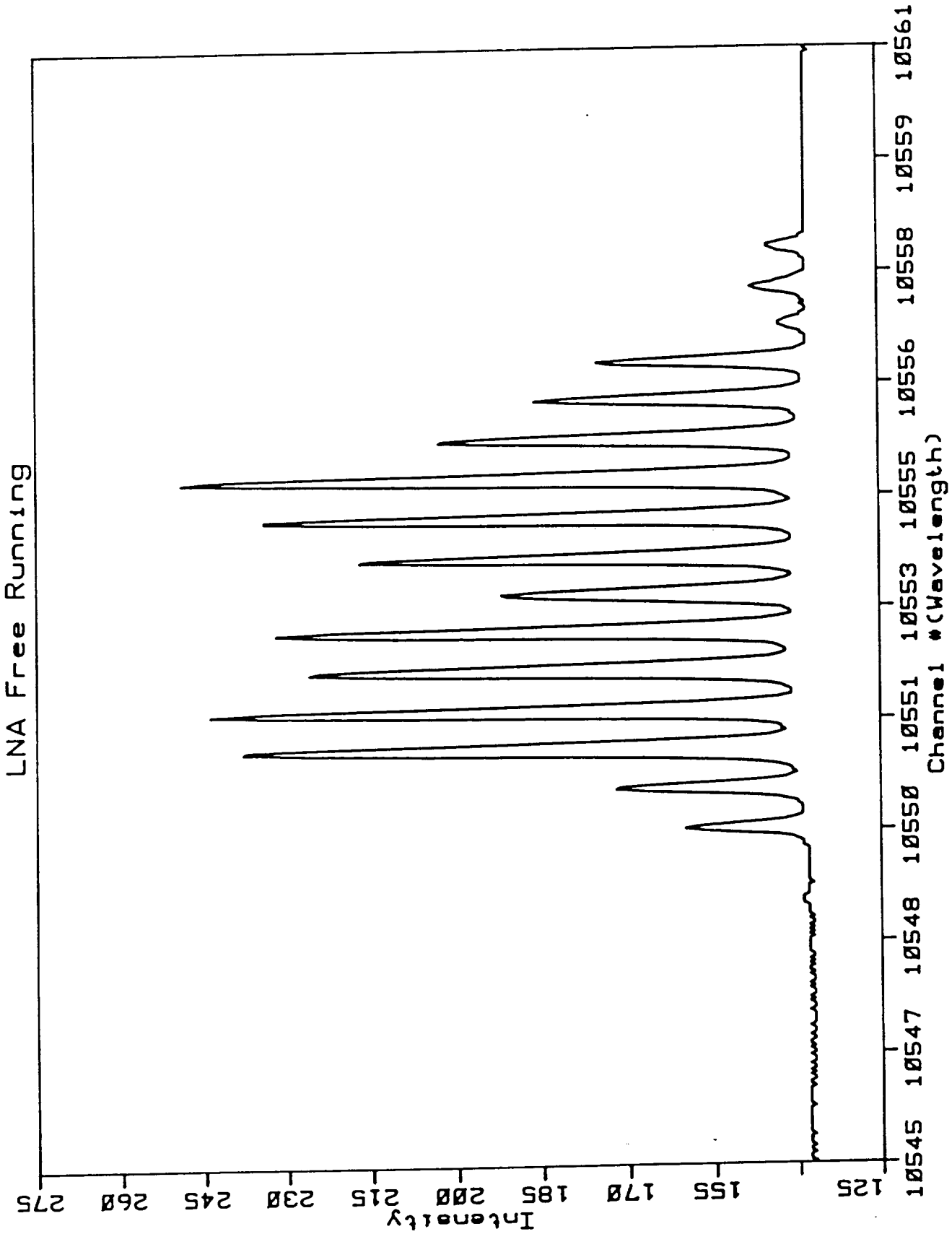

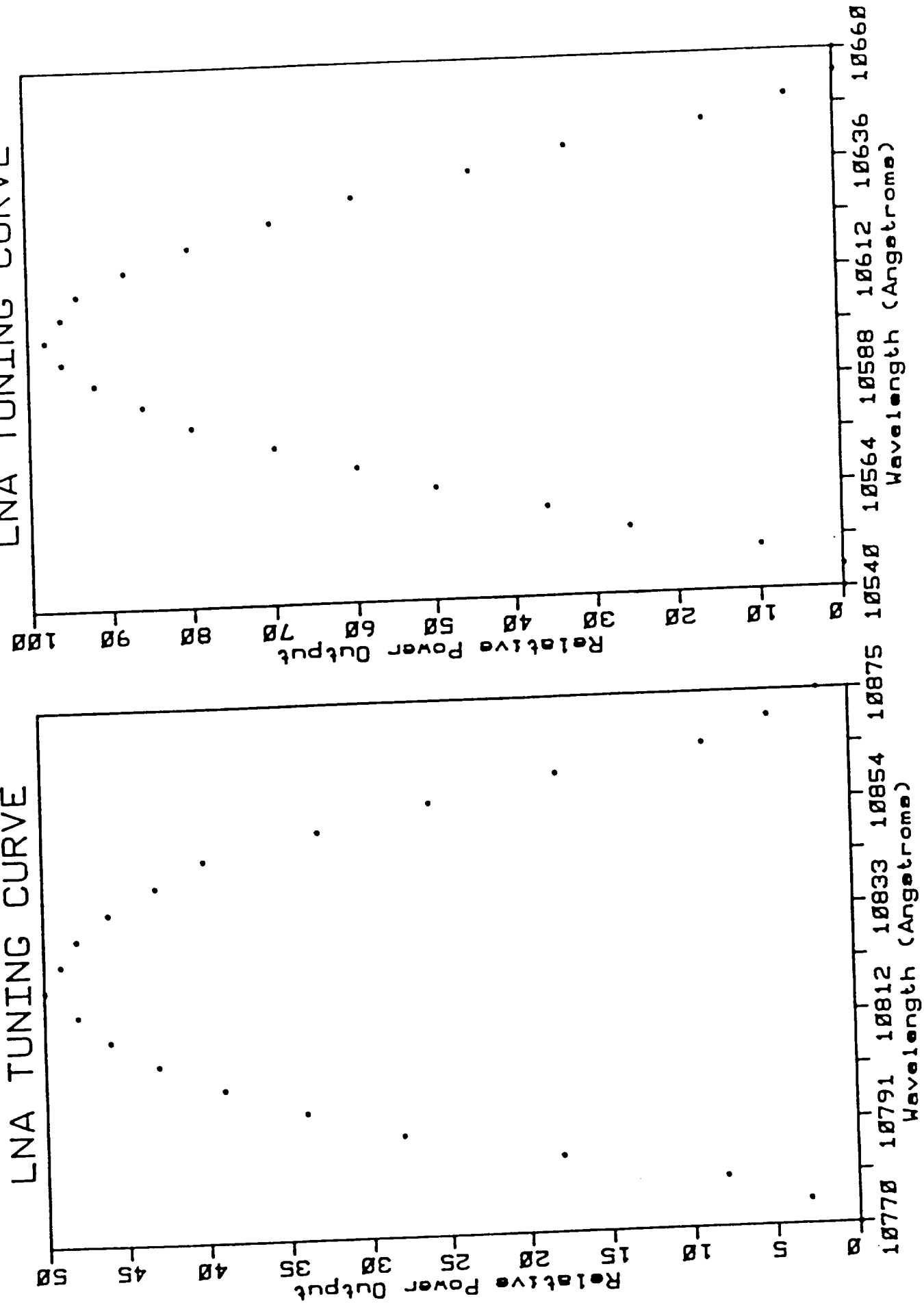

FIGURE 1.7 - LNA Laser Tuning Curve as Lyot Filter is Rotated

FIGURE 1.8 - Monochromator Scan of Laser Emission with Lyot Filter in Cavity

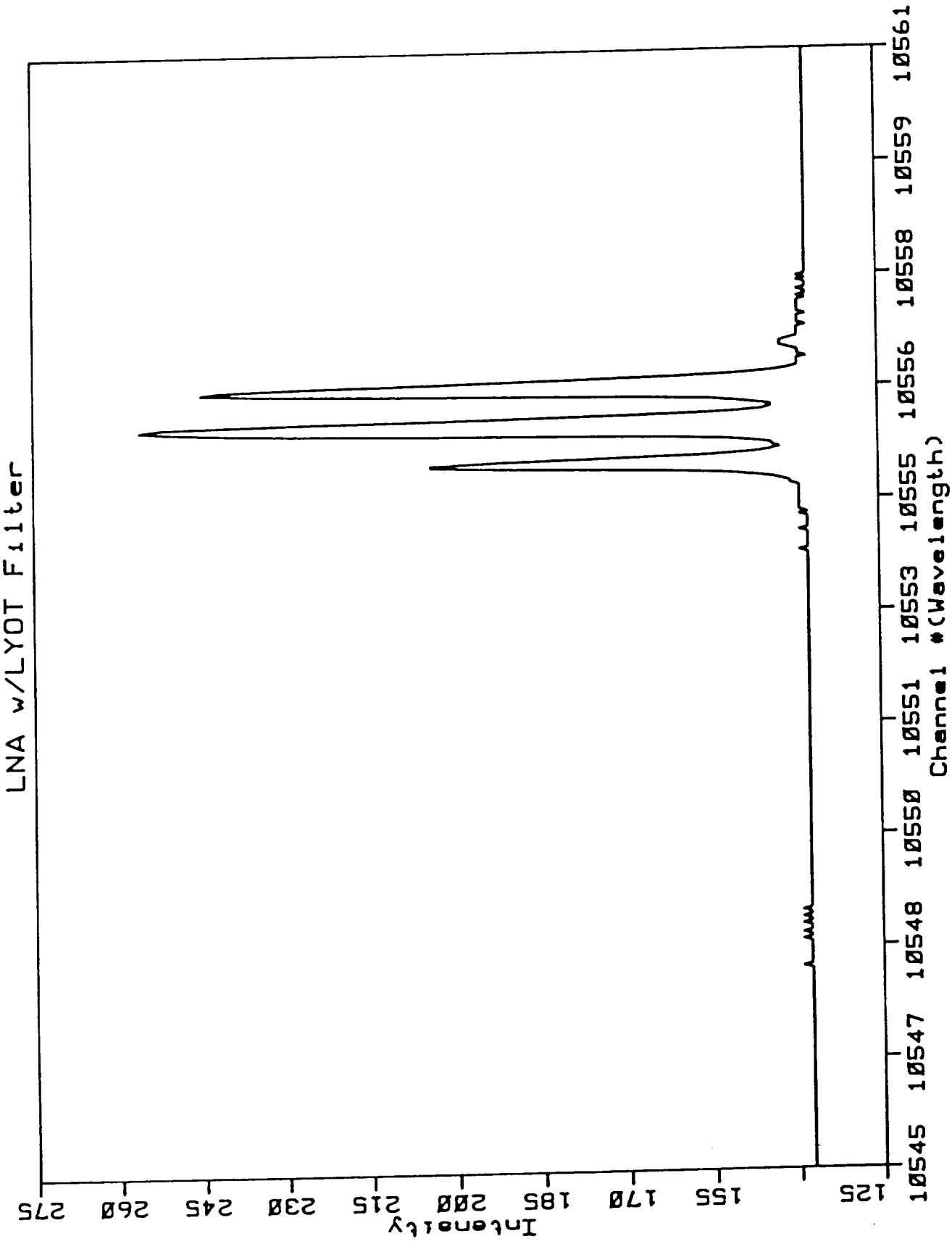

consists of a single component as is shown by the monochromator scan of Figure 1.9. The power output under these conditions is approximately 25 mw. The effective bandwidth of the laser output is 0.037 nm with the uncoated etalon in place.

With a single, 50% coated 0.5 mm etalon in the cavity the laser output at the helium transition is reduced to 20 mw. The laser output bandwidth is further reduced. With the thicker etalon a second emission peak separated by the etalon free spectral range may now appear. This second peak may be suppressed by careful alignment of the laser cavity or the insertion of a second, uncoated etalon. Examination of the mode structure of the laser with a Burleigh Scanning Fabry-Perot Etalon indicates oscillation in a single mode with a bandwidth of less than 40 MHz, the resolution of the scanning etalon. With either the Lyot filter or the special coated mirror in place in order to suppress lasing on the 1054 nm laser line, the laser power at the helium wavelength of 1083 nm is about 12 mw.

Figure 1.10 is a monochromator scan of the laser output with the 50% coated etalon in place. Figure 1.11 shows the single mode output of the laser obtained with the Burleigh instrument.

We can obtain the fluorescence spectrum of ^4He by passing the laser radiation through a helium discharge cell and tilting the solid etalon, thus changing the effective transmission peak. In order to obtain the spectral scan we use a stepping motor which is computer-controlled to uniformly tilt the etalon and hence change the laser output wavelength. As the laser wavelength is tuned through the helium absorption lines we observe the fluorescence scattered at right angles to the laser beam. The D_1 and D_2 transitions are now clearly resolved. The D_0 transition is, of course, well separated as shown in Figure 1.12.

Optical Pumping Signals

Briefly, the optical pumping process consists of passing a circularly polarized beam of light through a cell containing the helium atoms in which a weak electrical

FIGURE 1.9 - Monochromator Scan of Laser Emission with Uncoated Etalon in Cavity

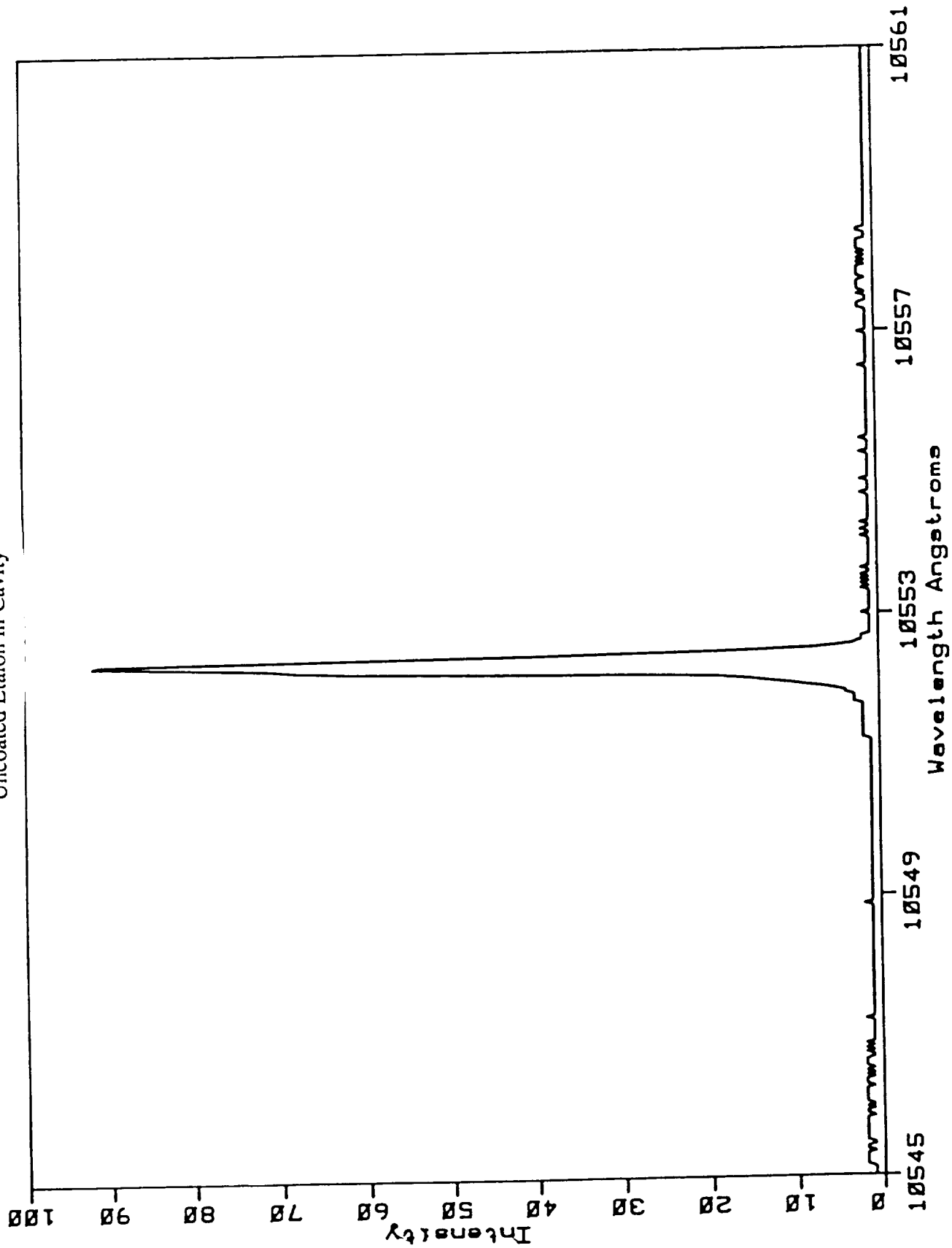

FIGURE 1.10 - Monochromator Scan of Laser Emission with 50% Coated Etalon in Cavity

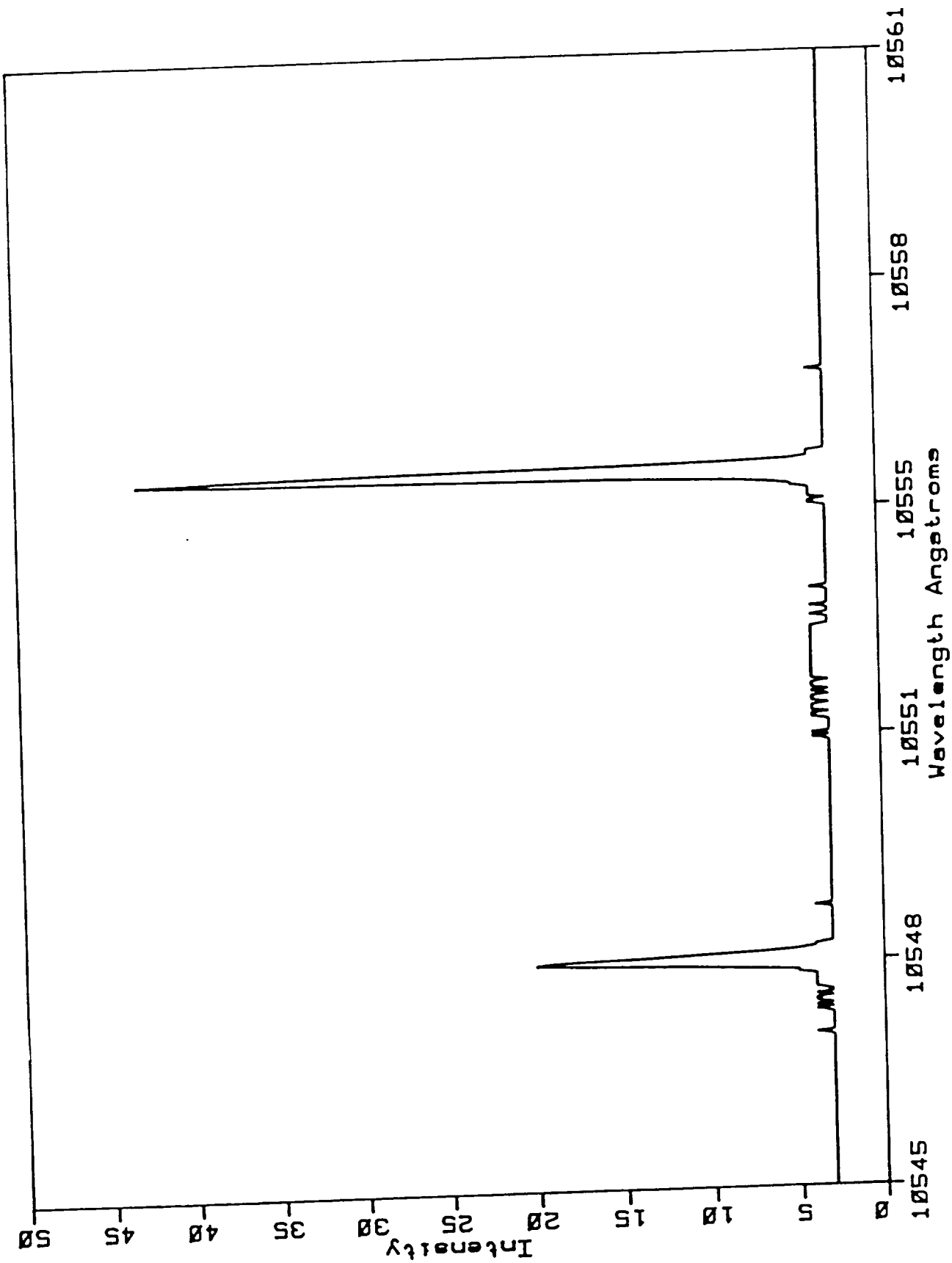

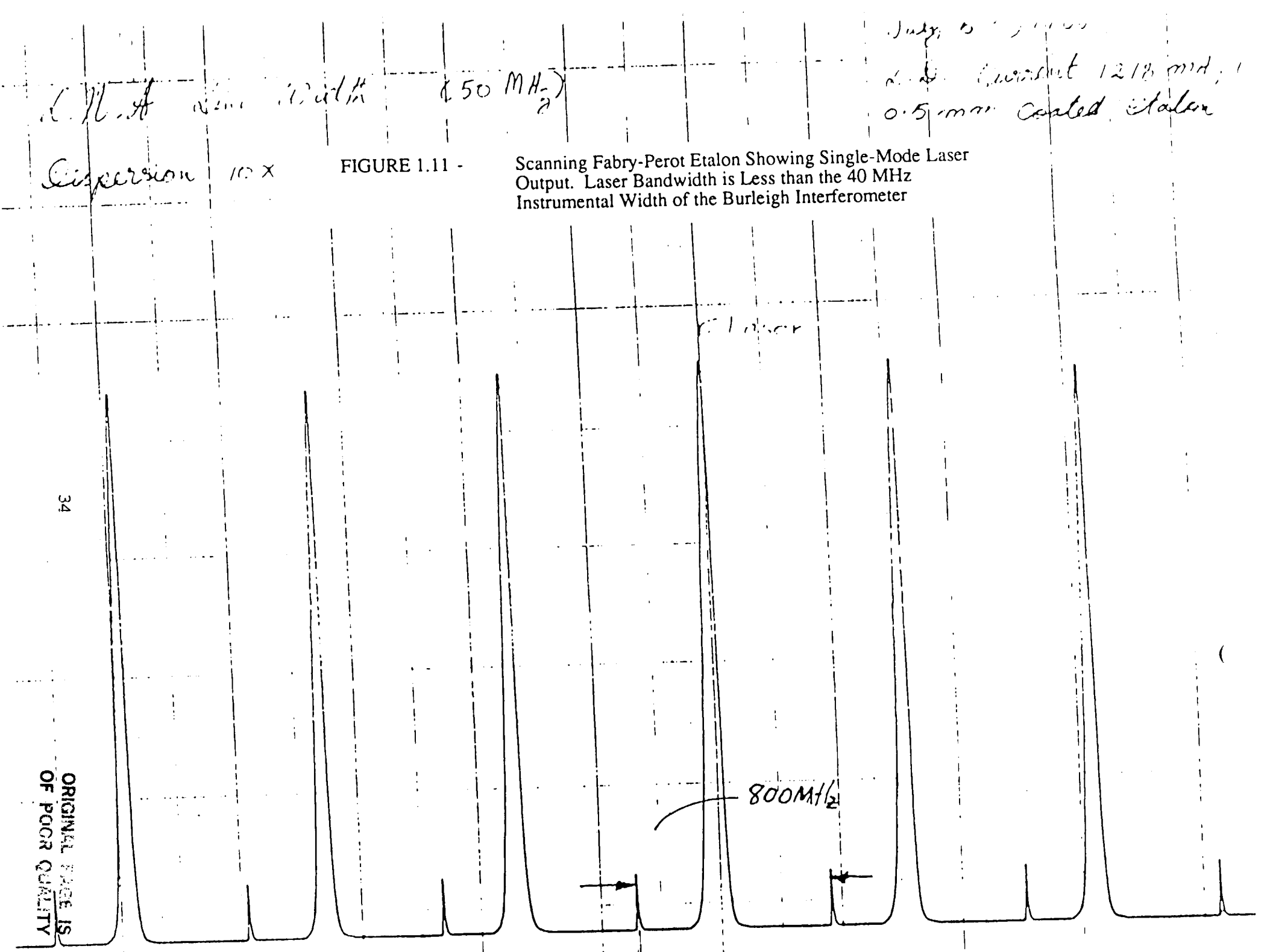

FIGURE 1.11 - Scanning Fabry-Perot Etalon Showing Single-Mode Laser Output. Laser Bandwidth is Less than the 40 MHz Instrumental Width of the Burleigh Interferometer

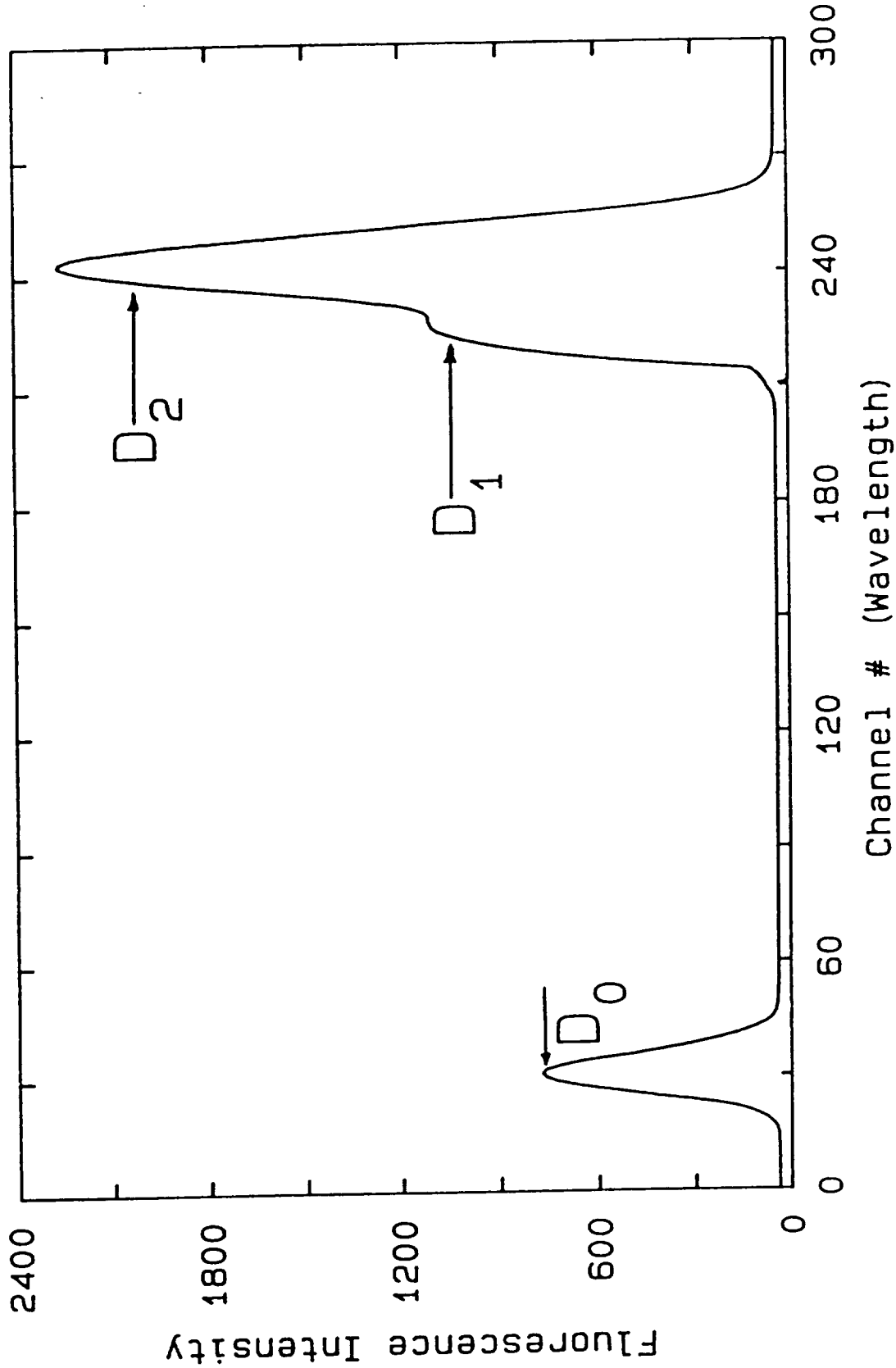

FIGURE 1.12 - Fluorescence Spectrum of Helium as LNA Laser Output is Scanned

discharge is maintained. The discharge populates the metastable levels of helium. The absorption and subsequent emission of this light by the metastable atoms generates a non-equilibrium population of the atoms in different magnetic substates; that is, it induces a magnetization in the ensemble. In ^{4}He the magnetization appears as an orientation of the electron spins of the metastable atoms. In the more complicated case of ^{3}He, the magnetization appears as an orientation of the nuclear spins in the ground state atom.

The original optical pumping experiments were performed with ordinary gas discharge lamps providing the optical pumping photons. The discharge lamps are electrically inefficient and are limited in the amount of power that can be obtained within the absorption linewidth. Typically, a discharge lamp provides a fraction of a milliwatt of pump power.

The new proposed applications require that large numbers of helium atoms be processed. This in turn requires that large numbers of photons at the appropriate resonance wavelength be available. A tunable laser source of many milliwatts at 1083 nm emitting in a bandwidth comparable to the Doppler broadened absorption width of helium would be an ideal source for this purpose. However, such tunable laser sources are not available commercially, and it has been necessary to develop them. In the sections following we describe the characteristics of the optically pumped ^{4}He ensemble. The optical pumping apparatus is schematically represented in Figure 1.13. The laser emission is circularly polarized and directed into the helium discharge cell along the axis of an externally applied magnetic field. The laser beam is expanded with a telescope to fill the cell diameter. The magnetic field of several gauss is generated by a Helmholtz pair. A residual magnetic field of approximately 0.5 gauss is along an axis orthogonal to the laser pump beam. Thus, when the Helmholtz coils are energized, the resultant field is along the pump beam direction: when the coil current is zero, the resultant field is perpendicular to the laser pumping beam. A coil current which oscillates between zero

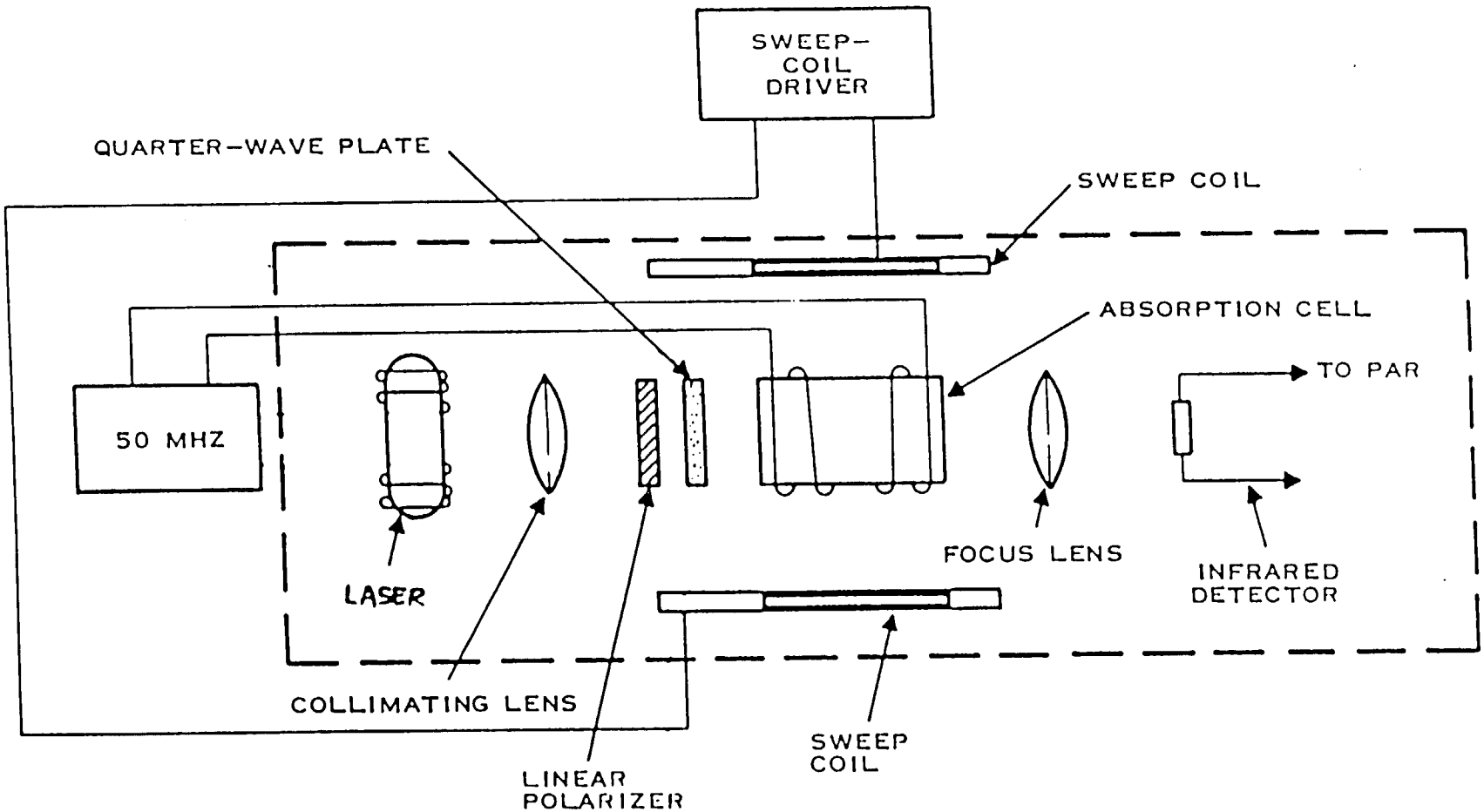

FIGURE 1.13 - Schematic Representation of the Optical Pumping Apparatus

and some non-zero value alternately permits the helium metastable atoms to be optically polarized and then depolarized. Our observations then as a function of the Helmholtz current indicate the efficiency of the optical pumping process.

The optical signals from the polarized-depolarized sample are detected optically both in transmission and/or in fluorescence. The polarization signals are shown in Figure 1.14 as the laser wavelength is scanned through the helium resonance transitions. The relative intensities of the optical pumping signals at the three resonance transitions are strongly discharge dependent with the D_1 intensity being favored by a weak discharge. The D_2 signal is invariably weak indicating the relative inefficiency of pumping with that frequency. In Figure 1.15 we show the dc levels of the transmitted intensity for the D_0 and D_1 components under the several conditions described above. Note that the D_0 transmitted signal changes by more than 60% when the sample is optically pumped. The D_2 component is almost completely absorbed by the weak discharge: the signals for the D_2 component are generally much smaller than either of the other two components.

1.3 YAP (Nd:$YAlO_3$) LASER

1.3.1 LASER CRYSTAL

Laser generation in Nd:$YAlO_3$ (YAP) was first reported by Massey and Yarborough[7] in 1971. Crystal quality was, however, poor and little was done with this system until recently. In 1986 cw laser emission on seven YAP laser lines at 1061.5, 1072.9, 1079.5, 1084.5, 1090.9, 1092.1 and 1098.9 nm within the $^4F_{3/2}$-$^4I_{11/2}$ transition was reported by Schearer and Leduc[8] using a modified cw. Nd:YAG laser cavity. They also tuned through the laser lines at 1079.5 and 1084.5 nm. With the availability of high power laser diodes, a number of very efficient, compact solid state Nd-doped YAG lasers have been reported[9]. More recently there have been reports on diode pumped $LaNdMgAl_{11}O_{19}$ lasers and Nd:$LiNbO_3$ lasers.[10]

FIGURE 1.14 - Optical Pumping Signals Obtained as the Laser Wavelength is Scanned

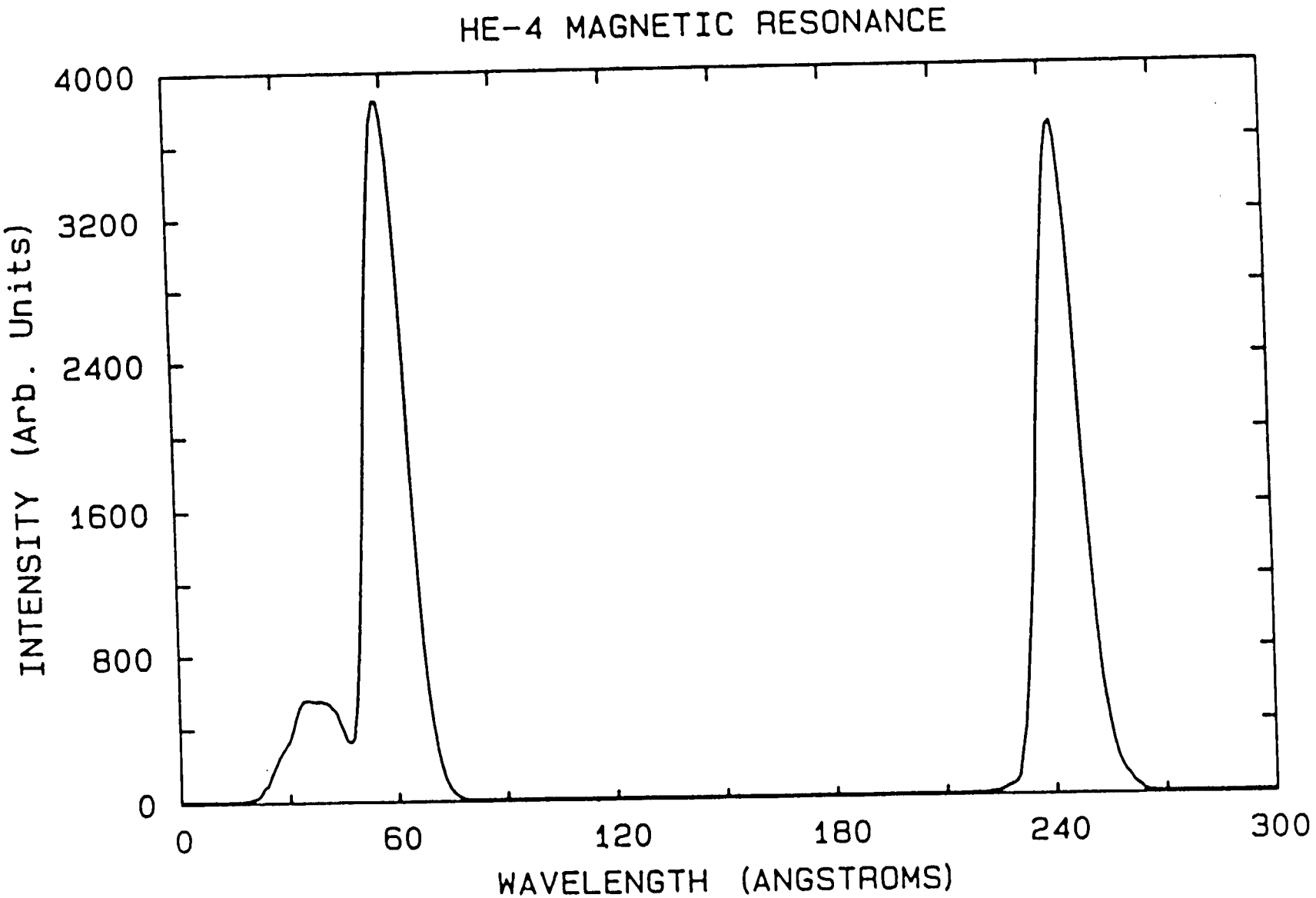

FIGURE 1.15 - DC Levels of Transmitted Light for the Spectral Components as the Sample is Polarized and then Unpolarized

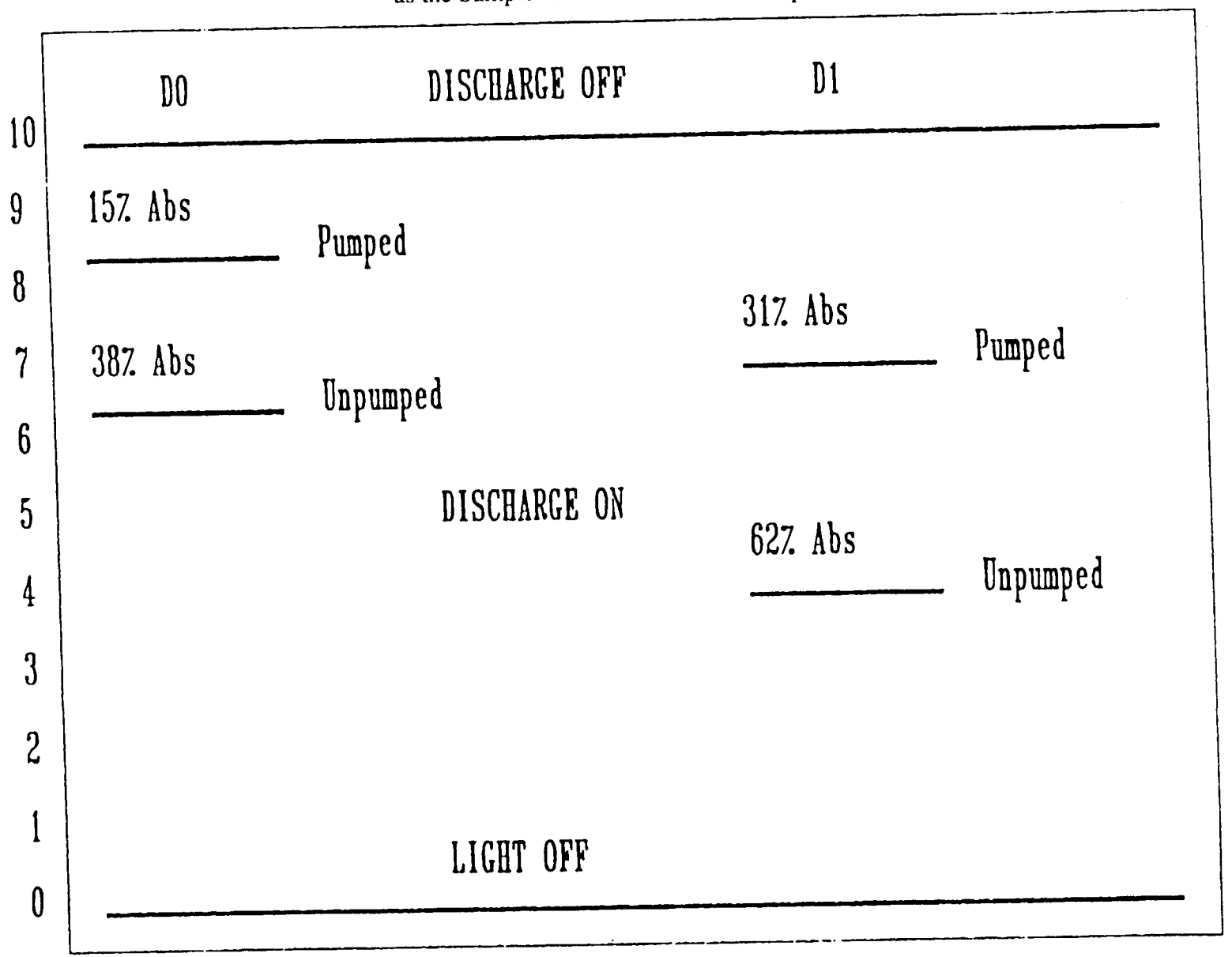

Searl et al.[11] recently obtained laser emission at 1341.1 nm ($^4F_{3/2}$-$^4I_{13/2}$ transition) in Nd:$YAlO_3$ when it was pumped by an 0.5 W. 40 stripe laser diode. Here we report the lasing performance and tuning characteristics of Nd:YAP laser lines originating from the $^4F_{3/2}$-$^4I_{11/2}$ transitions when pumped with a 500 mW high power laser diode.

The YAP crystal used in the work reported here was obtained from Airtron.[12] It had a 1 wt% Nd content and was 5 mm in length and 3 mm in diameter. It was cut along the crystal "a" axis. One end of the YAP rod had a high reflectivity coating at 1080 nm and high transmission at 800 nm. The other end was AR coated at 1080 nm. Thus, one end of the crystal also formed one end of the cavity. This provided a straight forward way to couple in the pump power while also minimizing the threshold power.

1.3.2 DIODE LASER PUMP SOURCE AND OPTICS

One of the attractive operating features of using the laser diodes is the good spectral match between the laser diode emission and the rare earth element (in this case Nd^{3+}) absorption band. The major absorption bands centered at about 520 nm, 590 nm, 740 nm and 800 nm (specifically 796 nm, 807 nm and 812 nm)[13,14] permits one to use the commercially available high power cw laser diodes. The laser diode utilized in this work was Spectra Diode model SDL2450. The lasing structure of this diode is 400x1 microns consisting of a 40 element array. At room temperature the diode wavelength was 805 nm with rated power output of 500 mW.

The laser diode output was collimated by an 8 mm focal length (Melles Griot 06GLC 002) lens. Due to the diffraction at the laser diode cavity the output of the laser diode has an asymmetric pattern and a 3 x anamorphic prism was used to correct this astigmatism before it was focused onto the YAP crystal by a 25 mm focal length (Melles Griot 06GLC 004) lens. The laser diode was cooled by peltier cooler attached to a water cooled heat sink and was maintained at about 17°C. A schematic diagram of our laser

cavity is shown in Figure 1.4. The cavity was about 40 cm in length providing space for a Lyot filter and one or more solid etalons for tuning purposes.

1.3.3 LASER PERFORMANCE AND TUNING CHARACTERISTICS

Figure 1.16 is the YAP laser gain curve at 1079.5 nm obtained with a 95% reflectivity output coupler. The YAP laser threshold occurred with 75 mW of diode power incident on the crystal. The YAP crystal absorbed more than 90% of the incident diode light at 805 nm. Over 100 mW of output power was achieved with 450 mW of laser diode light on the crystal. Due to the anisotropic nature of the stimulated emission cross sections of this material, the laser thresholds and gain coefficients of the various transitions for Nd^{3+} in $YAlO_3$ are dependent on the crystallographic orientation of the rod axis. Without polarization selective optics in the cavity, the oscillation is always polarized along the c axis either at 1079.5 nm or 1311.1 nm.

Oscillation on the main peak at 1079.5 nm can be suppressed by inserting a Lyot filter inside the cavity. In our case a two stage birefringent Lyot filter with thicknesses of 0.76 mm and 6 mm was inserted between the intra-cavity lens and the output mirror as shown. Depending upon the crystal orientation with respect to the orientation of the Lyot filter, different groups of laser lines are obtained. When the c crystallographic axis was parallel to the laser polarization, laser emission at 1072.9, 1079.5 and 1084.5 nm was obtained by tuning with the Lyot filter. The relative intensities of the lines with the 95% output coupler are shown in Figure 1.17. When the b axis of the crystal was made parallel to the laser polarization, three other lines at 1064.5, 1090.9, and 1098.9 nm were obtained as depicted by the dotted lines in Figure 1.17.

Tuning within a band was performed by inserting an 0.25 mm uncoated etalon inside the cavity. Coarse tuning to the major transitions utilized the double plate Lyot filter while fine tuning was obtained with the etalon. Figure 1.18 display the tuning range of the laser lines at 1072.9 nm, 1079.5 nm and 1084.5 nm when the YAP crystal c

FIGURE 1.16 - YAP Laser Gain Curve at 1079.5 nm

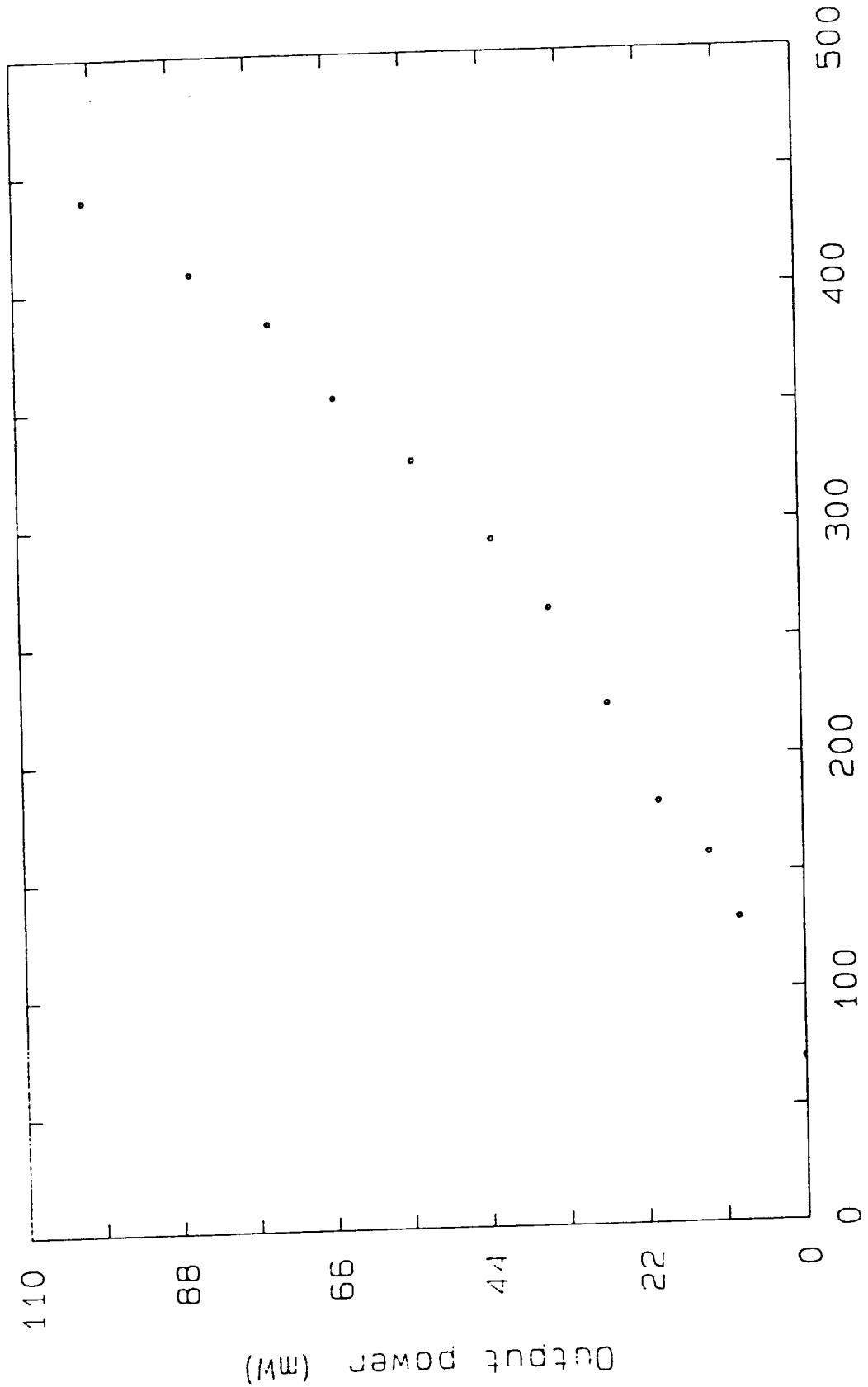

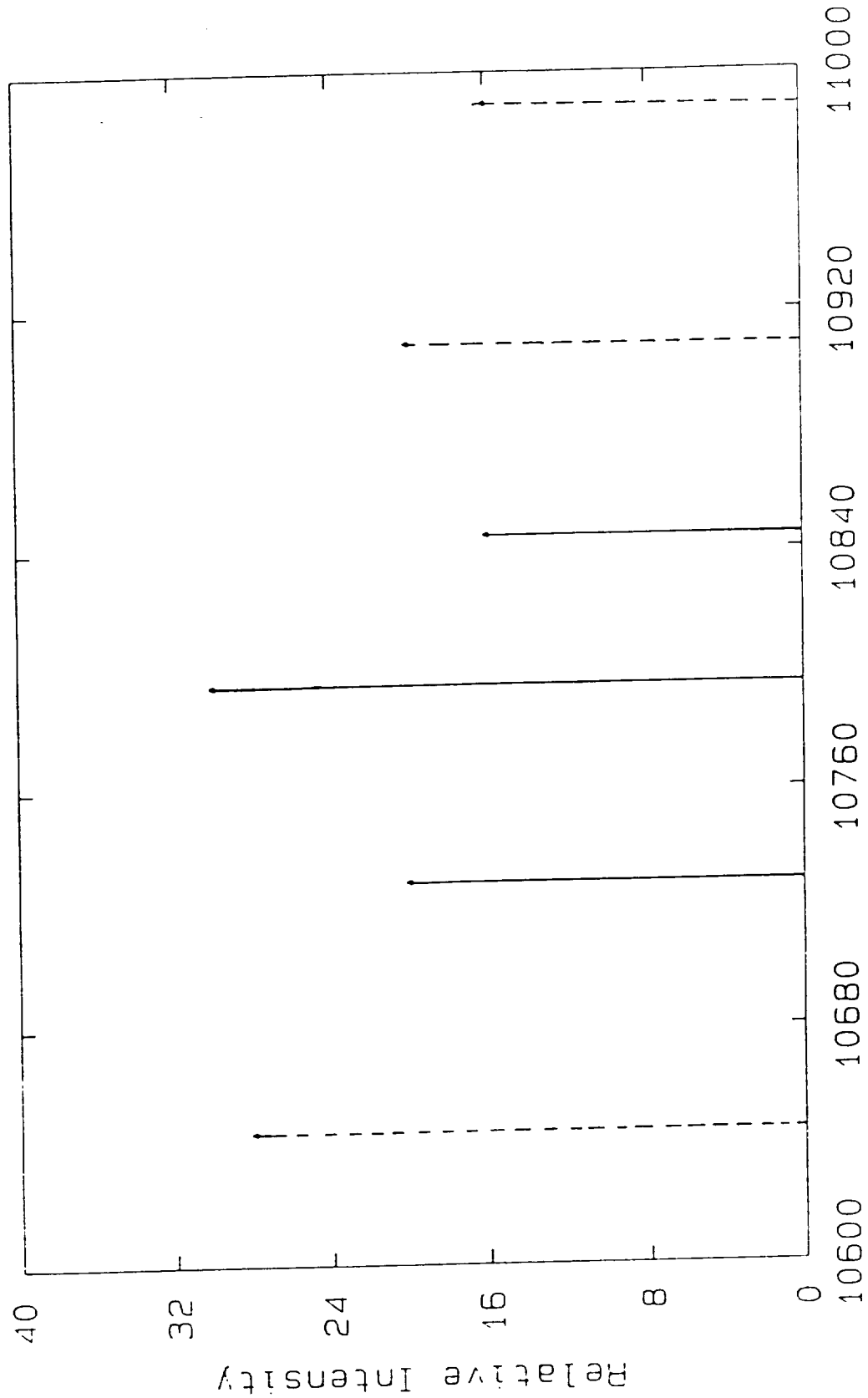

FIGURE 1.17 - YAP Laser Lines Obtainable with Lyot Filter

FIGURE 1.18 - Tuning Curves for 3 of the YAP Laser Transitions

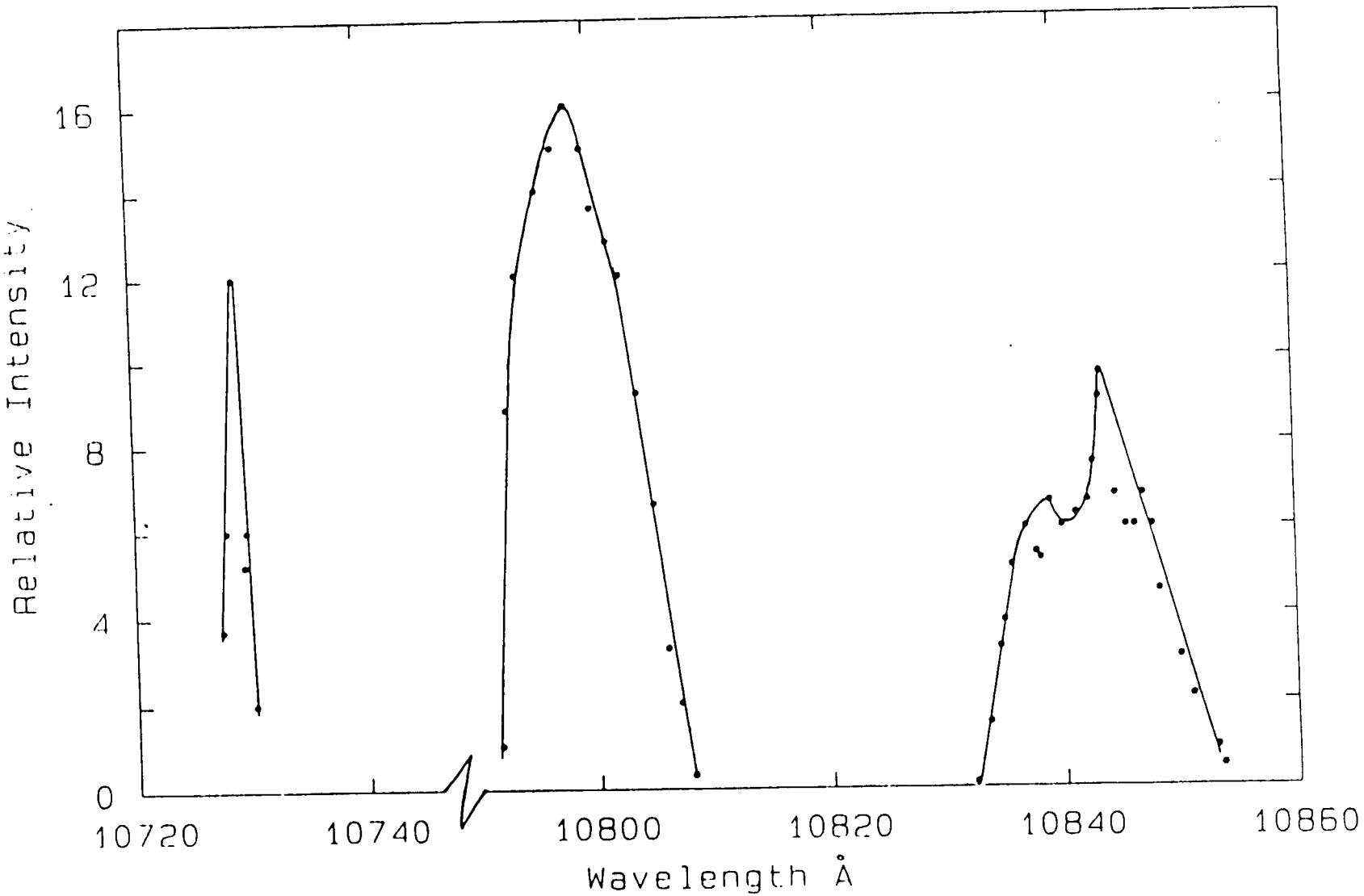

axis is parallel to the polarization of the laser. The tuning curves shown were obtained with a 98% output coupler. The best tuning performance was obtained with the laser diode case temperature set to about 17°C.

We also tuned this YAP laser at the other three laser lines: 1064.5 nm, 1090.9 nm and 1098.9 nm which were observed when the crystalline b axis was parallel to the polarization of the laser output. A single plate Lyot filter of thickness 1.5 mm was used in this case with the 0.25 mm uncoated etalon. The tuning range of these three lines is shown in Figure 1.19.

Conclusions

As indicated in Fig 1.17, we have obtained all the energy levels pertinent to the Nd:YAP laser lines of the $^4F_{3/2}$-$^4I_{11/2}$ transition manifold. The tuning curve of Figure 1.18 shows that we can obtain laser emission, although weak, near 1083.1 nm which is the resonance transition in Helium-3 (7 mw in an 0.012 nm bandwidth). Using an arc-lamp pumped Nd:YAP laser to optically pump helium atoms, spin-polarized Helium-3 nuclei and polarized metastable Helium-4 atoms have been obtained.[6] Nuclear targets of polarized ^{3}He nuclei have been developed using the arc-lamp YAP system. The work reported here suggests that diode-pumped systems may be useful in this application as more powerful diodes become available.

A significant advantage offered by laser diode pumping is system lifetime and reliability. Laser diodes have operating lifetimes exceeding 10^4 hours for cw operation. The absence of high voltages, high temperature load, and UV radiation encountered with arc lamps leads to a more benign operating environment for all solid state laser systems employing laser diode pumps. Spectra Diode Labs has recently demonstrated a 100 micron wide laser emitting over four watts cw power which is comparable to typical output powers of the bulky ion lasers.[15] Thus, the diode-pumped Nd:YAP system may be a useful alternative to Nd:YAG where tunability, efficiency, and portability are required.

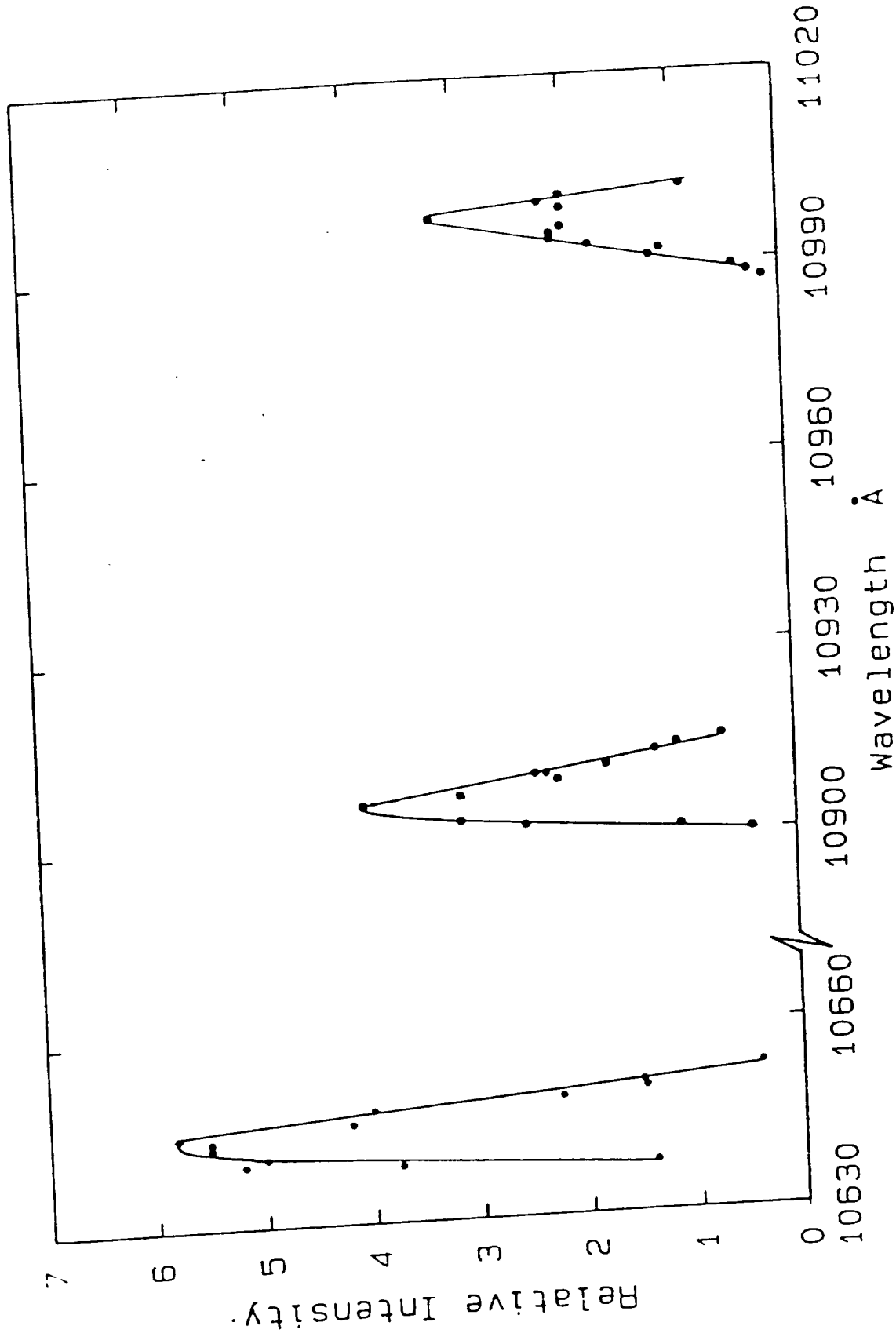

FIGURE 1.19 - Tuning Curves of 3 of the YAP Laser Lines with Opposite Polarization

1.4 LITHIUM NIOBATE (Nd:$LiNbO_3$) LASER

1.4.1 LASER CRYSTAL

Neodymium-doped lithium niobate crystals exhibit fluorescence in the near infrared region and Schearer et al.[16] have demonstrated that this laser material can be tuned to the helium resonance transition. The free-running wavelength of the output is at 1084 nm suitable for use in optical pumping of helium. Lithium niobate ($LiNbO_3$) is of commercial interest as a non-linear optical material for parametric processes, mode-locking, Q-switching, and frequency doubling applications. However, neodymium-doped lithium niobate crystals are not commercially available. The crystals used in this work were provided to us by McDonnell-Douglas Corp. of St. Louis, MO. The use of neodymium-doped lithium niobate, $LiNbO_3$ as an optical pumping source for helium is of interest because its other crystallographic properties, such as the piezoelectric, electro-optic, and non-linear optical effects can be used to control and vary the laser output.

The purpose of this work was to develop a Nd-doped $LiNbO_3$ tunable laser excited via its 590 nm absorption by a 3.0 W Ar ion laser pumping a dye laser. At 590 nm the absorption is maximum: thus the efficiency of conversion to the 1081 nm output from the $LiNbO_3$ is maximized. This laser was pumped via the 752 nm absorption by a 1 W Kr ion laser. The device is characterized by good efficiency, high gain, and low thresholds and is easily tunable in a region of the spectrum which contains the helium metastable resonance transitions. Fan et al. has also developed a Nd-doped $LiNbO_3$ pumped via the 590 nm absorption, but this laser was not tunable.[17] In essence, this research is an extension of Fan's work using the ideas introduced by Schearer. The Nd:$LiNbO_3$ crystals have a unique potential. It is the purpose of this research to describe our efforts at developing such a tunable laser.

Over the previous twenty years Neodymium-doped Lithium Niobate has been investigated for applications in lasers.[18,19,20] It is an interesting material which combines the lasing properties of the Nd^{3+} ion with the electro-optical and non-linear

optical properties of $LiNbO_3$. The work was initiated in a study done by Evlanova et al.[19] and has continued with renewed interest recently.[21] This material has an emission peak near 1084 nm which can be excited by light in the vicinity of 530, 590, 760, and 800 nm.[22] Nd-doped $LiNbO_3$ shows promise of being an alternative to YAG as a tunable laser in the 1084 nm region.

Nd-doped $LiNbO_3$ has a perovskite-like structure with orthorhombic symmetry.[23] The crystal is uniaxial with the optic axis along the c direction. The crystal can be optically excited along the a (or equivalently along the b), and the c directions with considerable difference in their lasing power. If the crystal is optically pumped from the a or b axis, the optic plane is elliptical and the crystal is consequently birefringent. $LiNbO_3$ is known to have a large birefringence.[24] The large birefringence allows the crystal to polarize the light giving a substantial lasing power. If the crystal is pumped from the c axis, the optic plane is circular, and the crystal has a low lasing power.

The Nd^{3+} donors in $LiNbO_3$ account for the lasing ability. A simplified version fo the appropriate energy-level scheme of Nd is given in Figure 1.20 where E_1 is the ground state and E_4 is an excited state. The energy difference (E_4-E_1) corresponds to a wavelength of approximately 590 nm. The energy level E_3 is an intermediate excited state with a lifetime of approximately 240 us. By optical pumping at 590 nm, Nd atoms in the ground state are stimulated. State 4 decays to state 3 by non-radiative decay. If the crystal is pumped "hard" the net result is to invert the population from E_3 to E_2. During the optical pumping, state 2 is not affected, implying $N_3 >> N_2$. State 3 subsequently decays to state 2 by stimulated emission if sufficient feedback is available to overcome losses due to spontaneous emission. The emitted photons have a wavelength of 1084 nm. Thus, a coherent radiation at 1084 nm builds up. The transition from state 3 to state 1 is not allowed by selection rules.

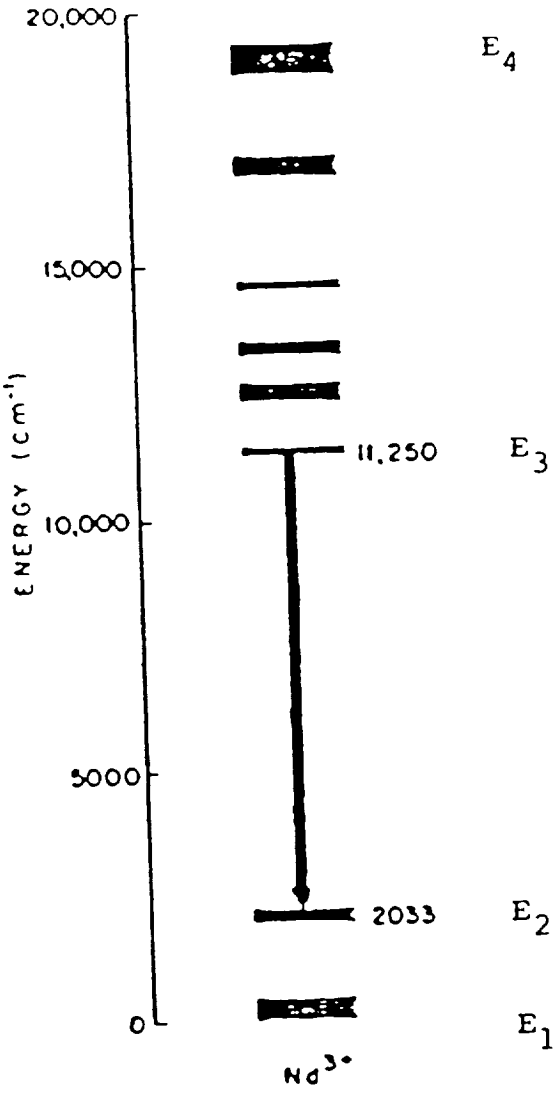

FIGURE 1.20 - Energy Level Diagram for Nd in Lithium Niobate

Figure 1.21 shows the absorption spectra of Nd-doped $LiNbO_3$ and Figure 1.22 shows the emission. These graphs were taken from the work of Cordova-Plaza et al.[21] The early work on Nd-doped $LiNbO_3$ was done on crystals of poor optical quality. The lasing power rapidly deteriorated with usage. The cause of the aging was attributed to inhomogenities caused or enhanced by the photovoltaic photorefractivity. This handicap severely limited the use of the Nd-doped $LiNbO_3$ laser. Recently, Fan et al.[21] made a solid solution of Nd-doped $LiNbO_3$ with 5-mol.% MgO. The addition of Mg to the melt and its incorporation into the crystal reduces the photorefractive damage to the crystal as shown by R. Gerson et al.[24] They obtained a crystal with greatly reduced aging in the output power. Aging still occurs if the crystal is excited via the 590 nm absorption, but if one of the longer wavelength absorption bands (e.g.) 750 nm) is used the laser power becomes stable "indefinitely".

Fan et al. has recently developed a Nd-doped $LiNbO_3$ pumped by an Ar+ pumped dye laser at 590 nm. Schearer et al.[16] also recently developed a Nd-doped $LiNbO_3$ laser pumped by a 1 W Kr+ laser at 752 nm. Both these lasers had good efficiencies, high gains and low thresholds. Schearer's laser was tunable in a region of the spectrum which contains the Helium metastable resonance line at 1083 nm.

1.4.2 PUMP SOURCE AND OPTICS

As indicated in a previous section, the Nd-doped $LiNbO_3$ can be pumped with one (or more) of several wavelength bands. The band at 595 nm, however, has the greatest absorption cross-section; consequently, pumping with this band should yield a laser of the highest efficiency and lowest threshold. The largest uncertainty was the role of photorefractive damage to the crystal caused by the pump light. It was known that photorefractive effects were serious at shorter pump wavelengths, but Schearer et al.[16] reported no deleterious photoeffects when the crystal was pumped with a Kr+ laser at 752 nm.

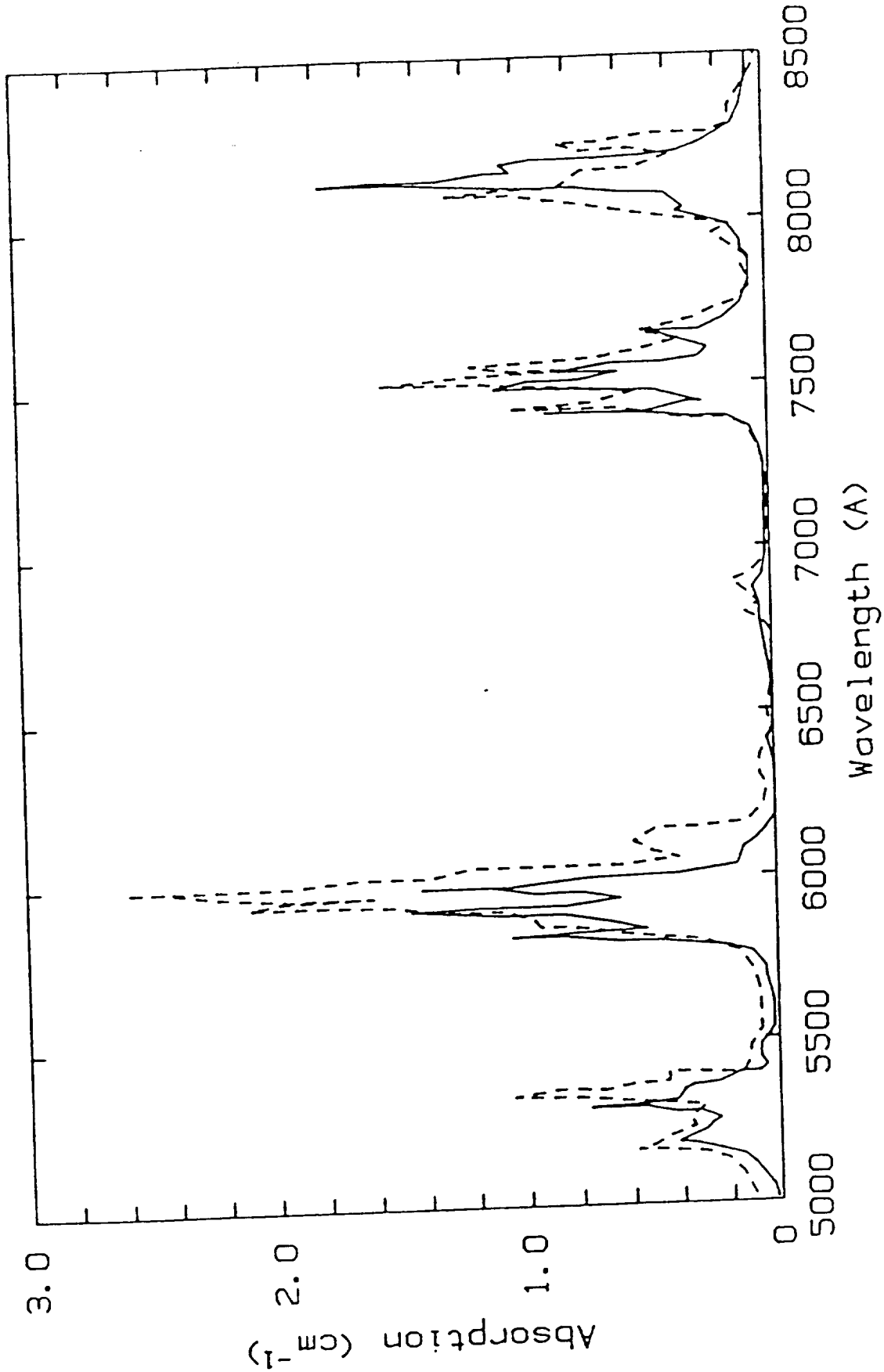

FIGURE 1.21 - Absorption Spectrum of Nd-doped Lithium Niobate

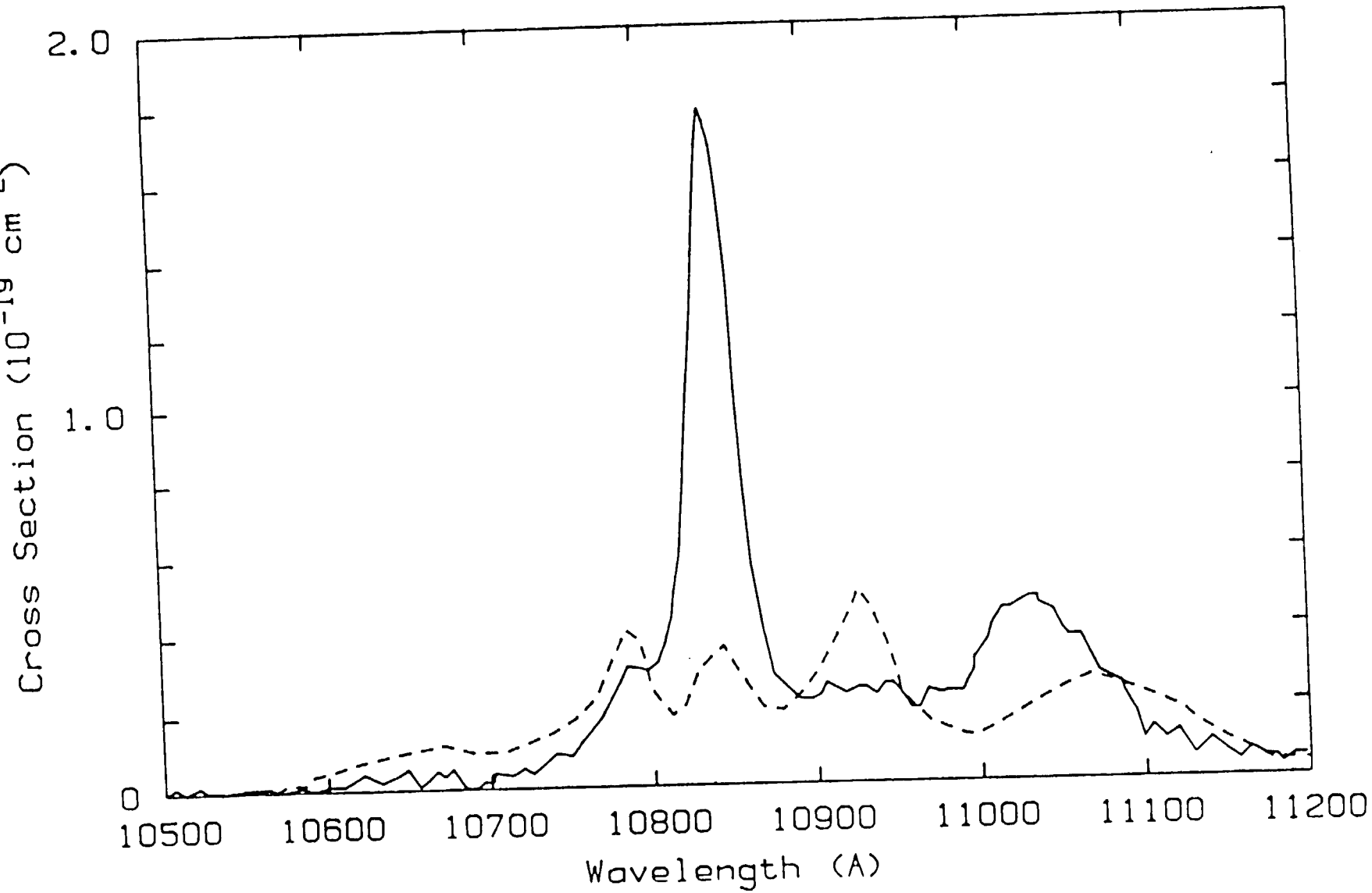

FIGURE 1.22 - Emission Spectrum of Nd-doped Lithium Niobate

Pumping with a cw 590 nm Source

The experimental setup used is shown in Figure 1.23. The pump light source was a series of two lasers. The first was a 3.0 W Ar+ laser which was used to pump a standing wave, cw jetstream dye laser operating with Rhodamine 6G dye. The dye laser was operated at a wavelength in the vicinity of 590 nm. The output wavelength of the Ar+ laser was 544 nm. The conversion efficiency from the Ar+ laser light into the 590 nm dye laser output was approximately 20%; thus, about 360 mw of laser light at 590 nm was available to pump the $LiNbO_3$ crystal.

The light out of the dye laser was directed towards a lens (L1) which had a focal length of 5 cm. The pump light was focused just inside the front surface of the $LiNbO_3$ crystal. The $LiNbO_3$ crystal had a high reflection (HR) coating on the surface facing the dye laser which, however, permitted almost complete transmission of the incident light (590 nm). The reflectivity of the crystal was nominally 100% at the desired lasing wavelength, 1083 nm. It thus, formed one end of the laser cavity. The opposite end of the crystal was AR coated at 1083 nm and had reflection losses of less than 0.2%. The crystal was coated by Virgo Optics, Orlando, FL.

A second lens (L2), identical to lens (L1), was placed behind the $LiNbO_3$ crystal. Both lenses were AR coated at 1083 nm in order to minimize reflective losses inside the cavity. The lens (L2) was used to define the stability of the cavity by focusing the infrared fluorescence from the crystal at a point beyond a plane mirror M2. The plane mirror, M2, was a partially reflecting mirror at 1083 nm and acted as the output mirror, coupling out a portion of the laser radiation produced inside the cavity.

The transmission of the mirror could be chosen between 1-16% by changing the coating and its thickness. The mirrors used in this experiment had transmissions of 1.2.5 and 16%. The output power from the $LiNbO_3$ crystal could be changed by varying the transmission of M2. The cavity length could be adjusted between 20 and 80 cm, but 60 cm was chosen throughout this experiment. Figure 1.24 shows the gain curve of

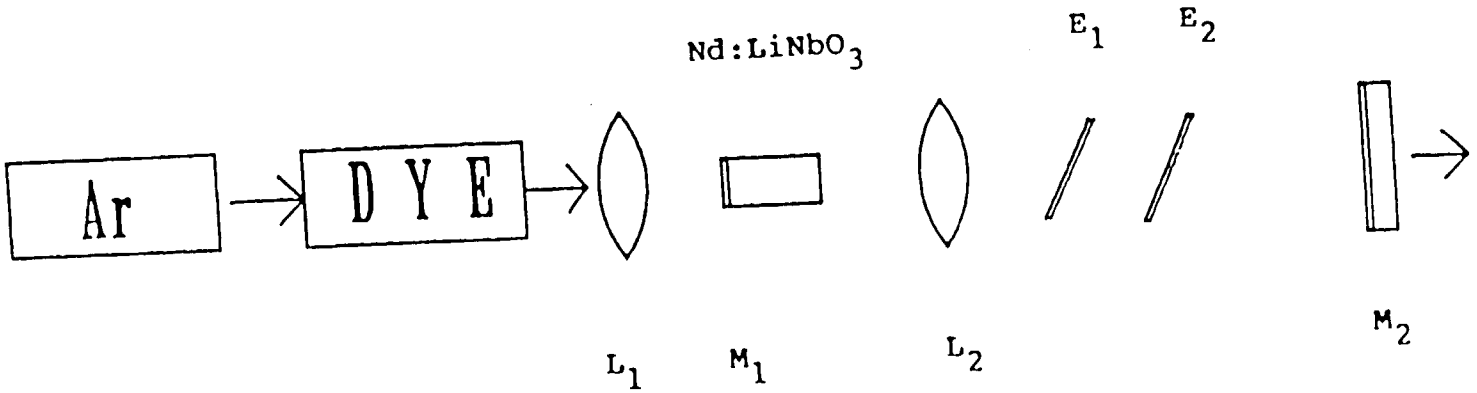

L_1 = focussing lens

L_2 = collimating lens

M_2 = plane output coupler

M_1 = HR coating on $LiNbO_3$ surface

$E_{1,2}$ = solid etaion

FIGURE 1.23 - Experimental Setup for Dye Laser Pumping of Nd-doped Lithium Niobate

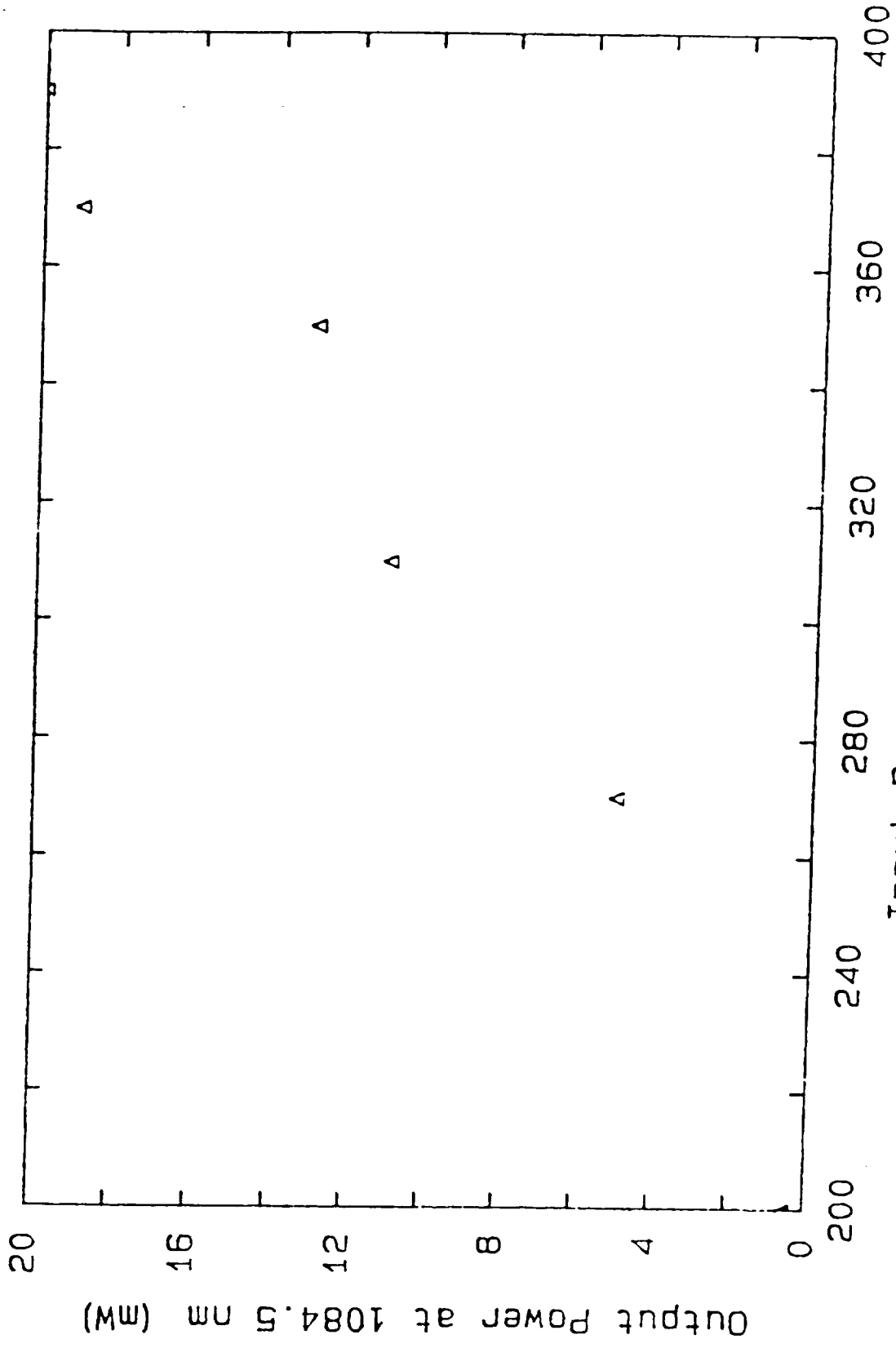

FIGURE 1.24 - Gain Curve for Nd:Lithium Niobate

Nd:$LiNbO_3$ laser at 1084 nm. The crystal was obtained from McDonnell-Douglas Corp. and was cut in the form of a rectangular parallelopiped, 4 mm x 4 mm x 10 mm and contained 0.15-wt% Nd. The long dimension of the crystal coincided with the crystalline 'b' axis.

When the cavity was configured as described above and pumped with the two laser system at 360 mW, the cavity lased in the vicinity of 1084 nm. The laser output was polarized along one of the short edges coinciding with the c axis. In the free-running mode, over 20 mW of laser power was obtained at the peak of the fluorescence shown in Figure 1.25.

The tuning characteristics of the laser were determined by inserting one or more solid etalons within the cavity. The solid etalons provide a variable frequency transmission as their thickness is changed by tilting the etalons. The bandwidth is varied by varying the relative thicknesses of the etalons or by using different reflective coatings on the etalon surfaces.

A Lyot filter could also be inserted within the cavity for tuning purposes. The Lyot filter (FL) is essentially a variable waveplate, allowing the cavity transmission to change with wavelength.[25] Tuning curves were taken with both cavity configurations. The Lyot filter was oriented at Brewster's angle, and its placement within the cavity is as shown in Figure 1.26. The tuning characteristics of the $LiNbO_3$ output with the Lyot filter in place was found by rotating the Lyot filter. All measurements were made at room temperature.

Pumping with a Pulsed Source at 590 nm

We have also investigated the use of a frequency-doubled, modulated YAG laser as a replacement for the AR+ laser pumping the Rh6G jet dye laser. The output of the doubled YAG laser consists of 150 ns pulses at a 6 kHz repetition rate. The peak pulse power is approximately 2 kW: the average power is 2 W at a frequency-doubled

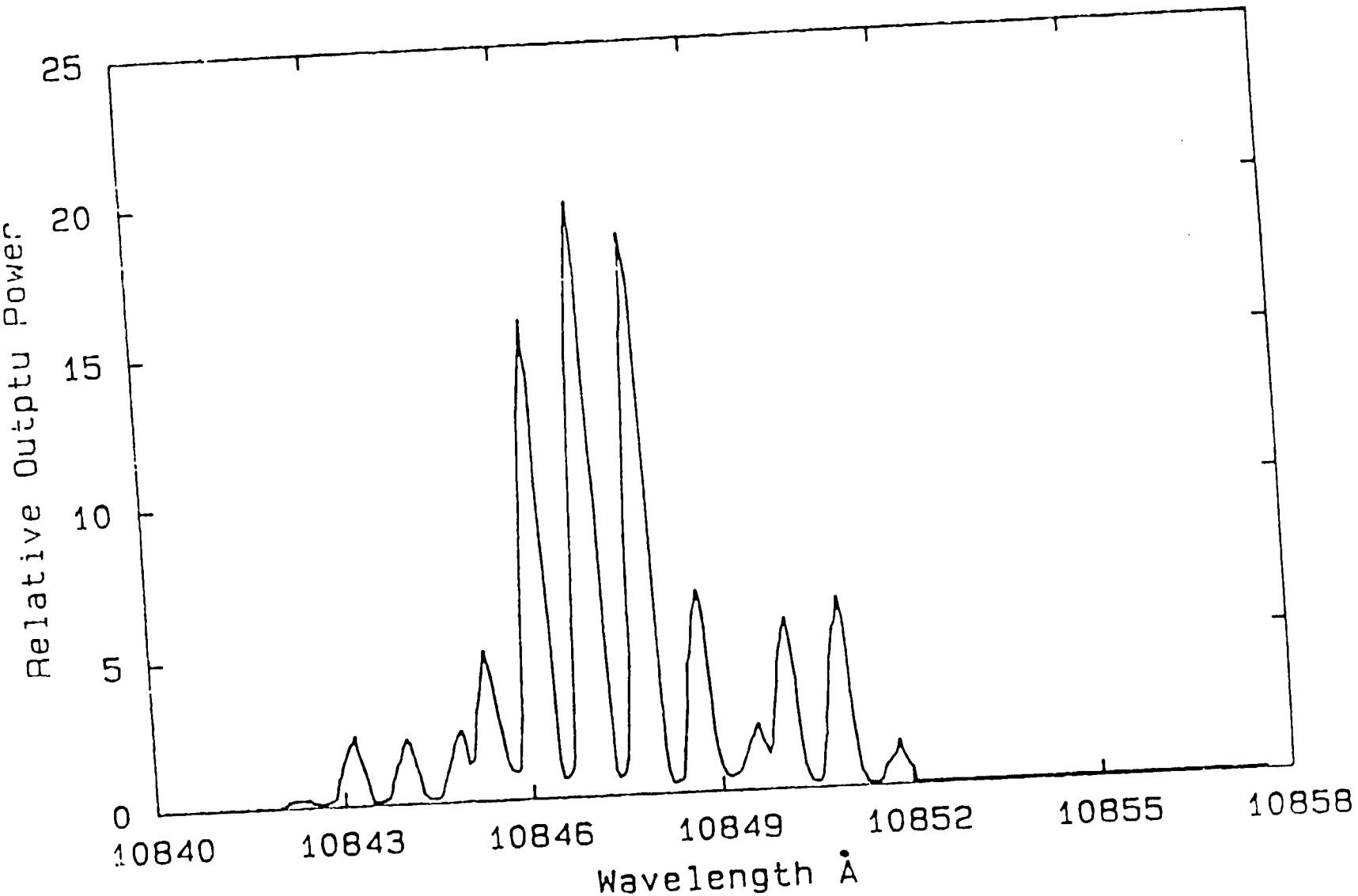

FIGURE 1.25 - Monochromator Scan of Nd:Lithium Niobate Laser in Free-Running Mode

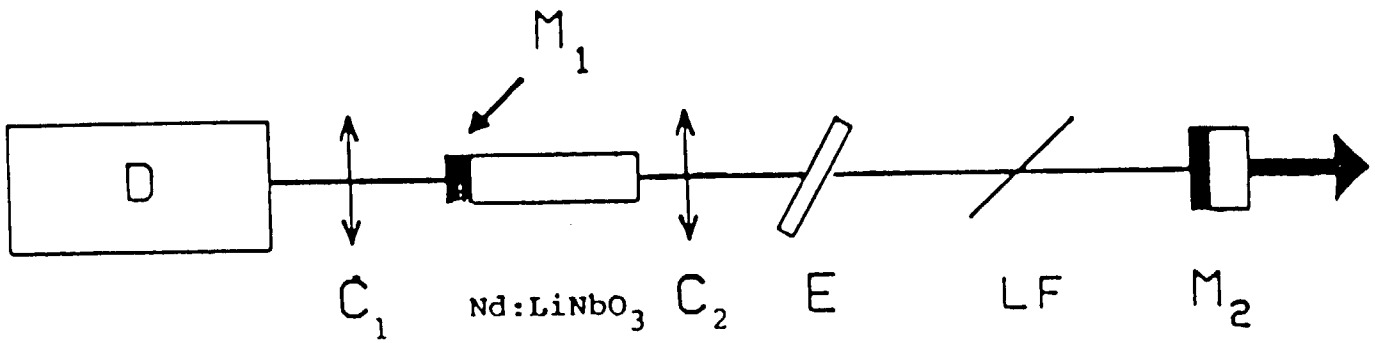

D = Dye laser

C_1 = focussing lens

C_2 = collimating lens

M_1 = HR coating on $LiNbO_3$ surface

M_2 = plane output coupler

$E_{1,2}$ = solid etaion

LF = Loyot filter

FIGURE 1.26 - Nd:Lithium Niobate Laser Cavity with Lyot Filter

wavelength of 532 nm. When this source is used to pump the dye laser we obtained an average power of 250 mW at 590 nm and a peak power of 250 W.

The average power of 250 mW is required in order to maintain an average population inversion in the Nd-doped $LiNbO_3$. The pulses from the dye laser could then, in principle, be used to investigate time-dependent processes within the solid-state laser. Figure 1.27 shows the dye laser pumping the Nd:$LiNbO_3$ laser which in turn is pumped by a Nd:YAG laser.

The Nd:YAG Laser is a cw (continuous-wave) laser in which the active lasing element is Neodymium within a crystalline lattice of Yttrium Aluminum Garnet (YAG). This system produces a cw output power of 60 W at 1060 nm when pumped by cw Kr arc-lamps. Included in the YAG cavity is an acousto-optic modulator which modulates the transmissivity of the laser cavity with the 150 ns, 6 kHz pulses described above. The acousto-optic Q-switch is a piezoelectric crystal which suffers a periodic change in its refractive index when an oscillating voltage is applied to the crystal. If the acoustic wavelength is of the order of the wavelength of the laser light, the material behaves as a diffraction grating. When the incident beam falls on the acoustic grating at an angle, Bragg reflection occurs so that a large portion of the incident beam is diffracted. This effectively reduces the gain to a point where the system stops lasing. This results in an increased "population inversion" which produces a laser output of "intense giant pulses". The frequency of the voltage applied to the Q-switch is 40 MHz, and it is modulated at the Q-switch frequency of 6 kHz. When the modulator is opaque to the circulating laser photons, the circulating power can build up to large values, 2 kW in our case.

The laser cavity also includes a second harmonic generator (SHG) which uses Lithium Iodate ($LiIO_3$), a birefringent crystal, as an active non-linear element to convert 1060 nm radiation to 532 nm radiation. This is known as frequency doubling. The Nd:$LiNbO_3$ cavity is now pumped with the modulated, dye laser light at 590 nm as before. The cavity remains identical to that described in the preceding section.

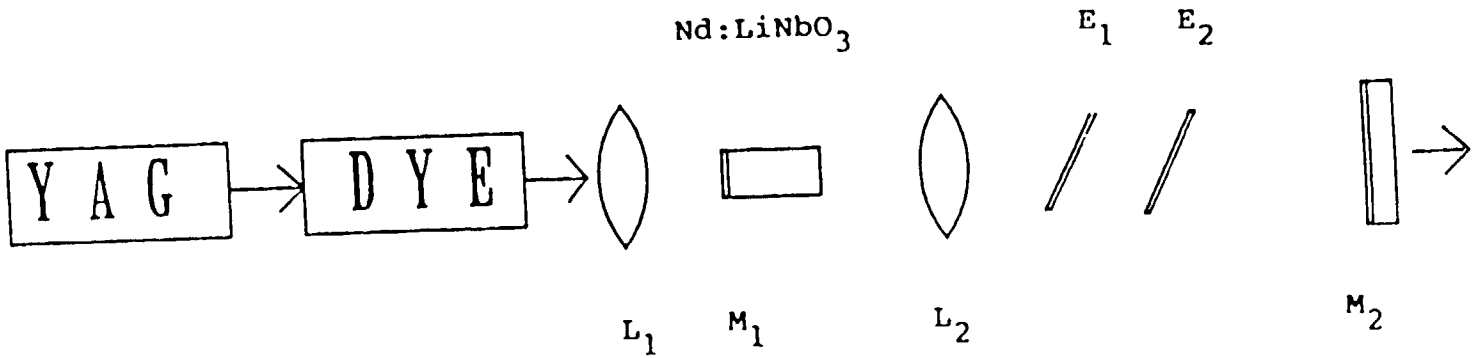

L_1 = focussing lens

L_2 = collimating lens

M_2 = plane output coupler

M_1 = HR coating on $LiNbO_3$ surface

$E_{1,2}$ = solid etalon

FIGURE 1.27 - Dye Laser-Pumped Nd:Lithium Niobate Laser

1.4.3 LASER PERFORMANCE AND TUNING CHARACTERISTICS

Figure 1.25 shows the output from the Nd-doped $LiNbO_3$ crystal without a Lyot filter or etalon in the cavity. A center peak is obvious at 1084.5 nm which arises from the stimulated emission of the pumped Nd^{3+} donors. There are several peaks on both sides of the center peak which arise from the Nd^{3+} fine structure. The electronic structure of the ground state of Nd^{3+} is $[Xc]4f^3$: the Nd atom gives up three 4f electrons to form Nd^{3+}. The three 4f electrons in Nd split the energy level creating a fine structure giving rise to the side peaks. The total output power in this free-running mode is 20 mW.

If a single 50% coated etalon of 1.0 mm thickness is inserted within the cavity, we obtain the spectrum shown in Figure 1.28. As can be seen, there are only three peaks. The etalon acts as filter. The frequency of the light transmitted by the etalon is given by

$$\nu_m = c/2nL\star\cos(\theta) \qquad (1)$$

where c is the speed of light in vacuum, n is the refractive index of the FP filter, L is the thickness of the FP filter, θ is the angle of orientation, and m is a positive integer. The wavelengths allowed by the filter are 1085.17, 1084.77, and 1084.4 (nm). Figure 1.29 shows the output from the crystal with one coated and one uncoated etalon placed in the cavity. As can be seen from Figure 1.29, only the center peak is transmitted. This is due to the fact that the transmission of the two etalons were a maximum only at 1084.8 nm. The width of this peak was 0.021 nm, and the output power was 11 mW. The output frequency can be changed by tilting the etalon; i.e. by changing the angle in Equation 1. Figure 1.30 shows the output from the crystal with a Lyot filter placed in the cavity. This graph shows the tuning characteristics of the crystal and represents the range of wavelengths over which our dye laser pumped cavity has enough gain to overcome losses. As can be seen from Figure 1.30, the maximum output power was 8 mW at 1084.8 nm. The output could be tuned over approximately a 4 nm region with at least half the maximum output. The lasing wavelength is changed by rotating the Lyot filter. The technique of frequency selection takes advantage of the fact

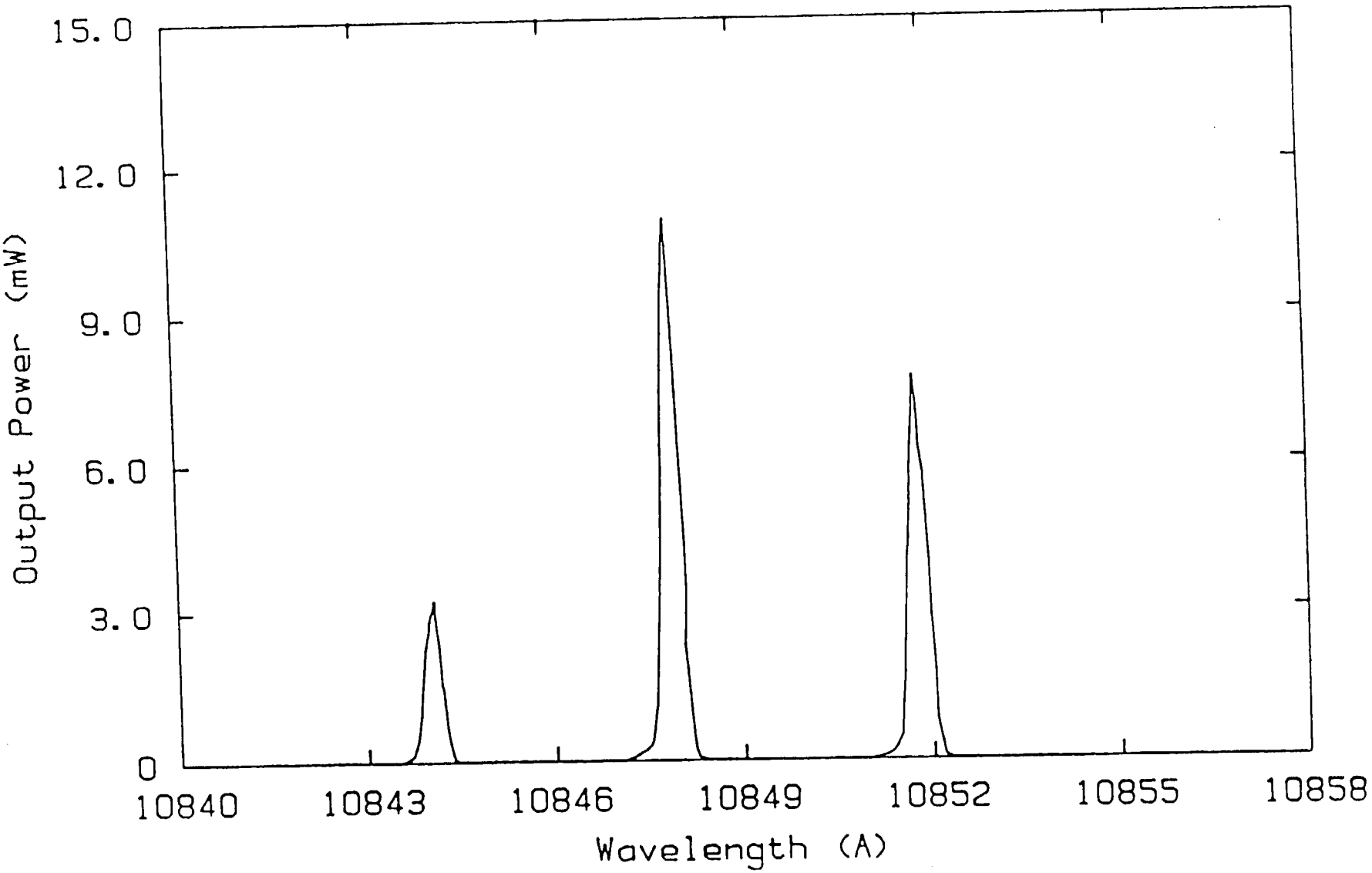

FIGURE 1.28 - Monochromator Scan of Nd:Lithium Niobate Laser with Etalon in Cavity

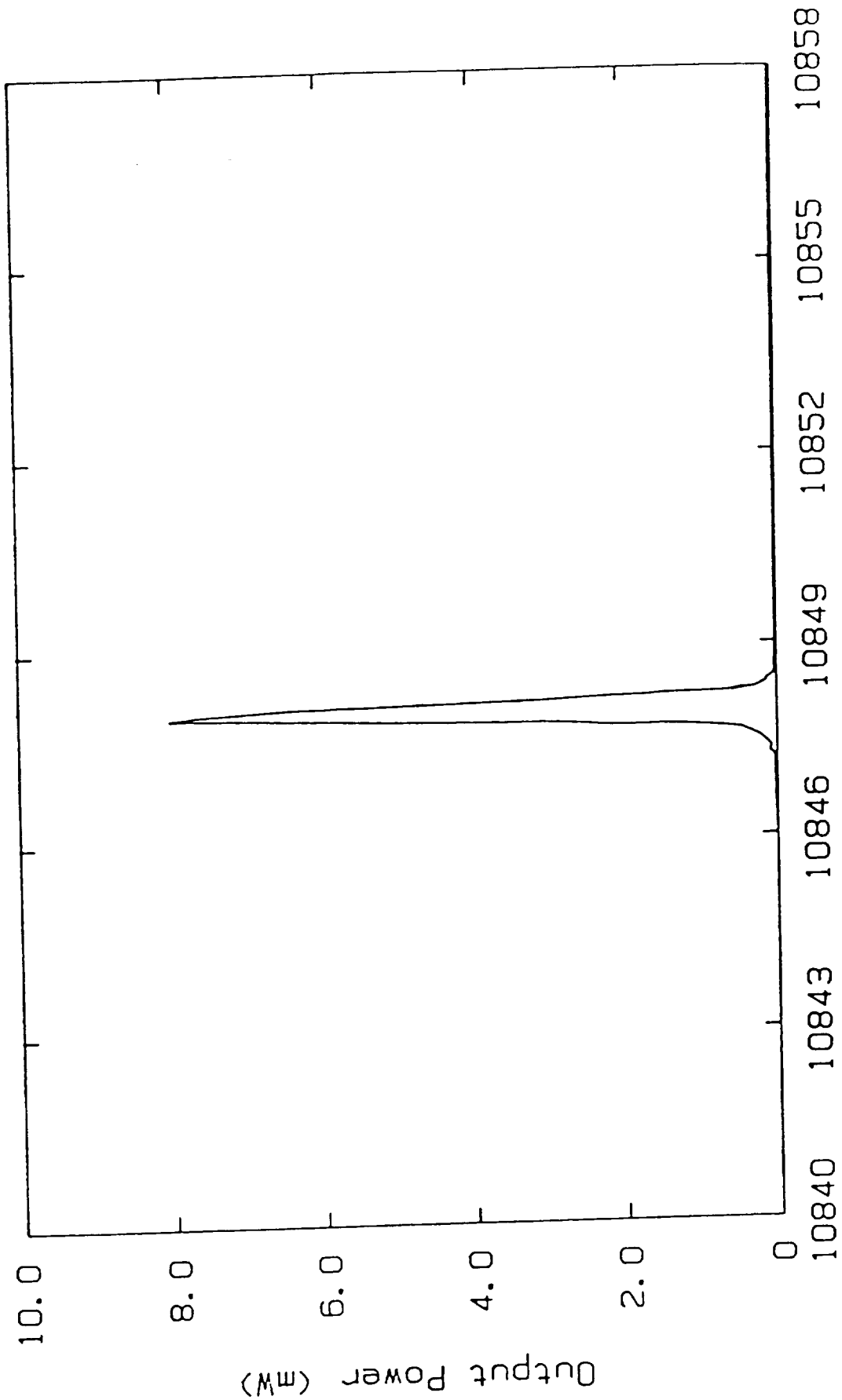

FIGURE 1.29 - Monochromator Scan of Nd:Lithium Niobate Laser with 2 Etalons in the Cavity

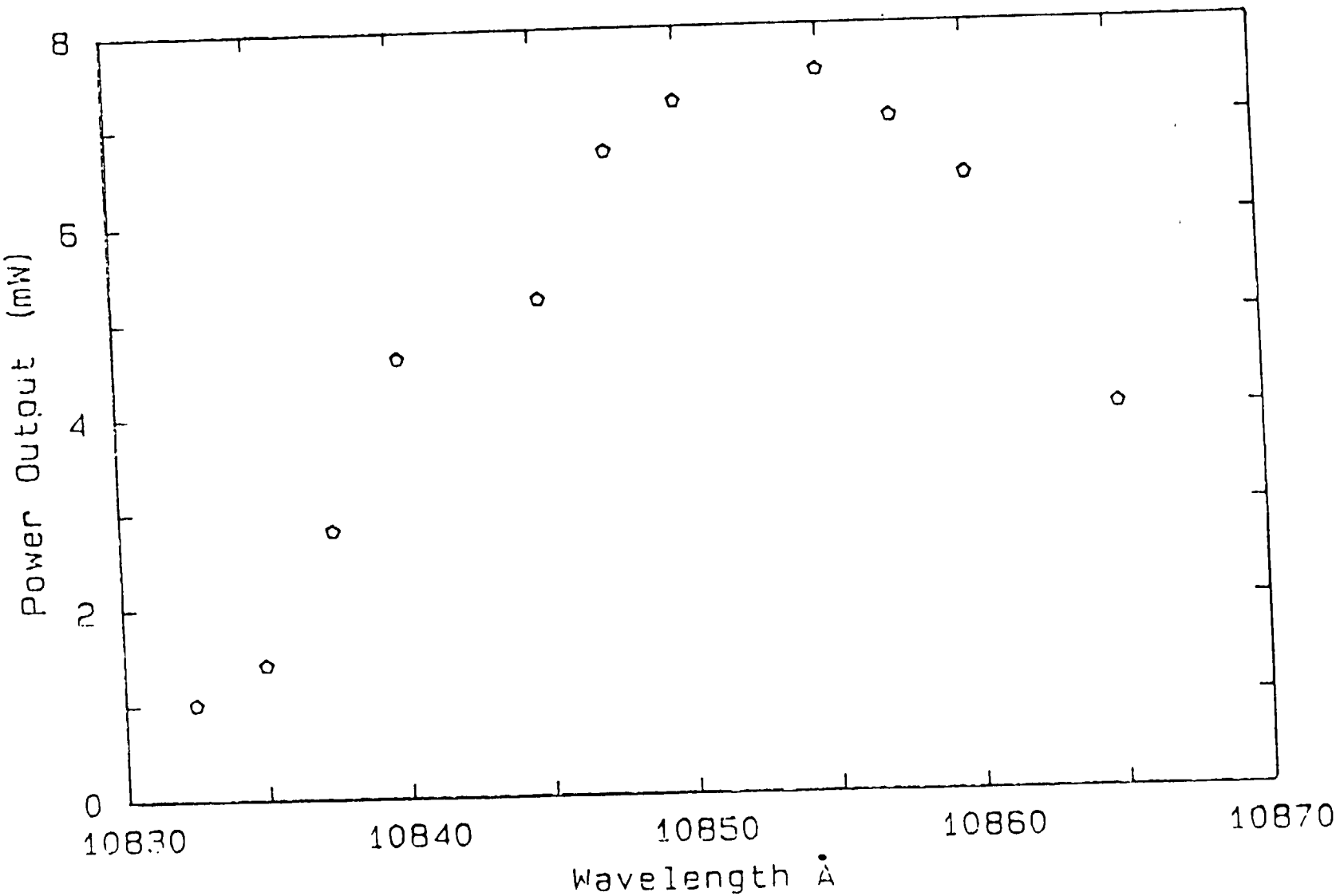

FIGURE 1.30 - Nd:Lithium Niobate Laser Tuning Curve Obtained with Lyot Filter

that a low gain laser can operate only with the polarization that is transverse magnetic (TM) with respect to any intracavity elements oriented at Brewster's angle. A single birefringent plate has the property of transforming the incident TM polarization into some elliptical polarization composed of both TM and TE (transverse electric) linear polarization components. A useful filter must be efficient, and such a filter tuned to the peak of the laser gain curve should cause little or no degradation of the output power. It is also important that the birefringent filter display smooth, continuous tuning as the orientation of the device is gradually altered.

When the laser light is incident on the Lyot filter, it undergoes a phase shift. The light then transverses the whole length of the cavity before again undergoing a subsequent phase shift. The phase shift of the light is given by Equation 2 where δn is the difference in the index of refraction of the ordinary and extraordinary rays in the crystal, i.e. its birefringence. Thus

$$\delta\phi = 2 \star \delta n \star x \star \cos(\theta)/\lambda \qquad (2)$$

where x is the filter thickness and λ is the wavelength. Equation 2 can be solved for λ. This relationship is given in Equation 3.

$$\lambda = 2 \star \delta n \star x \cos(\theta) \star 2 \star \pi/\lambda \qquad (3)$$

where $\delta\phi = 2\pi$ K and K is an integer.

The only wavelength which can pass through the Lyot filter is given by this equation. Thus by adjusting the Lyot filter, the laser output from the $LiNbO_3$ crystal could be tuned over a 4 nm region. Figure 1.30 shows the maximum output power obtained from the tuned $LiNbO_3$ laser as a function of the output power. The positions of the elements within the cavity were adjusted initially for maximum power output and then left unchanged as the pump power was reduced. The threshold under these conditions was 20 mW.

Unfortunately, beyond observing that the $LiNbO_3$ crystal could be efficiently pumped as described in the earlier section, we were unable to make any systematic

measurements on the power output and tuning characteristics. At this point the second harmonic generating crystal in the YAG laser suffered irreversible damage. A replacement crystal was obtained too late to incorporate the results into this thesis.

A Nd-doped $LiNbO_3$ tunable laser excited via its 590 nm absorption band generated by an Ar ion laser-pumped Rh6G dye laser has been developed. The output power was 20 mW when the pump power incident on the Nd:$LiNbO_3$ crystal was 360 mW. The luminescence due to the electronic fine structure of the 4f electrons of Nd was filtered out by an etalon with a 50% reflective coating. The output power was tuned over approximately a 4 nm region with at least half maximum output power.

A primary goal was to obtain useful tunable, laser emission at the 1083 nm transition wavelength of the 2^3S_1 helium atom. The data of Figure 1.30 clearly indicates that one can tune this crystal to the desired wavelength. With the added promise of non-linear phenomena which can be generated with this crystal, we have a unique system for helium optical pumping experiments.

REFERENCES - SECTION 1

1 D. L. Sipes, Appl. Phys. Lett. 47, 74 (1985).

2 Laser Focus, January 1987, p. 6 and D. J. Krebs, McDonnell-Douglas, private communication.

3 R. J. Mears, L. Reckie, S. B. Pook, and D. N. Payne, Electron. Lett. 22, 159 (1986).

4 L. D. Schearer, "Polarization of 2^3S_1 Metastable Helium Atoms by Optical Pumping", in Advances in Quantum Electronics, J. R. Singer, ed. (Columbia University Press, NY, 1969) pp. 239-251.

5 F. D. Colegrove, L. D. Schearer, and G. K. Walters, Phys. Rev. 132, 2561 (1963).

6 C. L. Bohler, L. D. Schearer, M. Leduc, P. J. Nacher, J. Zachorowski, R. G. Milner, R. D. McKeown, and C. E. Woodward, J. Appl. Phys. 63, 2497 (1988).

7 G. A. Massey and J. M. Yarborough, Phys. Lett. 18, 576-579 (1971).

8 L. D. Schearer and Michele Leduc, IEEE J. Quantum Electron. QE-22, 756-758 (1986).

9 D. L. Sipes, Appl. Phys. Lett. 47, 74 (1985).

10 A Cordova-Plaza, et. a. Optics Lett. 13 (1988).

11 D. Searl, B. Fieldman, and R. Burnham, Topical Meeting on Tunable Solid-State Lasers, Technical Digest, pp. 23-25, MC 3-1 (1987).

12 AIRTRON, Inc., Morristown, NJ.

13 M. Bass and M. J. Weber, App. Phys. Lett. 17, 395 (1970).

14 M. J. Weber, M. Bass, and K. Andringa, Appl. Phys. Lett. 15, 324 (1969).

15 D. R. Scrifes, W. Streifer, G. L. Harnagel, D. F. Welch, and J. Berger, Topical Meeting on Tunable Solid-State Lasers, Technical Digest, pp. 11-14, MB2-1 (1987).

16 Laird D. Schearer, M. Leduc, J. Zachorowski, "CW Laser Oscillations and Tuning Characteristics of Neodymium-Doped Lithium Niobate Crystals", IEEE J. Quant. Elect. QE-23, 11 (1987).

17 T. Y. Fan, A. Cordona-Plaza, M. J. F. Digonnet, R. L. Byer, and H. J. Shaw, Opt. Soc. Am. 3, 140 (1986).

18 Amado Cordova-Plaza, Michel J. F. Digonnet, and Herbert J. Shaw, "Miniature CW and Active Internally Q-Switched Nd:MgO:$LiNbO_3$ Lasers", IEEE J. Quant. Ele. QE-23, 2 (1987).

19 N. F. Evlanova, A. S. Kovalev, L. S. Korienko, A. M. Prokhorov, and L. N. Rashovich, "Stimulated Emission of $LiNbO_3$ Crystals with Neodymium Impurity", JETP Lett. 5, 29 (1967).

20 G. Zhong, J. Jiah, and Z. Wa, in Proceedings of International Quantum Electronics Conference (Institute of Electrical and Electronic Engineers, New York (1980) p. 631.

21 A. Cordova-Plaza, T. Y. Fan, M. J. F. Digonnet, R. L. Byer and H. J. Shaw, "Nd:MgO:$LiNbO_3$ Continuous-Wave Laser Pumped by a Laser Diode", J. Opt. Soc. Am. 13, 209 (1988).

22 L. F. Johnson and A. A. Ballman, "Coherent Emission from Rare Earth Ions in Electro-optic Crystals", J. Appl. Phys. 40, 279 (1969).

23 G.-G. Zhang, J. Jian, and Z.-K. Wu, in Proc. 11th Int. Quantum Electron. Conf., p. 631, IEEE Cat. 80, CH 1561-0 (1980).

24 R. Gerson, J. F. Kirchoff, L. E. Halliburton, and D. A. Bryan, "Photoconductivity Parameters in Lithium Niobate", J. Appl. Phys. 60, 3553 (1986).

25 D. B. Preuss and J. L. Gole, "Three-Stage Birefringent Filter Tuning Smoothly Over the Visible Region: Theoretical Treatment and Experimental Design", Appl. Opt. 19, 702 (1980).

2.0 LASER PUMPING APPARATUS AND EXPERIMENT FOR HELIUM OPTICAL PUMPING DEMONSTRATION

2.1 EXPERIMENT DESIGN

We wish to observe Hanle signals and n = o, p = 1 parametric resonance of 2^3S_1 metastable helium atoms in a discharge cell by optically pumping the helium atoms with a tunable Nd:LNA laser. These resonances can be used to construct a sensitive magnetometer such as the VHM for the measurement of very small magnetic fields. Since magnetometer sensitivity is proportional to the slope of the parametric resonance signal (signal amplitude divided by linewidth), the relative sensitivity could be determined by comparing the slopes for single line laser pumping with similar quantities obtained from conventional helium lamp pumping. We wished to establish the potential for developing ultra-sensitive resonance magnetometers using single line laser pumping and demonstrate for the first time laser pumping of a magnetometer sensor. The results of the laser pumping experiments described in Sections 2 and 3 were published in J. Appl. Phys. 64 (12), 6615 (1988) which is included as Appendix 1.

Laser pumping could result in a new generation of optically pumped helium magnetometers which have been used since the early 1960s to measure interplanetary, planetary, and cometary magnetic fields.[1,2,3] These existing instruments use 1083 nm radiation from an rf electrodeless discharge helium lamp to optically pump a sample of 2^3S metastable helium atoms. The pumping radiation consists of the three spectral lines D_0, D_1, and D_2 around 1083 nm corresponding to the 2^3S-$2^3P_{0,1,2}$ transitions. The pumping beam both optically polarizes the sample and monitors the ensemble polarization.[4]

A rate equation analysis of the optical pumping process predicts the inefficiencies resulting when the ensemble is pumped by the natural output from a helium discharge lamp. The optical pumping signal, defined as the change in the transmitted light that occurs when the sample goes from the pumped to the unpumped condition, consists of the contributions from each of the three spectral components present in the

lamp, D_0, D_1, and D_2. The D_1 and D_2 components produce signals of opposite polarity and nearly equal intensity so that their contribution to the total signal is negligible.[5] Thus, the fractional change in the transmitted light signal as the sample is pumped by a discharge lamps is typically 0.1%.

An obvious solution is to use a tunable emission line source to avoid this cancellation. However, until recently there were no lasers available which matched the helium absorption lines at 1083 nm and could be used to test this solution. In this experiment we have used Nd-doped, $La_{1-x}Nd_xMgAl_{11}O_{19}$ crystals in a laboratory laser pumped by a high power, cw diode laser to produce tunable emission at 1083 nm.[6] We were able to evaluate single line optical pumping for use in high sensitivity helium magnetometers. Zero-field parametric resonance techniques[7] were used to observe single line laser pumping and compare the resonance signals with those obtained using conventional helium lamps. The initial results obtained from laser pumping in a helium magnetometer sensor using the Nd:LNA laser pumped with a high power diode laser are described in Section 3.

It is more convenient to use parametric resonances rather than paramagnetic resonances to compare resonance signals generated by optical pumping since no rf fields perturb the optically pumped sample.[8] It does, however, require that the experiment be conducted in a region of low magnetic fields. The low field region found inside a mu-metal room at the Magnetic Test Facility at the Jet Propulsion Laboratory was used for our experiments. The shield eliminated the major part of the earth's field and residual fields can be controlled or eliminated using Helmholtz coils within the shield.

2.2 OPTICAL PUMPING APPARATUS

The optical pumping apparatus is shown in Figure 2.1 and has been described in detail in Ref. 8. The amplitude of the resonance signal for the optically pumped metastable level was measured using the Hanle effect. With the optical pumping apparatus located in zero field inside the JPL Magnetic Shield a field H_0 is applied

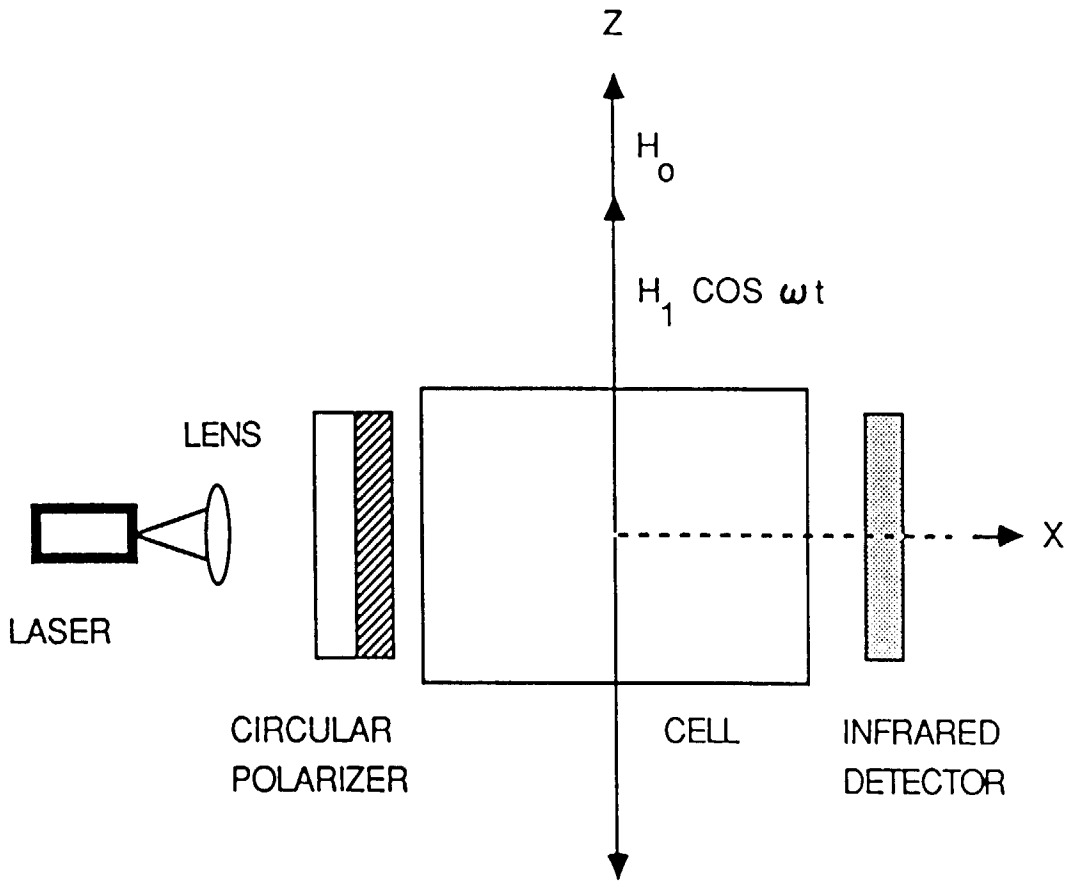

FIGURE 2.1 - Schematic Representation of the Helium Magnetometer. The Cell Containing the Helium Gas is Placed in a Nominally Zero Magnetic Field. H_0 and $H_1 \cos \omega t$ are Fixed and Oscillating Magnetic Bias Fields Produced by Helmholtz Coils.

perpendicular to the beam direction. The signal along the pumping beam direction is proportional to M_x where

$$M_X = \frac{Mo}{1+(\omega\tau)^2} \tag{1}$$

and M_O is the optically induced magnetic moment in the gas, τ is the decay time of M_X and ω is the Larmor precession frequency.

Since our primary interest in the tunable solid-state laser is as a radiation source for single line optical pumping, a direct comparison of laser pumped resonance signals and resonance signals produced by radiation from a typical rf electrodeless helium lamp of the type commonly used in helium magnetometers is desirable. The key parameter is the slope of the resonance curve at the inflection points which is proportional to the resonance amplitude divided by the linewidth. This quantity has been shown[8] to be proportional to the slope of the dispersion shaped curve at zero field for the n=0, p=1 parametric resonance which is observed on the transmitted light beam as a signal proportional to

$$M_X = M_O J_O\left[\frac{\gamma H1}{\omega}\right] Jp\left[\frac{\gamma H1}{\omega}\right] \frac{\omega_o\tau}{1+(\omega_o\tau)^2} \sin p\,\omega t \tag{2}$$

The term H_1 is the parametric drive field which in the present experiment is a 30 KHz field applied perpendicular to the direction of the optical pumping beam. The resonance signal described by Eq. 2 is monitored by the infrared detector with its output directed to a lock-in amplifier tuned to 30 KHz. The lock-in output is displayed on an X-Y recorder. We have demonstrated in an earlier paper that the slope for the dispersion signal is proportional to the minimum detectable signal for a magnetometer operating on this resonance.[7,8] Maximum signal size can be obtained when the amplitude of the 30 KHz drive field is adjusted to the optimum value as determined by the Bessel function solutions to the phenomenological Block type equation describing the n=0, p=1 parametric resonance (Eq. 2).

2.3 TUNABLE SOLID-STATE LNA LASER

The essential features of a diode-pumped LNA laser shown in Figure 2.2 are described in Ref. 9. The LNA crystal is a cylinder, 5 mm in diameter and 5 to 10 mm in length, grown in LETI (Grenoble). The rod axis coincides with the crystalline c-axis. The two polished parallel faces are antireflection coated for $\simeq 1.06$ m. It is excited longitudinally by CW diode arrays focused on one end of the crystal. It uses two diode arrays; the two beams are superimposed through a polarizing beam splitter. Each diode array (model 2420 H1 from Spectra diode Lab) delivers 200 mW at a current of 500 mA. One diode emits at 797 nm, the other one at 801 nm, both wavelengths within the absorption band of LNA. The light emitted by the diode is collimated by corrected lenses of large aperture (Melles Griot 06 GLC 002) and focused on the crystal through a lens of focal length 18 mm. The LNA laser cavity consists of a plane mirror M_1 (2 mm thick, with high reflectivity for the laser radiation and high transmission for the pump radiation) and a plane output mirror M_2 of low transmission T (T ranging from 1 to 4%); the cavity includes an AR coated lens L of focal length 25 mm. The total cavity length is approximately 13 cm. The transverse waist of the gaussian beam in this cavity is of the order of 100 μm, approximately matching the pump spot size (of the order of 150 μm).

The results are shown in Figure 2.3. Without selective elements in the cavity the LNA laser emits on the main fluorescence peak at 1054 nm. The output power is plotted as function of the pump power on the crystal, which absorbs 85% of the incident light. The two curves refer to different values of the output coupler transmission T. For T = 1% the threshold is 100 mW and the slope efficiency 7.3% (emitted power/absorbed power); for T = 4% the threshold increases to 180 mW and the slope efficiency to 9.5%. These thresholds are substantially higher than those observed by replacing the LNA crystal by a YAG crystal in the cavity. Such a difference can be attributed to the losses in the crystal, which have been measured to be of the order of 5%.

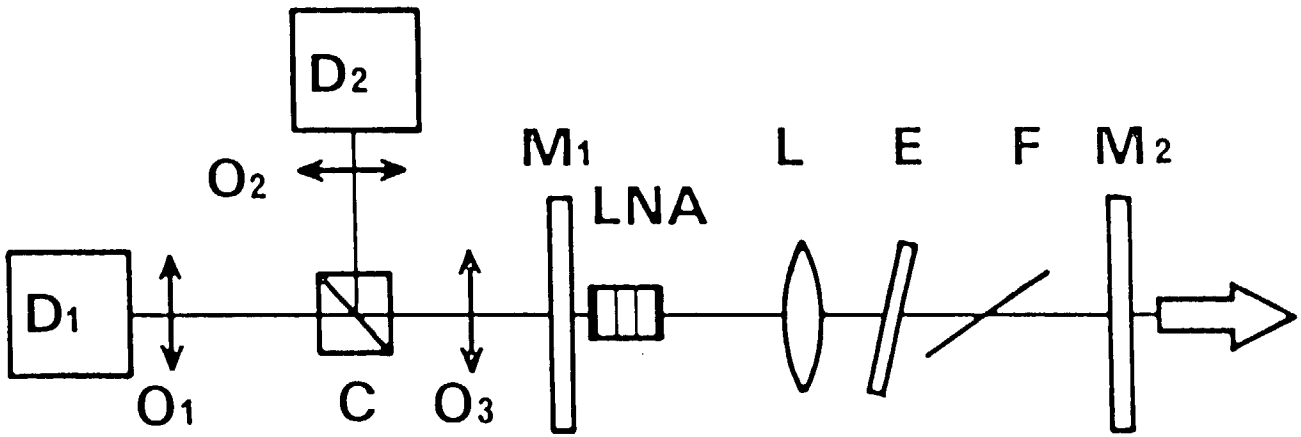

FIGURE 2.2 - The Cavity Used for the LNA Laser Pumped by Two Semiconductor Laser Arrays.
D_1 and D_2 are the Semiconductor Laser Arrays.
O_1, O_2, and O_3 are the Focusing Optics.
O is a Polarizing Beam-Splitter.
M_1 is a Dichroic Plane Mirror.
M_2 is a Plane Output Mirror of Transmission T.
L is a Lens Antireflection Coated for 1.06 μm.
For Tuning the Wavelength, Selective Elements are Added: A Single Plate Birefringent Lyot Filter F and a Solid Etalon E.

FIGURE 2.3 - Output Power of the Laser as a Function of the Pump Power. The Two Lines are for Different Transmission Values T of the Output Mirror (O : T = 1%, Δ : T = 4%).

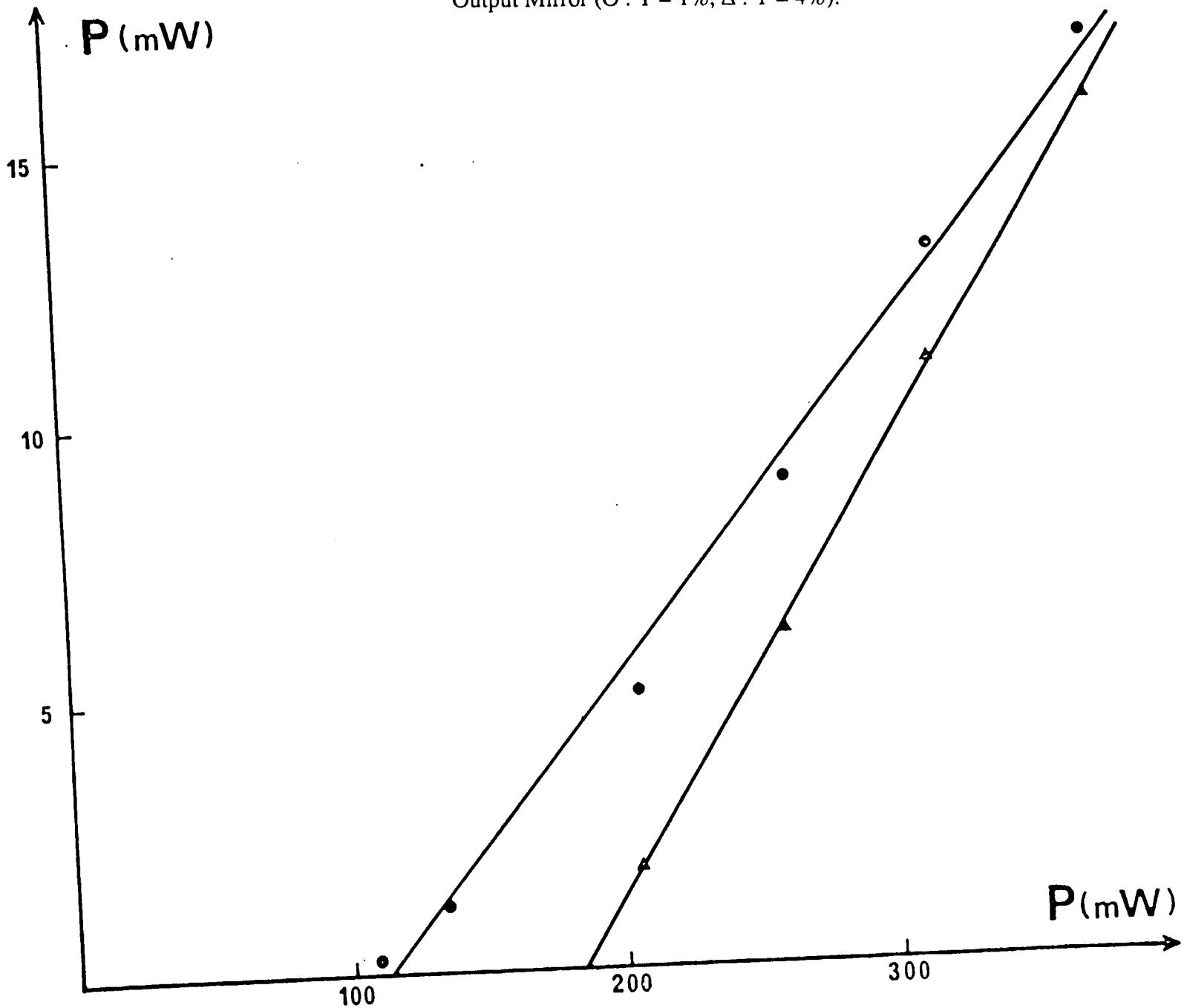

Tuning the frequency of the LNA laser was achieved by inserting a single plate birefringent Lyot filter L (a 1 mm thick quartz plate) at the Brewster angle in the cavity. Oscillation on the main peak at 1054 nm could be suppressed, and tuning around 1082 nm was then possible. Fine tuning was accomplished with a thin, solid etalon E (a 1 mm non-coated plate of fused silica). The observed laser bands are shown in Figure 2.4. The helium transition at 1083 nm can easily be reached; the power of the LNA laser obtained at this wavelength is typically 3 mW. The laser beam is linearly polarized according to the Lyot filter orientation.

The LNA laser set-up shown in Figure 2.1 was used to observe the fluorescence of ^4He metastable atoms. The laser beam was passed through a spherical glass cell (4 cm in diameter) filled at 1 torr with ^4He, in which a weak RF discharge was sustained. When the LNA laser frequency was scanned through the 2^3S_1 - $2^3P_{0,1,2}$ transition by tilting etalon E, the absorption of the laser beam was monitored; the D_0 line was clearly resolved from the group of the D_1 and D_2 lines; only partial resolution of the D_1 and D_1 components was possible, due to the Doppler width of the atomic absorption profile at room temperature (2Ghz). These results indicate that the LNA laser bandwidth is on the order of or smaller than 2Ghz. The largest absorption rate was observed with a laser tuned on the D_2 line and was of the order of 60% at the moderate discharge levels used here.

Several improvements of the LNA diode-pumped laser we made for this experiment. These changes resulted in the laser cavity shown in Figure 2.5. Mirror M_1 was eliminated since the dichroic coating was deposited directly on one surface of the LNA crystal itself. This should improve the laser efficiency because the cavity beam waist can be better. The pair of diode lasers was replaced by a single 1W, GaAlAs diode, model 304W from SONY Corp. A special coating was applied to the output coupler which obviated the need for the Lyot filter. A 50%, 0.25 mm thick etalon was used for wavelength tuning. With the diode providing a pump power of about 550 mW (1.6 V,

FIGURE 2.4 - Tuning Curves of the LNA Laser Obtained with a 1 Plate Lyot Filter and a Solid Etalon in the Cavity. The Pump Power is About 360 mW on the Crystal.

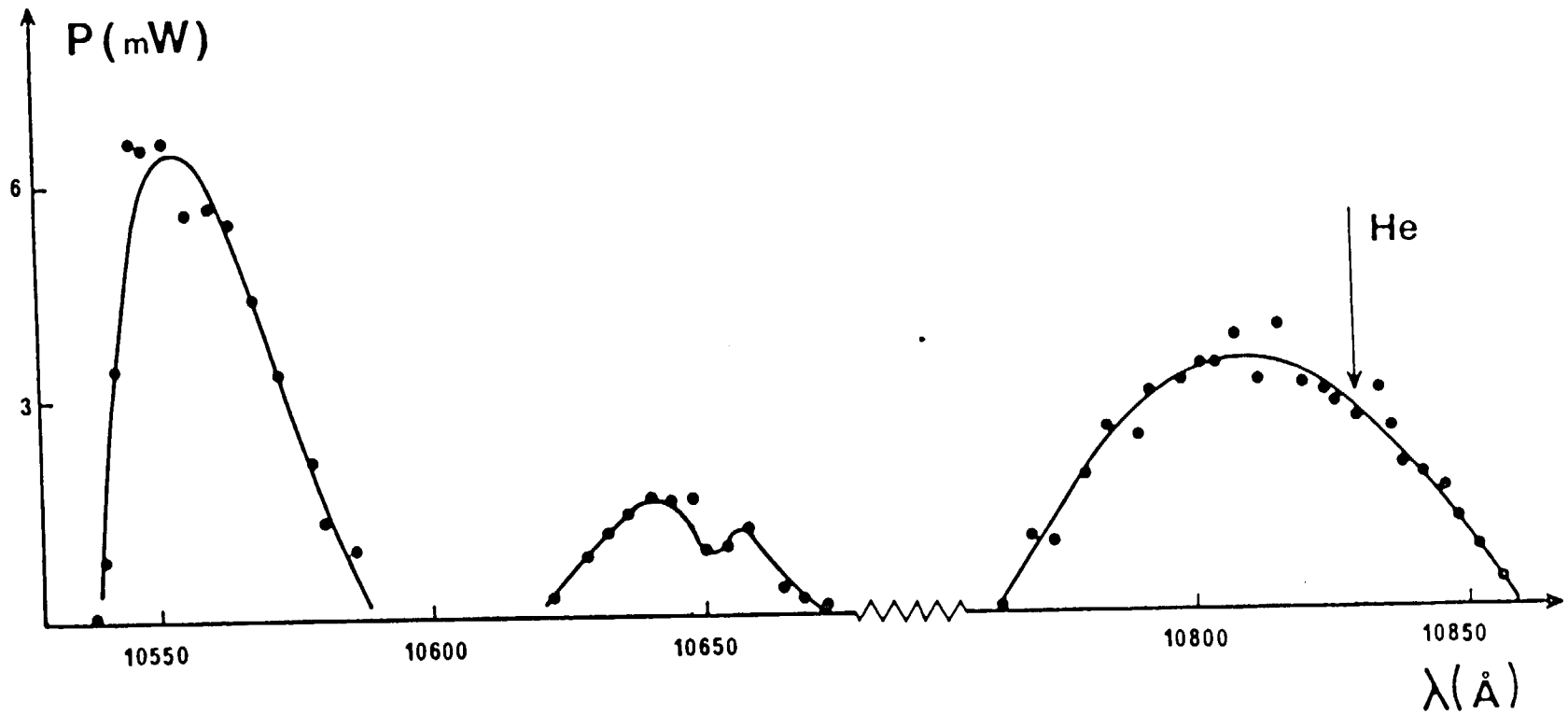

FIGURE 2.5 - Block Diagram of Improved LNA Laser Use for Parametric Resonance Experiments.

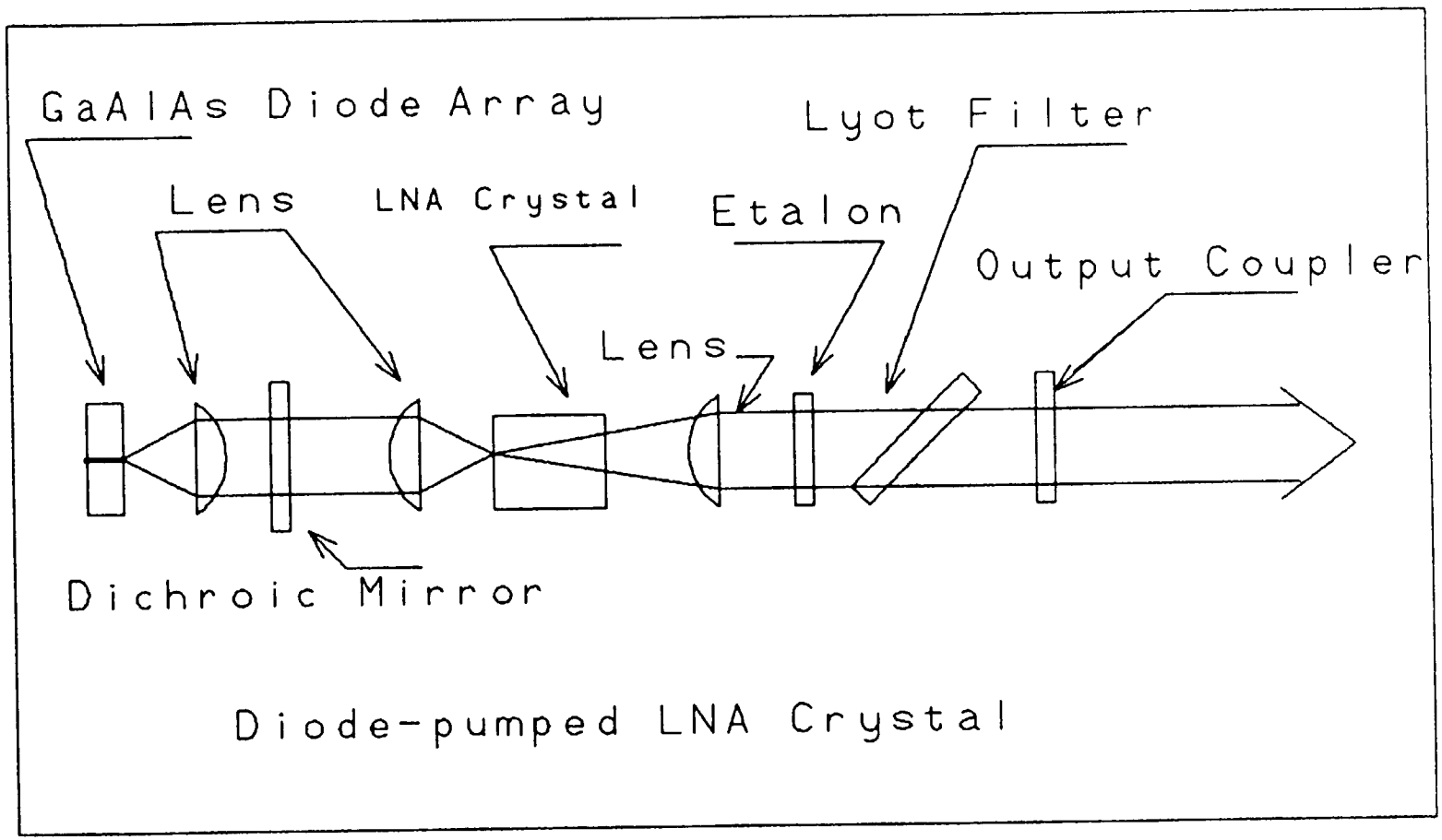

890 mA) the LNA laser output at 1083 nm is typically several mW. The scattered light from a helium cell registered as the laser wavelength is tuned through the resonance lines is shown in Figure 2.6. The resolution of the D_1 and D_2 lines shown suggests that the laser linewidth is less than the Doppler width (1.8 GHz).

The laser is easily tuned to each of the three desired transitions and is stable for adequate periods of time without operator intervention. With the SONY diode operating at maximum output, the laser power at the helium transition exceeded 10 mW. For the experiments described below, the diode was operated with a power input of approximately 1.0 W. The laser was placed on an optical bench outside the magnetic shield and the laser beam was directed by mirrors through a hole in the shield and along the optical pumping axis of a helium cell placed at the center of the magnetic shield.

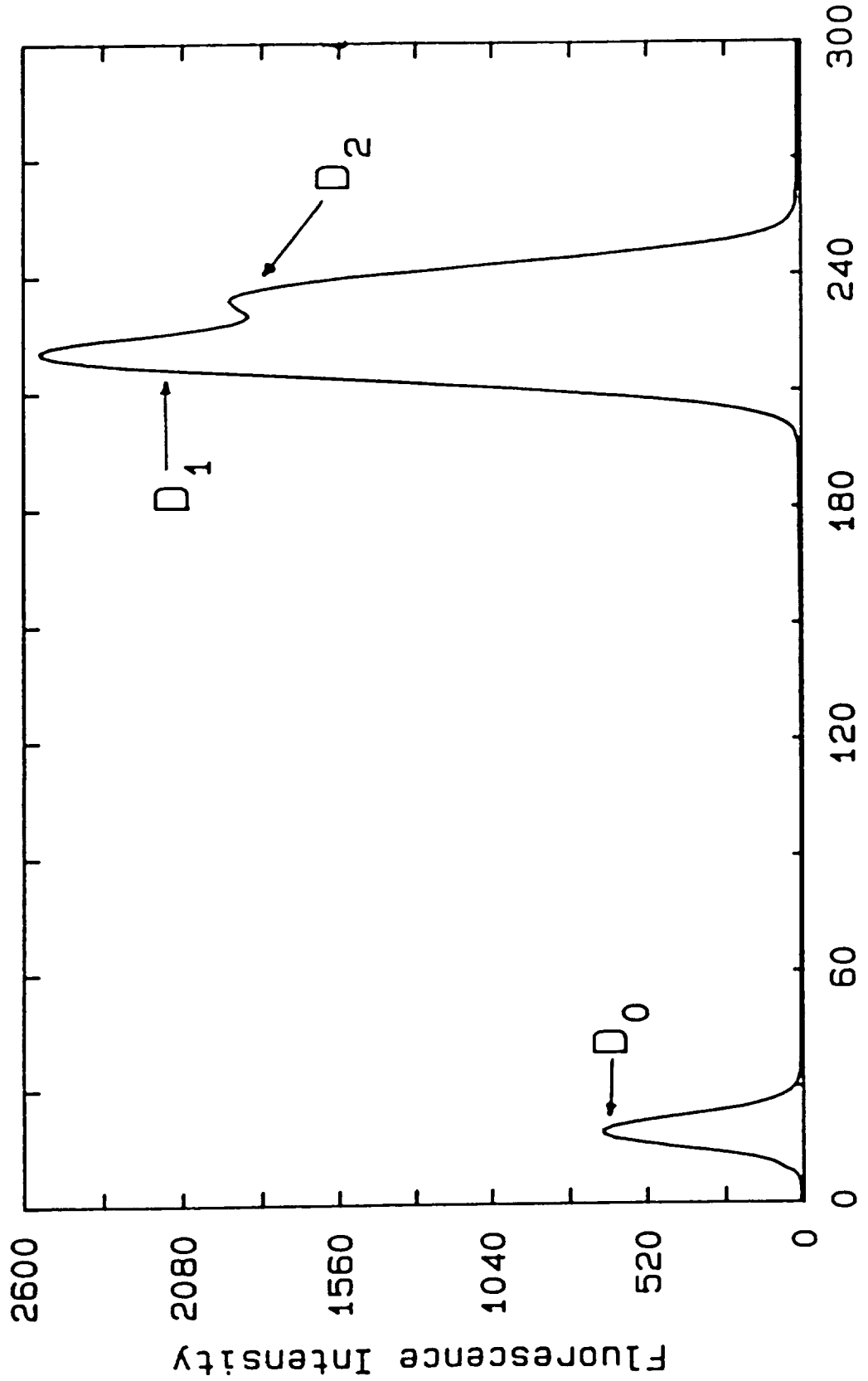

FIGURE 2.6 - Shown is the Fluorescence Spectrum from the He^4 Metastable Atoms as the Laser is Scanned Through the 23S-23P Transitions. The D_0 to D_1 Separation is About 0.1 nm. The Laser Frequency is Changed by Tilt-Tuning the Etalon.

REFERENCES - SECTION 2

1 R. E. Slocum and F. N. Reilly, "Low Field Helium Magnetometer for Space Applications", IEEE Trans. on Nuclear Science Vol. NS-10, 165 (1963).

2 B. V. Conner, "Space Magnetics: The Mariner V Magnetometer Experiment", IEEE Trans. of Magnetics Vol. MAG-4, 391 (1968).

3 A. M. A. Frandsen, B. V. Conner, J. Van Amersfoort, and E. J. Smith, "The ISEE-C Vector Helium Magnetometer", Trans. Geo. Electronics Vol. GE-16, 195 (1978).

4 L. D. Schearer, Advances in Quantum Electronics, ed. J. R. Singer (Columbia University Press, 1961), pp. 239-251.

5 L. D. Schearer, Phys. Rev. 160, 76 (1967).

6 L. D. Schearer, M. Leduc, D. Vivien, A. M. Lejus, and J. Thery, IEEE J. Quant. Electr. QE22, 713 (1986).

7 R. E. Slocum, "Zero-Field Level-Crossing Resonances in Optically Pumped 23S1 He4", Phys. Rev. Letters Vol. 29, 1642 (1972).

8 R. E. Slocum and B. I. Marton, "Measurement of Weak Magnetic Fields Using Zero-Field Parametric Resonance in Optically Pumped He4", IEEE Trans. on Mag., Vol. MAG-9, 221 (1973).

9 J. Hamel, A. Cassimi, H. Abu-Safia, M. Leduc, and L. D. Schearer, Optics Comm. 63, 114 (1987).

3.0 LASER PUMPING EXPERIMENTS

3.1 EXPERIMENTAL PROCEDURES

We were able to observe both the Hanle signals and the n=o, p=1 parametric resonance by monitoring the pumping radiation passing through the cell as described in Section 2.0. Distinct resonance curves were observed for each of the three lines D_0, D_1, and D_2 even though the D_1 and D_2 absorption line is barely resolved spectroscopically. For comparison of the laser curves with the resonance curves produced by a standard rf electrodeless discharge helium lamp used in space magnetometers, the sample of helium atoms in the standard helium cell was further restricted to a column 42 mm long and 16 mm in diameter. The sample length was set by the cell length and the sample diameter was set by the diameter of the infrared detector.

When the pumping light intensity increases, the resonance line is slightly broadened. It is therefore important to measure not only the amplitude of the resonance of the parametric resonance signal but also the slope at zero field which is effectively the resonance line amplitude divided by the linewidth.

3.2 TEST RESULTS

Single Line Pumping Resonance Signal Amplitude

The amplitude of the resonance signal for the optically pumped metastable level was measured using the Hanle effect. With the optical pumping apparatus located in zero field inside the JPL Magnetic Shield, a field H_0 was applied perpendicular to the beam direction as shown in Figure 2.1. The oscillating field at 400 Hz has a period greater than the relaxation time of the optically pumped helium. Maximum amplitude must be greater than the half width of the resonance curve which is 150 nT. As the field sweeps through zero field, a signal is produced at 800 Hz which is proportional to the amplitude of the resonance curve. The optical resonance signal was detected by monitoring both the intensity of the pumping beam transmitted through the cell and by

monitoring light scattered from the absorption cell in a direction parallel to the direction of the applied magnetic field.

The resonance signal was examined for each of the three helium lines generated by 2P-2S transition by etalon tuning the laser through lines at 1082.908 nm [D_0], 1083.025 nm [D_1], and 1083.034 nm [D_2]. Lines D_1 and D_2 are barely resolved in the absorption cell, however, two separate resonance signals clearly separated by a null were observed as shown in Figure 2.6. The laser linewidth is estimated to be less than 100 MHz. A typical resonance curve is shown in Figure 3.1 for monitoring of light through the cell. The resonance observed by monitoring scattered light is shown in Figure 3.2.

For a laser power level of 1.39 mW the relative amplitudes of the Hanle signal measured in the transmission mode are:

D_0---0.71

D_1---1.00

D_2---0.16

The same resonance was observed by monitoring resonance radiation scattered from the cell normal to the pumping beam direction along the direction of the sweep field. The resonance signal amplitudes have the following ratios:

D_0---0.41

D_1---1.00

D_2---0.06

The D_1 line is clearly the choice for producing optical pumping signals. In this initial evaluation the D_1 signal for scattered light detection was a factor of 2.3 times larger than the signal for transmitted light detection.

Relative Resonance Slope for Magnetic Field Measurements

Using the parametric resonance method with a 30 KHz drive field swept about zero field, the slope for a helium lamp pumped signal was compared with the slope for

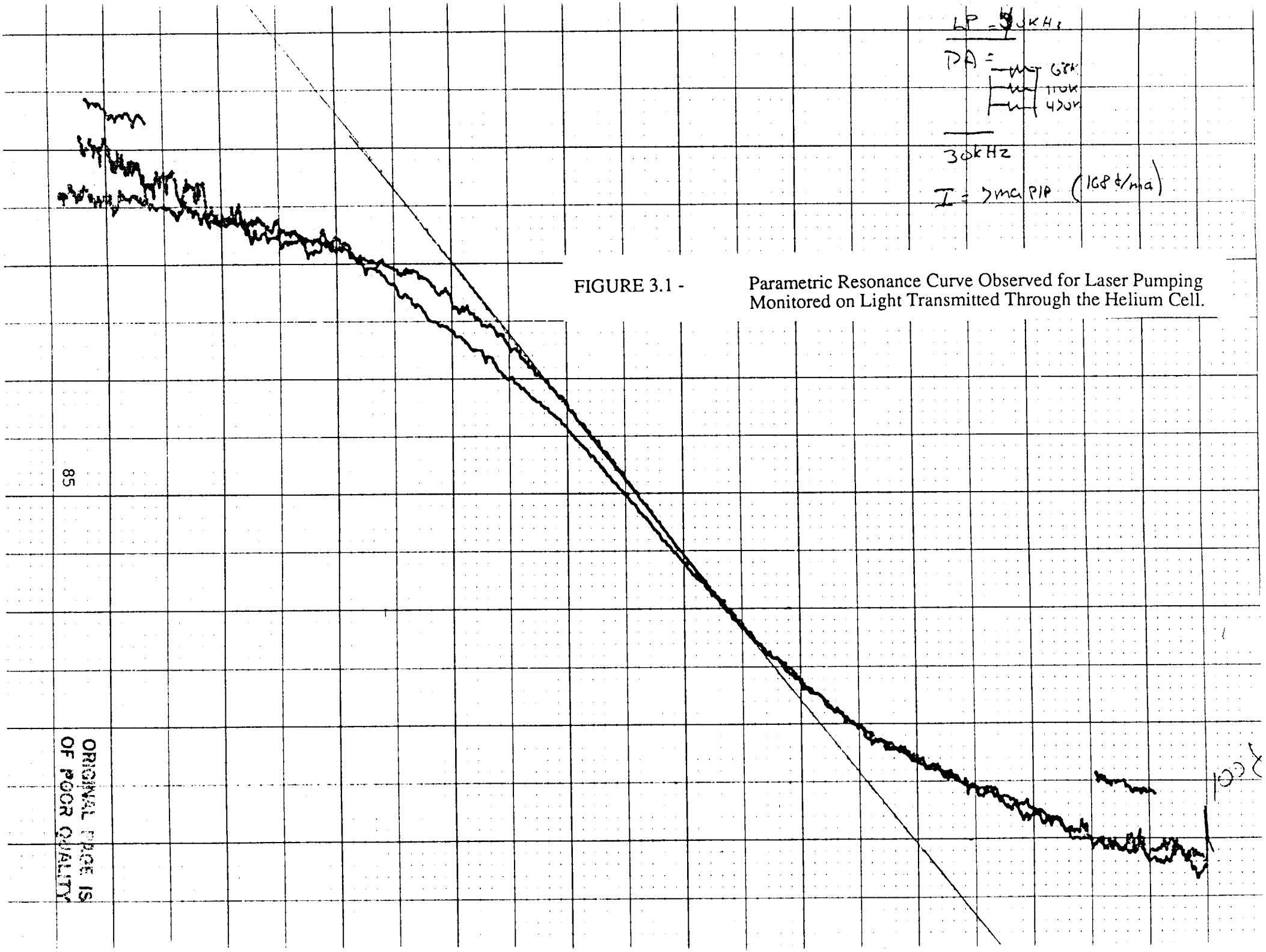

FIGURE 3.1 - Parametric Resonance Curve Observed for Laser Pumping Monitored on Light Transmitted Through the Helium Cell.

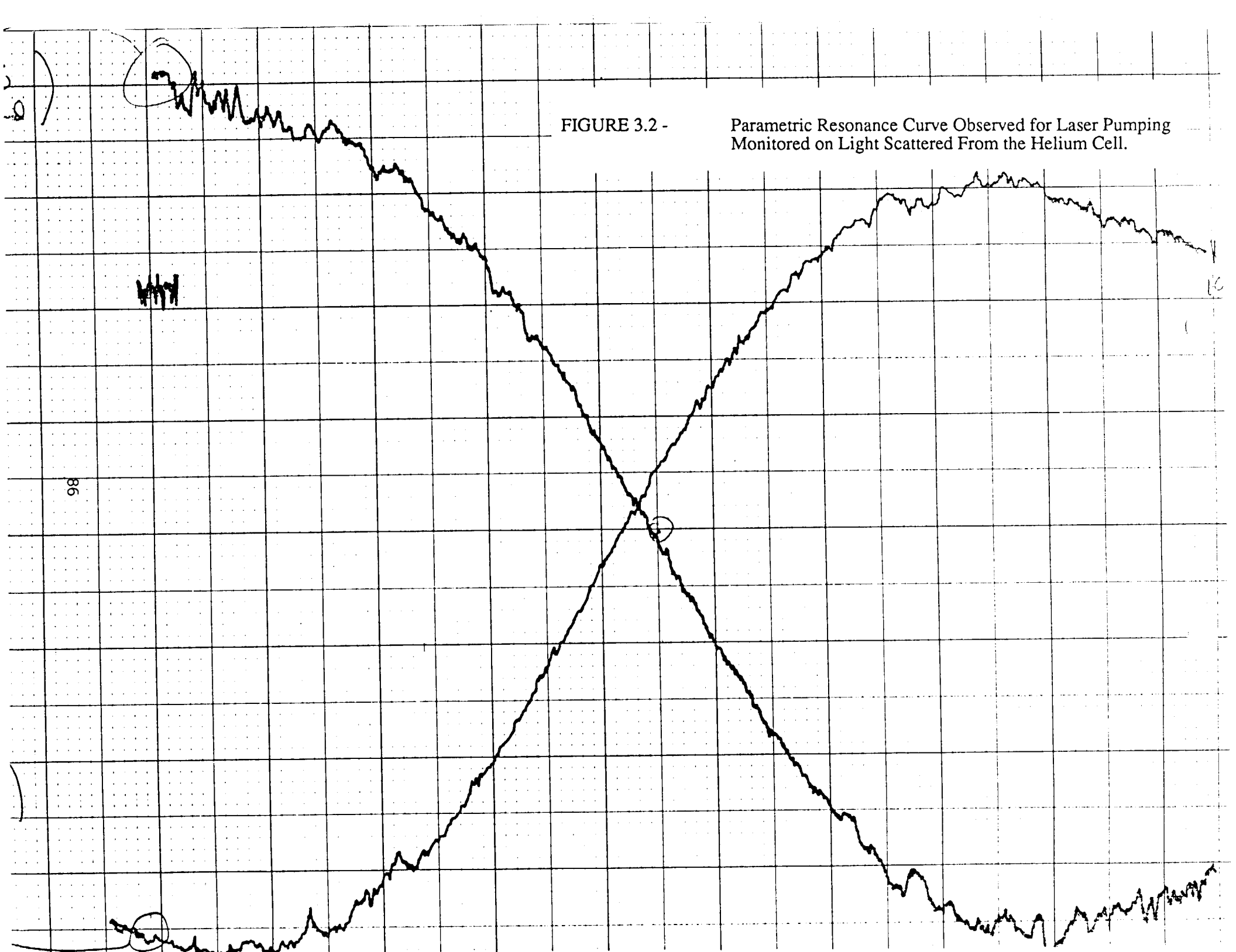

FIGURE 3.2 - Parametric Resonance Curve Observed for Laser Pumping Monitored on Light Scattered From the Helium Cell.

the D_1 laser line which generated the largest resonance signal. The two curves are shown in Figure 3.3. The comparison was made for a volume fo the cell defined by the cell length [42 mm] and the diameter of the large-area silicon infrared detector [16 mm] which is approximately 15% of the 32 mm diameter cell's volume. The laser pumped resonance exhibited an observable light broadening; however the signal amplitude resulted in a slope increase of 45.

3.3 CONCLUSIONS

We were able to experimentally demonstrate single line pumping in the 2^3S level of helium 4 and obtain resonance signals more than an order of magnitude greater in strength than those produced by conventional helium discharge lamps. As the diode laser pumped Nd:LNA laser was tuned through the D_0, D_1, and D_2 transitions three distinct resonance signals were produced.

Optical broadening of the resonance line as well as the resonance signal amplitude must be taken into account in predicting potential improvements in magnetometers using laser pumping. A direct comparison of the slope of lamp pumped signals and laser pumped D_1 signals was made using the n=1, p=1 parametric resonance. Under otherwise identical conditions we found the slope of the D_1 laser signal to be 45 times greater than the lamp pumped signal.

No attempt was made to minimize the noise contributed by the solid state laser. It can be concluded, however, that for the case of laser noise which is equal to that of current rf discharge helium lamps, laser pumped magnetometers can be built which have sensitivities at least two orders of magnitude greater than the current instruments. Since the present day helium space magnetometers have a sensitivity of 0.01 nT, our current effort will proceed toward achieving sensitivities of 0.1 pT.

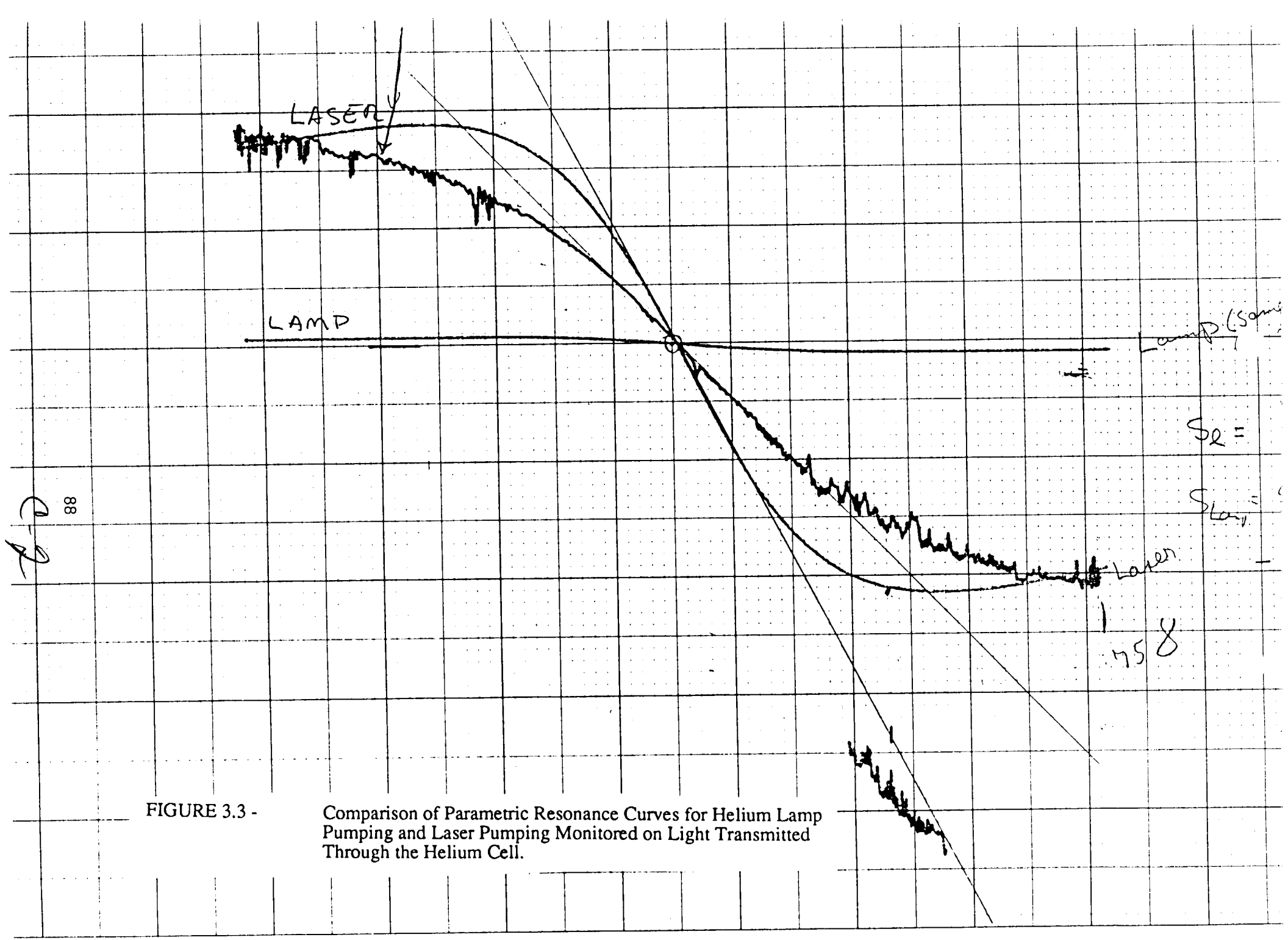

FIGURE 3.3 - Comparison of Parametric Resonance Curves for Helium Lamp Pumping and Laser Pumping Monitored on Light Transmitted Through the Helium Cell.

4.0 TUNABLE SOLID-STATE LASER (1083 nm LNA) FOR LASER PUMPED MAGNETOMETER

4.1 INTRODUCTION

We describe in Section 4.0 the tunable LNA used for the scalar magnetometer experiments. This LNA laser will be delivered to JPL at the conclusion of The Phase II Report. The neodynium-doped LNA laser crystal ($La_{.85}Nd_{.15}MgAl_{11}O_{19}$) is pumped longitudinally with a laser diode array emitting 800 nm radiation. The LNA has an absorption at 800 nm and fluoresces at 1054 nm and 1083 nm. The crystal is placed in a laser cavity that reflects primarily at 1083 nm out one end of the cavity and transmits at 1054 nm. This forces the crystal to lase at 1083 nm. Placing an Etalon in the cavity permits selecting the He D_0 or D_{12} lines. The D_0 absorption line is well resolved, but the D_{12} lines are so close that we achieve only partial resolution . The D_0 and D_{12} radiation has sufficient power to permit visual observation (with a Snooper Scope) of fluorescence in an excited He cell. A helium magnetometer has operated using the D_0 or D_{12} radiation.

4.2 DESCRIPTION

4.2.1 OPTICAL COMPONENTS

Laser Diode (LD) - The optical components are shown in a block diagram form in Figure 4.1. The laser diode purchased from Spectra Diode Lab is capable of delivering 0.500 watts of 797 nm radiation when driven at 930 mA. Its temperature could be selected and maintained between 5°C and 30°C. The laser diode consists of an array of lasers in a stripe 100 x 1 micron. The radiation is emitted in a highly divergent beam.

Focusing Lens (L) - The lens L has high light gathering power, is of short focal length and converts diverging into a parallel beam.

Anamorphic Prism (AP) - The anamorphic prism compresses the elongated cross section of the beam into a beam of a rectangular cross section of 0.5 by 0.9 cm.

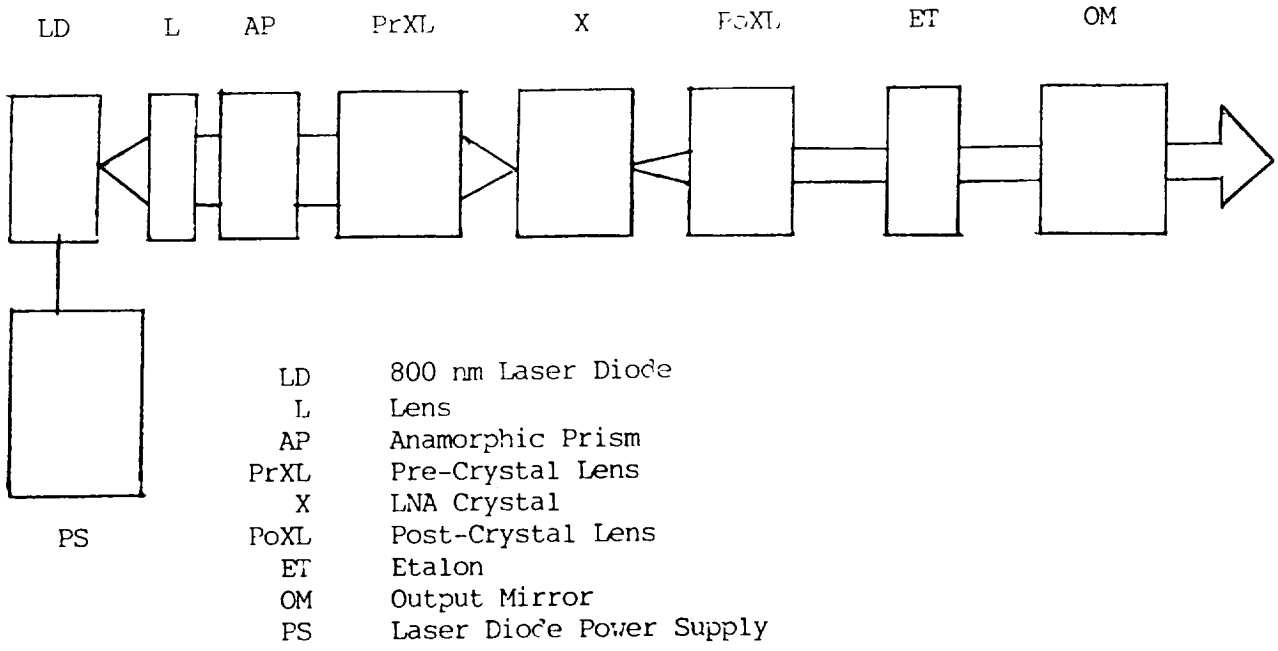

FIGURE 4.1 - LNA Laser Block Diagram

This allows the pre-crystal lens (PrXL) to focus the beam into a sharp point on the surface of the crystal.

Pre-Crystal Lens (PrXL) - The pre-crystal lens concentrates the beam into a fine point onto the face of the LNA crystal. The lens has focusing adjustments.

LNA Crystal (X) - The crystal is 5.0 OD and 10.0 mm length. One end is A/R coated for 1083 nm. The other end is coated with a dialectic mirror that has > 85% transmission at 800 nm and 100% reflection at 1083 nm. This end allows pumping with radiation from the laser diode and at the same time it is one end of the laser cavity at 1083 nm. The crystal is in a mechanical mount that permits: a) tilting about a vertical and a horizontal axis and b) positioning the crystal parallel to its axis, so that different spots on the crystal face may be selected.

Post Crystal Lens (PoXL) - This lens converts the 1083 nm divergent radiation into the parallel 1083 nm laser beam. This lens is plano convex with 1.5 inch focal length. It is mounted mechanically so that it may be tilled about a horizontal and vertical axis, positioned with its axis coinciding with the optic axis and may be focused along the optic axis.

Etalon (ET) - The etalon is tilted about a vertical axis to select the D_0 and D_{12} lines. Fine tuning is possible by tilting the etalon about the horizontal axis. It is a solid quartz plate 0.3 mm thick and coated with dielectric on both surfaces each giving 50% reflection.

Output Mirror (OM) - The output mirror is 1/4 inch thick glass polished to $\lambda/20$ flatness and coated with dielectric material to give >98% reflection at 1083 nm and >80% transmission at 1054 nm. This prevents lasing at 1054 nm and assists selection of 1083 nm lasing radiation. This mirror is mounted to allow tilting about a vertical and horizontal axis. This output mirror is the other end of the laser cavity and is parallel to the plane surface of the LNA crystal which is the other end of the laser cavity.

4.2.2 MECHANICAL COMPONENTS

The mechanical components are used for mounting the optical components. In general, it is desirable to have fine control in positioning the optical components along the X-, Y- and Z- axis. The mechanical components are mounted on an optical rail and have provision to clamp them rigidly to the rail. If the X- axis is along the rail, then the mounts usually have motion perpendicular to the rail, Y- axis. It is desirable to have vertical motion Z- axis but for some mounts this is not readily available. This limitation places the burden on the operator to carefully select the mounts.

Laser Diode - The mount provided fine tuning along the Y- and Z- axis. X- axis motion along the optical bar provided adequate freedom.

Lens - Anamorphic Prism - The lens is semi-permanently mounted to the anamorphic prism. The height along the Z- axis can be set without fine tuning. This height is chosen so that its optic axis lies along the optic axis of the pre-crystal lens. When this is correct, the laser beam travels parallel to the optical bar. The position along the X- axis can be fixed. The position along the Y- axis should be at the center across the bar and may be nonadjustable, as the fine tuning on the laser diode compensates for the fixed Y- position of the anamorphic prism. During final alignment, the combination laser diode, lens and anamorphic prism are adjusted so that the beam travels along the center of the optical bar and at a constant height above the bar. The laser diode position along the X- axis is chosen so that the rays in the laser beam is parallel throughout its path along the optical bar.

Pre-Crystal Lens and Crystal - The pre-crystal lens and crystal rail mount has only course X- adjustment. The lens and crystal have fine Y- adjustment. The lens has an additional fine X- adjustment. The crystal has Y- and Z- fine adjustment and in addition may be tilted about the horizontal and vertical axis. The tilt permits making the reflecting surface of the crystal, which is one end of the cavity, parallel to the output mirror which is the other end of the cavity.

Etalon - The etalon has X- positioning along the optical rail but no Y- or Z-positioning. It has fine tilt about the horizontal and vertical axes. The large diameter (1.0 inch) of the etalon eliminates the need for motion along the Y- and Z- directions.

Output mirror - The output mirror has positioning along the X- axis and none along the Y- and Z- axis. It has fine tilt control about the horizontal and vertical axes. The large diameter (1.0 inch) eliminates the need for motion along the Y- and Z-directions.

Shock mounting - The optical rail is mounted to an aluminum rail 1.0 inch x 9.0 inch x 48 inches. The aluminum rail floats on a bubble plastic surface resting on a table.

4.3 SETUP PROCEDURE

The set up procedure is required to assure that each optical element fulfills its function for lasing and tuning. Each component must be matched to the output of the preceding optical element. A methodical, planned approach is required to position basic optical components followed by positioning and adjustment of the remaining optical elements.

4.3.1 LASER DIODE, LENS AND ANAMORPHIC PRISM

These three elements are assembled and set up as a unit. The lens is mounted in the anamorphic prims holder. This assembly is mounted on the center of the optic rail at a height above the rail equal to the height of the pre-crystal lens height above the rail. The laser diode is placed before the anamorphic prism at the center of the rail and aligned so that the beam travels at a constant height above the rail and the beam does not change its cross section dimension as the beam is observed along the rail. During intermediate set up procedure the beam cross section will be changed as required during the alignment of other optical elements. The laser diode lens and anamorphic prism final alignment produces slightly convergent beam, which comes to a cross section with dimensions 0.5 x 0.5 mm.

4.3.2 CRYSTAL AND PRE-CRYSTAL LENS

The crystal in its complete mount is placed about 12 inches from the anamorphic prism down the rail. The crystal height is adjusted so that lateral position of the crystal is at the center of the laser beam. The pre-crystal lens is removed. The laser diode position is moved along the rail slightly away from the anamorphic prism so that the beam converges into a vertical line on the crystal. The beam is reflected back onto the anamorphic prism mounting. The crystal is tilted by the use of adjusting screws until the aperture of the anamorphic prism is at the center of the beam returned from the crystal. Note that the crystal is placed in its mount with reflecting surface facing the anamorphic prism. This completes the adjustment step of the crystal.

The pre-crystal lens is placed into its mount. The convergence of the laser is changed so that the beam is returned to the anamorphic prism mount. The lateral position of the pre-crystal lens and crystal is adjusted until the return beam is centered across the aperture to the anamorphic prism. This completes the preliminary adjustment. At this point, the pre-crystal lens and crystal assembly is removed from the rail and set aside to make room for the next element.

4.3.3 OUTPUT MIRROR

The laser diode position along the rail is readjusted until the beam forms a vertical line at a position about 12 inches from the anamorphic prism. As stated above, the vertical line image is centered across the rail and the height is unchanged from that discussed above. The output mirror is positioned on the rail so that the line image impinges on the output mirror. The output mirror tilt is adjusted with the screws till the beam is returned to the anamorphic prism mount. The tilt is adjusted so that the return beam is centered over the opening in the anamorphic prism. The output mirror is oriented so that the coating reflecting the 1083 nm radiation is towards the laser diode. This completes the preliminary adjustment.

4.3.4 POST-CRYSTAL LENS

The post-crystal lens in its mount is placed on the rail between the anamorphic prism and the output mirror. The lens position is adjusted by the use of X-, Y- and Z-axis adjustments to locate the center of the lens on the beam center. In addition, the tilt of the lens is adjusted so that the plane surface of this plano convex lens is normal to the laser beam. The lens is adjusted so that the beam is reflected and centered over the anamorphic prism mount. This completes the preliminary adjustments.

4.3.5 ETALON

The pre-crystal lens and output mirror are removed from the rail. The etalon in its mount is placed on the rail. The horizontal and vertical tilts are used to adjust the etalon so that beam is returned to the anamorphic prism so that the beam is centered over the anamorphic prism aperture. This completes the preliminary adjustment.

4.3.6 ASSEMBLING THE SYSTEM

The assembled laser is shown in Figure 4.2.

Laser Diode, Lens and Anamorphic Prism - The laser diode, lens and anamorphic prism are assembled at one end of the rail. The position of the diode along the rail is adjusted so the laser beam remains at a constant height along the center of the rail and the beam cross section at the other end of the rail forms a square of about 5 mm to the side. The beam is slightly convergent. The laser diode current is adjusted to about 450 mA.

Pre-Crystal Lens and Crystal - The mount holding the pre-crystal lens and crystal is placed in the laser beam with the pre-crystal lens between the anamorphic prism and the crystal. The position along the rail is such that it allows easy access to the adjusting knob on this mount. The course adjustment of the pre-crystal lens is used to bring the laser beam into a sharp point focus onto the surface of the crystal. The fine positioning screw allows fine tuning at a later step.

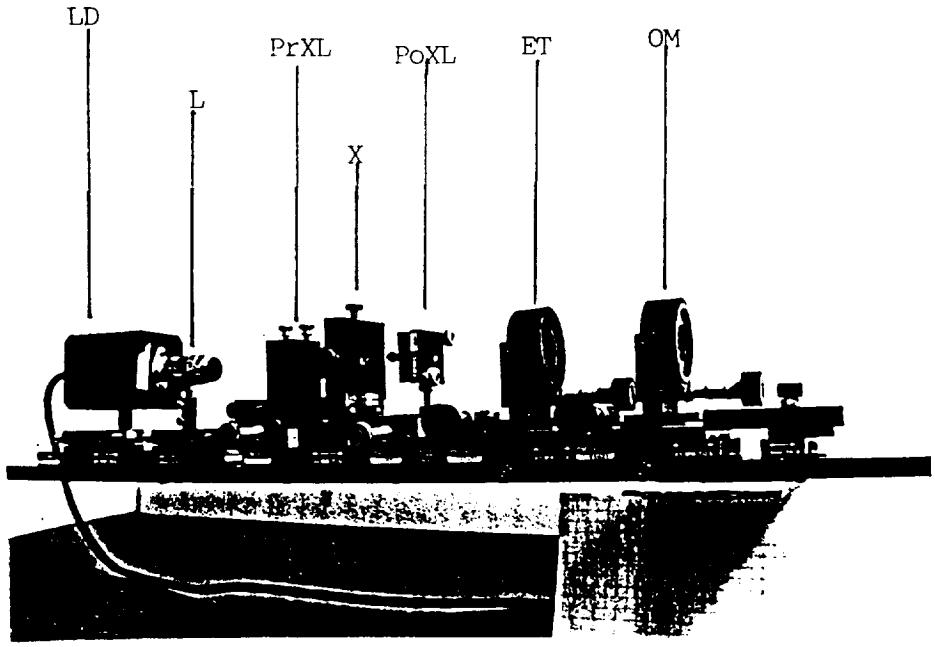

FIGURE 4.2 - LNA Laser System. Note that the anamorphic prism was not used here.

Post-Crystal Lens - The post-crystal lens mount is placed on rail and is used to focus the fluorescent output beam from crystal into a parallel beam along the center of the rail at the height that the beam would be at the center of the output mirror. Some of the pumping radiation may be observed on a target placed at the other end of the rail. The cross-section of this beam is rectangular in shape slightly smaller than the cross section of the beam as it leaves the anamorphic prism. This determines the approximate position of the post-crystal lens along the rail.

Output Mirror - The output mirror in its mount is placed along the rail at a distance from the output lens sufficient to permit placing the etalon and its mount on the rail later.

Etalon - The etalon is not placed on the rail during the procedure of lining up the laser system to lase. Having assembled the components we now turn to tuning the system to make it lase.

4.4 TUNING PROCEDURE

Lasing at 1054 nm - The LNA crystal fluoresces strongly at 1054 nm followed by lesser intensity at 1083 nm as shown in Figure 4.3. Preliminary optics alignment should be aimed at allowing the system to lase at 1054 nm as this intermediate goal simplifies the task. To this end, the output mirror to be used is the one that has >98% reflection and T<2% transmission at 1054 and 1083 nm. The system will lase at 1054 nm because the fluorescence is stronger than at 1083 nm.

Focusing the Pumping Beam on the LNA - The first step is to use the pre-crystal lens to focus the pumping radiation into a fine spot on the mirror face of the LNA crystal. Set the laser diode current at about 650 mA. Use the fine screw to focus the pumping radiation into a very fine spot on mirror end of the crystal (it should be on the input side). When the spot appears to glow with white radiation, this is adequate focusing for the first step. The crystal fluoresces strongly at this spot. Fluorescence is

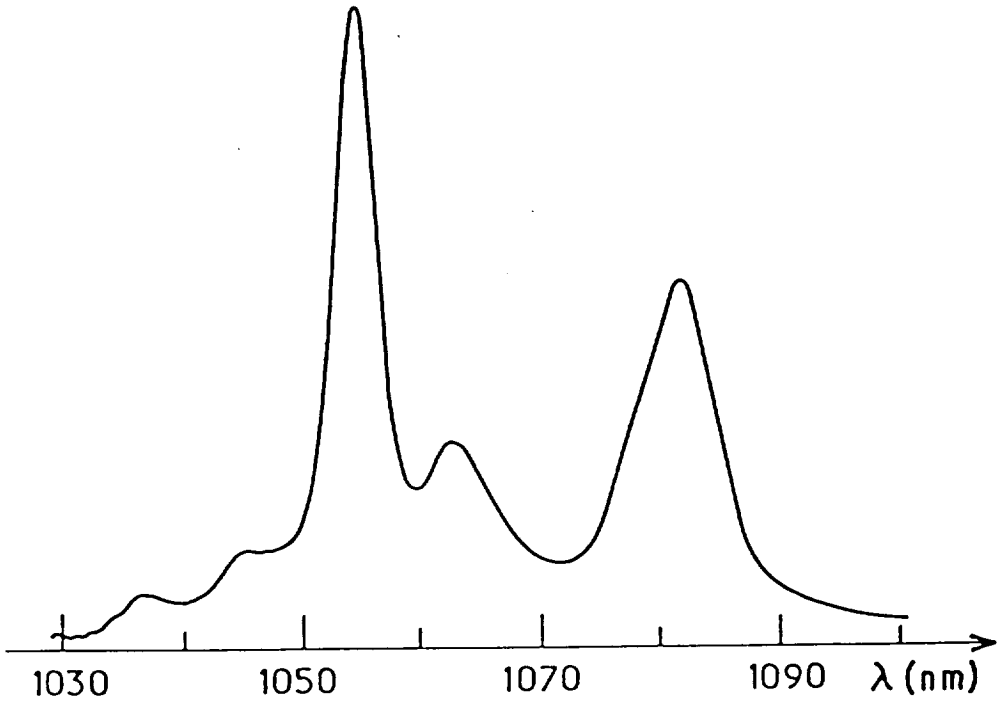

FIGURE 4.3 - Fluorescence of LNA at 1054 and 1083 nm.

also present at the crystal outer edge along the full length of the crystal as observed with an I.R. Snooper Scope.

Post-Crystal Lens and Output Mirror - The post-crystal lens and the output mirror are adjusted alternately to achieve lasing. One observes with an I.R. Snooper Scope the beam on a target at the end of the rail and notes that there is a rectangular area. One adjusts the output mirror tilt about the vertical and horizontal and looks for a bright spot (which is image of the fluorescent spot on the crystal). The image responds to the output mirror adjustments. If there is no bright spot then one uses the fine adjust to change the position of the post-crystal lens. A loosening of the screw that clamps the mount to the rail may also be used for a course change of the position of the post-crystal lens along the optical bar. The position of the post-crystal lens is changed while adjusting the horizontal and vertical to tilt the output mirror and observations are made to look for the bright spot that responds to the tilting of the output mirror. If the spot appears in view then the tilt of the output mirror is adjusted until the spot is in the central area of rectangular image. i) If the brightness of this spot then increases several tens or hundreds fold, then lasing is occurring. One tunes the pre-crystal lens laterally to brighten the laser spot. The tilt of the crystal is adjusted as well as the tilt of the output mirror. The post-crystal lens positions along the optical bar (the X- direction) is fine tuned to increase the laser output. A detector may be used to advantage to read the power of the laser beam while all available adjustments are tuned for maximum laser output. ii) If lasing does not occur, one proceeds with all adjustments to change the spot until lasing occurs. Tuning the laser becomes a skill acquired by experience. Pump laser diode current may be increased to about 780 mA to aid in the search. When the laser has been properly aligned and it lases, threshold current may be as low as 500 mA or less.

Lasing at 1083 nm - Lasing at 1054 nm means that the position and tilting of the pre-crystal lens, crystal and post-crystal lens as well as the output mirror has been

properly adjusted and tuned so that the various optical components cooperate to achieve lasing. One may now tune to achieve lasing at 1083 nm.

Output Mirror - The output mirror (R >98%, T <2%) is replaced with one that has R <80% at 1054 nm and R >98% at 1083 nm as well as T >20% at 1054 nm and T <2% at 1083 nm. This mirror favors lasing at 1083 nm. If lasing had occurred at 1054 nm then lasing at 1083 nm would require only tuning the tilt of the output mirror. Monitoring the laser beam with a light meter would permit one to maximize the laser efficiency by fine tuning in succession all the optical elements. Place the etalon on the optics bar between the output mirror and post-crystal lens.

Etalon - The etalon R = 50%, t = 0.30 mm, is used to tune for He D_0, D_{12} lines. When the etalon is tilted for zero order the lasing occurs with greater power. One may begin tuning the etalon to produce the beams at the three He lines. One observes the tuning by searching for fluorescence in a helium cell. As one tunes, the etalon lasing may disappear, so tune the output mirror. Lasing may fluctuate with etalon tilt, adjust the output mirror tilt to maximize the laser beam output at He D_0, D_{12}. Experience helps, perseverance is essential.

Helium Cell - The helium cell excited with R. F. power is placed in the path of the laser beam beyond the output mirror. An I.R. Snooper Scope is used to observe fluorescence.

He D_0, D_{12} Lines - By using a chopped laser beam and mechanically tuning the etalon, we observed and recorded the fluorescence with a lock-in amplifier and recorder. A trace of the He D_0, D_1 and D_2 line fluorescence is shown in Figure 4.4. D_0 is well resolved but D_1 and D_2 are only partially resolved.

4.5 PERFORMANCE CHARACTERISTICS

Evaluation was done after laser was made operational. Some typical data was obtained and is presented here. Observation was made in fluorescence with the He cell mode:

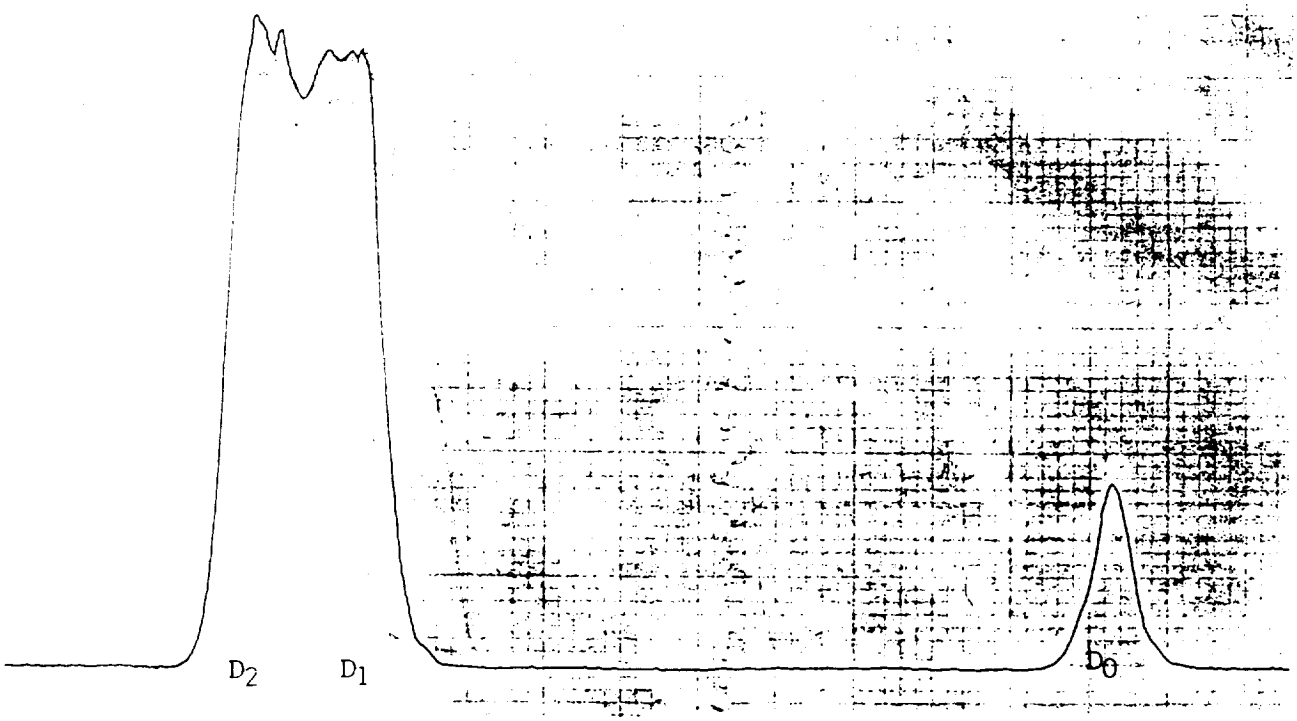

FIGURE 4.4 - Fluorescence of the He D_0, D_1 and D_2 radiation by a scanning LNA laser. Diode: 807 mA 14.5°C.

1054 nm	
Mirror	R 95% (1054 - 1085 nm)
Laser Diode	820 mA 14.5°C
Output and Background	20.0 mW
Background	7.0 mW
Laser	13.0 mW
1083 nm	
Mirror:	R >98% (1083 nm)
	R <20% (1054 nm)
Laser Diode	839 mA 14.5°C
Output	1.8 mW
Threshold	470 mA 14.5°C

Usually the D_{12} lines are partially resolved and are considerably stronger than the D_0. Under some condition for reasons that were not investigated, the power of D_2 was greater than D_1 by a factor of at least 2 times and for D_0 by a factor about 5 times as shown in Figure 4.5. No wavelength locking was done for the LNA. The major effort was applying the LNA laser to Helium magnetometer application which is discussed in Section 6.0.

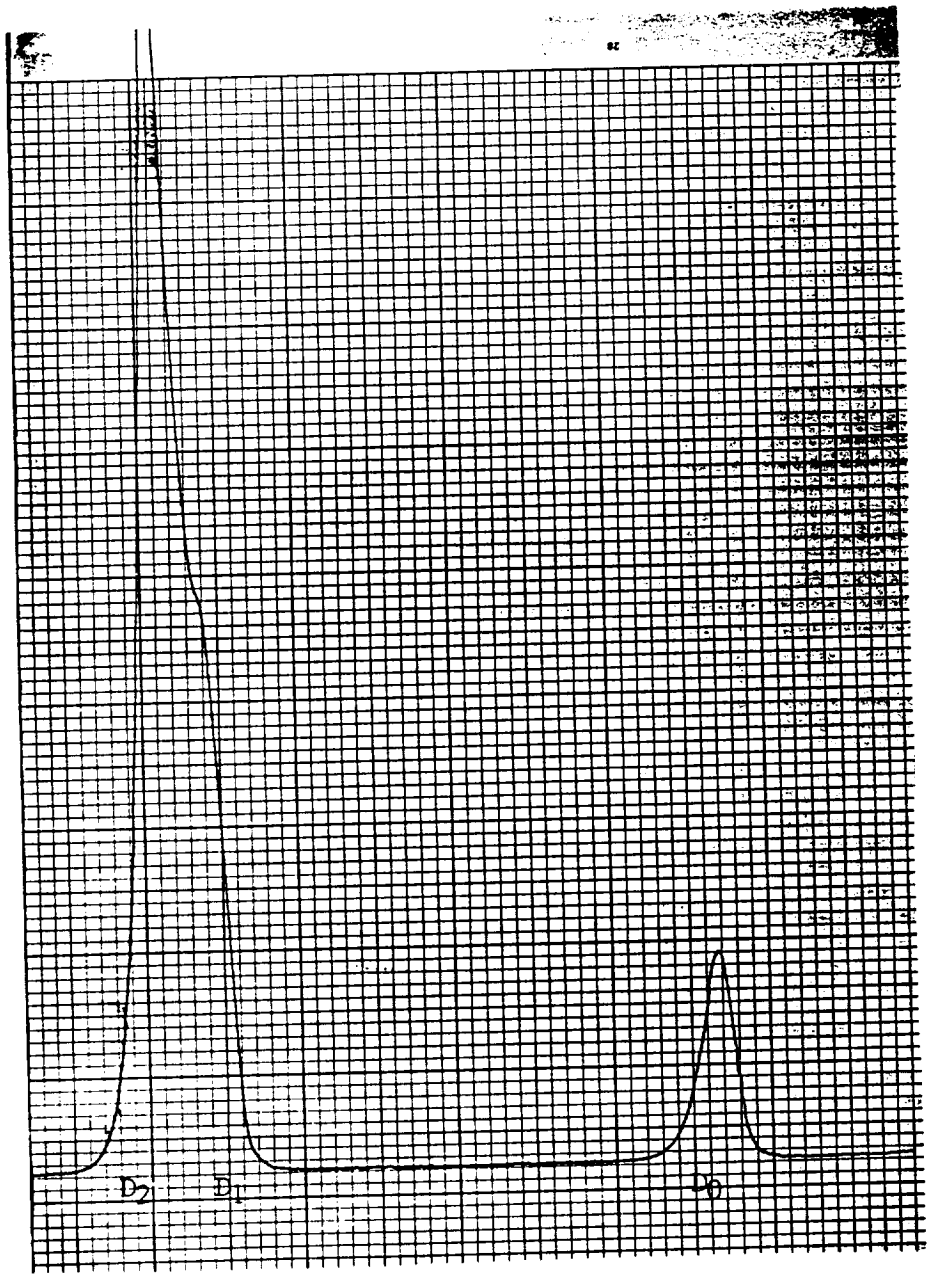

FIGURE 4.5 - LNA laser emitting radiation at D_2 that is 2x greater than D_1 and about 5x than D_0.

5.0 PROTOTYPE LASER-PUMPED MAGNETOMETER

5.1 SENSOR DESCRIPTION

In order to investigate the impact of laser pumping on magnetometer performance a laboratory laser-pumped magnetometer was designed and assembled. The sensor head was constructed of standard helium magnetometer components mounted in special optical tubes.

It was necessary to design, construct, and assemble a locked-loop control system which is designated the digital resonance spectrometer (DRS). The DRS can be operated as a locked-loop scalar magnetometer mode or for evaluation of the components and assemblies for the sensor head. A block diagram of the complete measurement system is shown in Figure 5.1. The DRS electronics are designed to measure 0.1 pT variations in the ambient magnetic field when the sensor head satisfies the following equation for minimum detectable signal:

$$W \times B^{1/2}/(S/N) \leq 1 \times 10^{-4} \text{ nT}. \quad (1)$$

Here W is the helium absorption linewidth in nT. When W is 100 nT, then $S/N \geq 1 \times 10^6$ in a 1 Hz bandpass is required to achieve a minimum detectable signal of 0.1 pT rms. The resolution of the DRS is a factor of 10 better than the instrument design goal of 1 pT.

5.2 SENSOR HEAD

The sensor head components were mounted inside an assembly of PVC pipes and associated fittings shown in Figure 5.2. This construction was selected because of the low cost and the requirements for non-magnetic materials. The absorption cell and excitation coils were mounted in a double tee at the center of the sensor head. The double tee VC joins the two pipes which are used to mount magnetic optical components at distances up to 95 cm from the cell.

A PVC Helmholtz coil pair was fabricated which can be mounted on the center tee assembly in either the transverse or longitudinal orientation with respect to the light beam. These coils are used in the transverse orientation for initial observation of optical

FIGURE 5.1 - BLOCK DIAGRAM OF LAB MAGNETOMETER AND DIGITAL RESONANCE SPECTROMETER

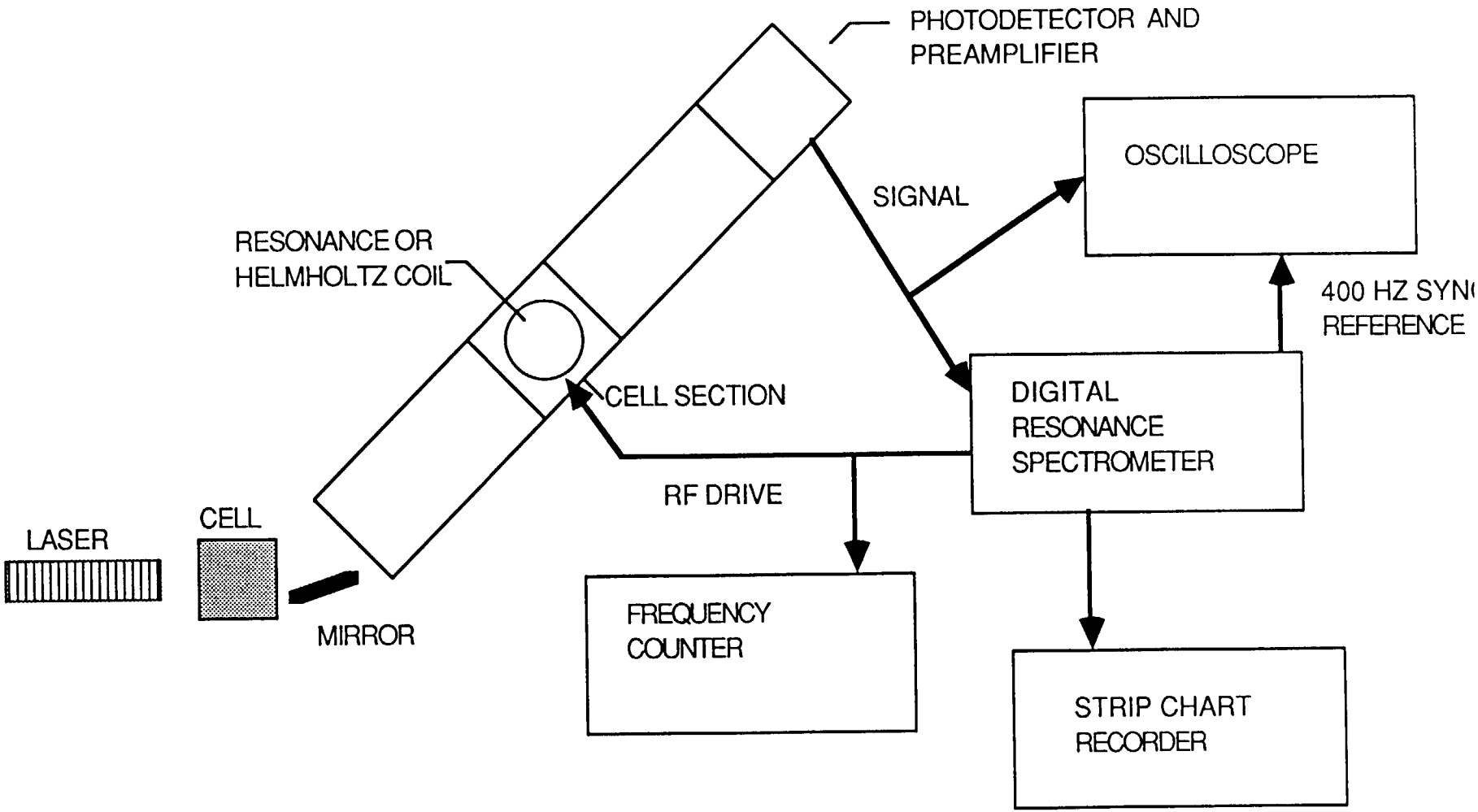

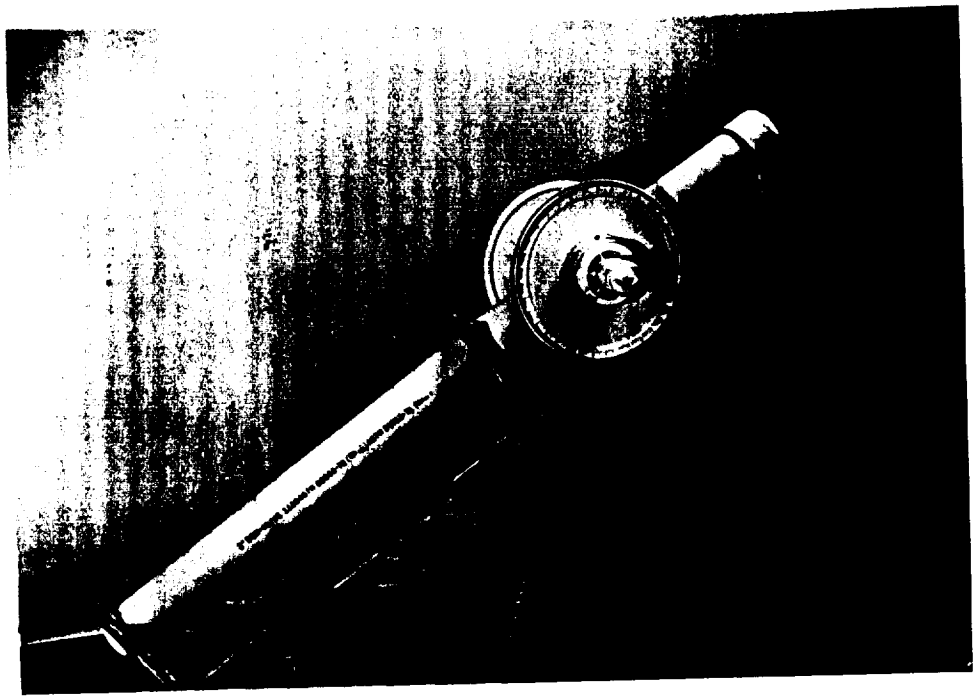

FIGURE 5.2 - MECHANICAL MOUNTING FOR LABORATORY LASER PUMPED MAGNETOMETER

pumping signal-to-noise as critical parameters such as cell excitation levels are adjusted. A nonmagnetic free-standing mount was designed and built which aligns the optical path of the laser light with the earth's magnetic field.

The sensor photodetector assembly consists of a silicon photodetector with a peak response at 1083 nm which is connected to a transimpedance preamplifier recommended by the detector manufacturer. The output of the preamplifier is a/c coupled to a voltage amplifier when required for baseline measurements using a helium lamp. When using the laser, one or more neutral density filters can be mounted in front of the photodetector to adjust the incident light intensity so that the preamplifier operates in a linear region. The photodetector, preamplifier, and amplifier are packaged in a shielded can with an opening for light to reach the photodetector.

Specifications and typical performance for the photodetector and transimpedance amplifier are:

Photodetector

Active Area	0.1 inch x 0.1 inch
Responsivity	$\geq$0.45 μ amp/μ watt
Dark Current	<0.1 μ amp
Noise Current	< 0.20 p amp

Transimpedance Amplifier

Equivalent Input Noise Current	3 p amp/Hz$^{1/2}$
Forward Transfer Impedance	12 k ohms
Input Impedance	300 ohms
Output Impedance	4 ohms

When the amplifier is used with the photodetector, the equivalent input noise current is approximately 6 pamp/Hz$^{1/2}$. The photodetector and transimpedance amplifier noise does not make a measurable contribution to the overall magnetometer system noise.

5.3 LOCKED-LOOP ELECTRONICS AND DIGITAL OSCILLATOR (DIGITAL RESONANCE SPECTROMETER)

In order to investigate the laser pumped magnetic resonance line in helium, a source is required to supply an rf drive field at the Larmor frequency of helium resonance (in the neighborhood of 1.5 MHz). Polatomic developed a high precision digital

oscillator which can provide this drive field and be incorporated in a resonance loop which locks the oscillator to the magnetic resonance frequency of the helium sample. The loop must have an effective resolution of 0.1 pT in order to utilize the anticipated laser pumped sensitivity. The digital oscillator is the key element in the P.C. keyboard controlled digital resonance spectrometer as shown in Figure 5.3.

The DRS electronics features a P.C. controlled system which serves as an operation interface with the electronics. Through the P.C. keyboard controls, an operator can select among several applications programs and initialize all critical parameters including logging file, starting frequency, sweep width and sample interval time. The electronics package built around the digital oscillator can serve as an open loop station magnetometer, a scalar magnetometer resonance loop, resonance spectrometer for line shape studies, and dual sensor gradiometer. All of these functions are controlled by the P.C. keyboard and programs.

A limited capacity for data archiving is activated by momentarily switching off the system run switch. The software is flagged to exit the application program and store the 14,000 word buffer into a disk file. The data period covered by the disk file depends on the sample interval time, e.g. at a sample interval time of 0.2 sec/point, approximately 3/4 hour of data can be stored. This is adequate to demonstrate data having an upper frequency of interest near 1 Hz.

A laboratory pulse generator provides a positive going pulse at an 800 Hz rate. This pulse string is used as a system phase clock. The rising edge of the pulse starts the analog-to-digital (A/D) conversion of the magnetometer error signal which is completed in approximately 0.1 m sec. The falling edge of the pulse activates the transfer of the digitized error signal (error word) to the P.C. The P.C. application program performs all necessary computations before the next rising pulse edge.

In the P.C. the error word is algebraically added to a scaled frequency number which is output as a 32-bit word to a latched register on the digital oscillator board

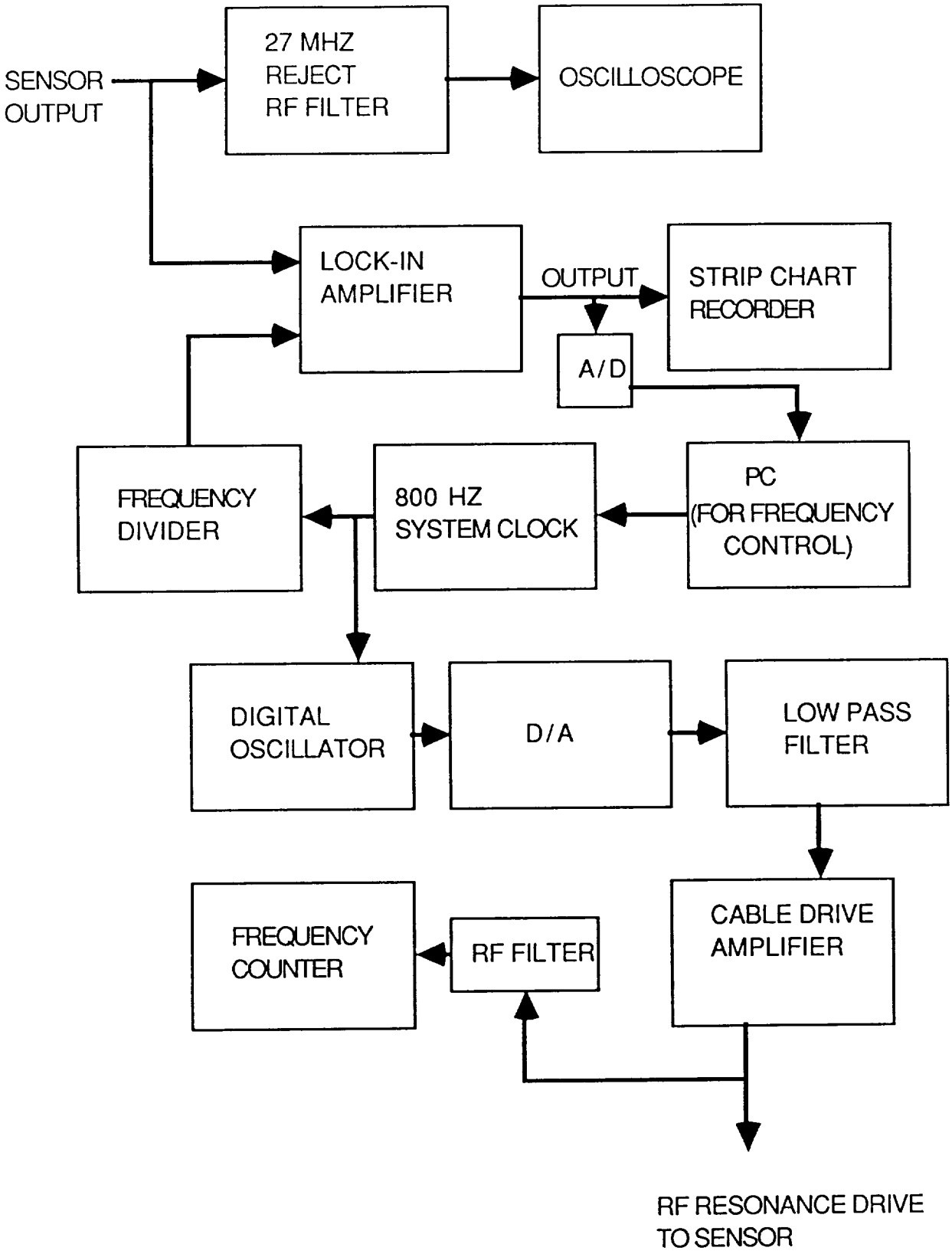

FIGURE 5.3 - BLOCK DIAGRAM OF DIGITAL RESONANCE SPECTROMETER

(D.O.). The sine wave frequency of the D.O. is determined by this word at a 10 MHz sample rate as defined by the equation

$$f = \frac{DELTA}{t \times N} \qquad (2)$$

where f is the output frequency, t is the sample interval time (i.e. 1×10^{-7} sec) and N is the number of stored, equally spaced sine wave values (2^{16} in number). The maximum value for DELTA must not exceed N/2 to satisfy the Nyquist criteria [$f \leq 1/(2 \times t)$].

To determine the frequency resolution consider DELTA, a 32-bit word, to have 16-bits to the right of the Q-point since the 16 most significant bits exhaust the enumeration of the 2^{16} memory locations. Thus the frequency resolution may be computed from equation to be

$f = 2.33 \times 10^{-3}$ Hz or

H = 0.083 nT

The high stability (5×10^{-10}) 10 MHz clock (Implementation difficulties forced operation at 5×10^{6} Hz with double the resolution and half the maximum usable frequency.) in the D.O. selects the sine wave digital values from the memory and a digital-to-analog converter followed by a low pass filter with a 2.5 MHz cut frequency and a line driver provide the r.f. resonance signal to the sensor field coils. A gain control is provided for adjusting the resonance r.f. level. The digital oscillator board is shown in Figure 5.4.

5.4 SIMULATED SENSOR PERFORMANCE

An electronic simulator of the helium resonance was designed and built in order to test the locked loop concept and apparatus prior to the availability of a suitable helium resonance signal. The resonance simulator utilized design depends upon a crystal resonance actively broadened to resemble the helium paramagnetic resonance. Figure 5.5 shows the differentiated simulated resonance generated by a frequency modulated excitation frequency and a lock-in amplifier. The differentiated curve was found to have a linewidth of 300 Hz. Open-loop noise measurements resulted in 1.74 micro-volts rms

FIGURE 5.4 - PHOTOGRAPH OF DIGITAL OSCILLATOR BOARD

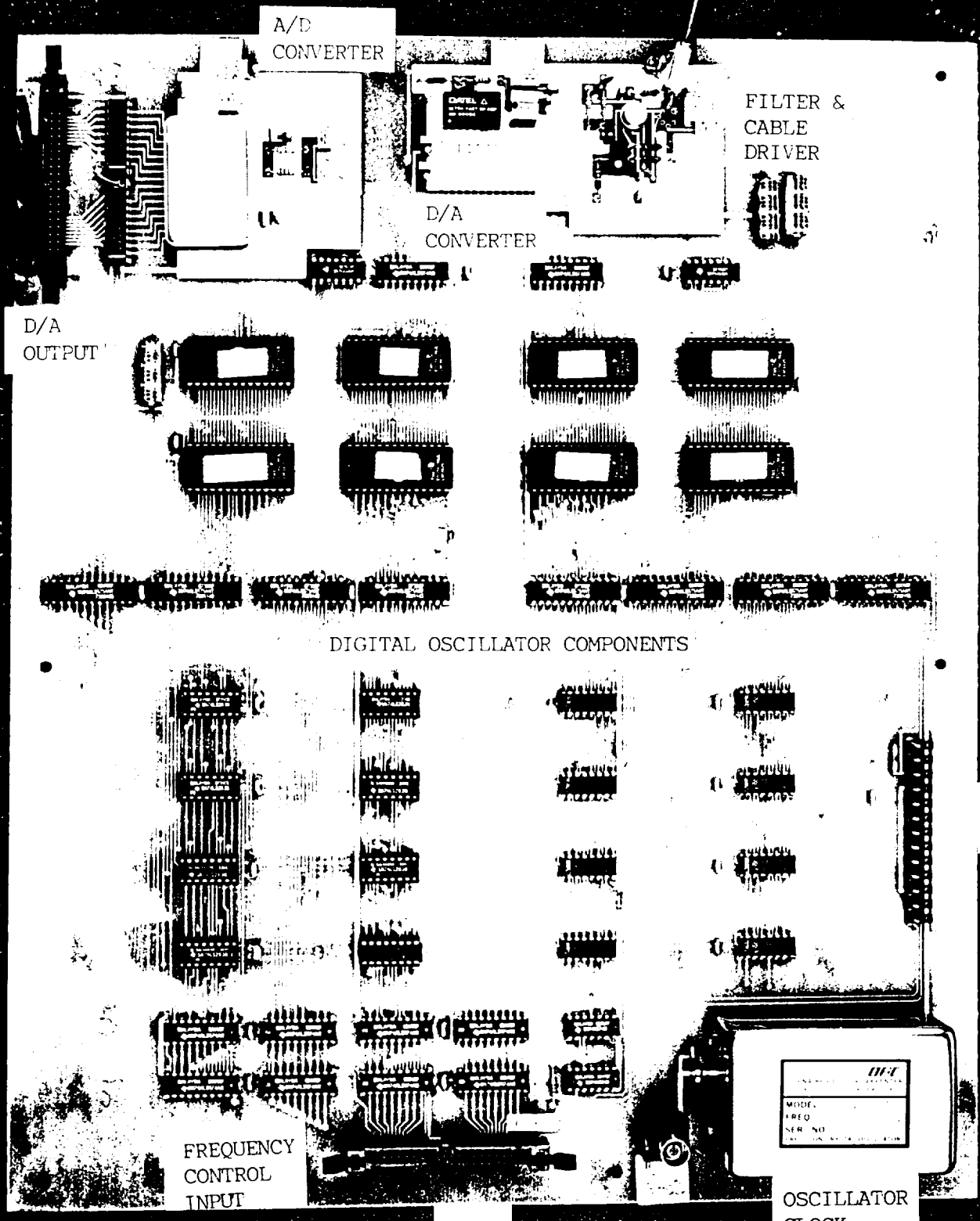

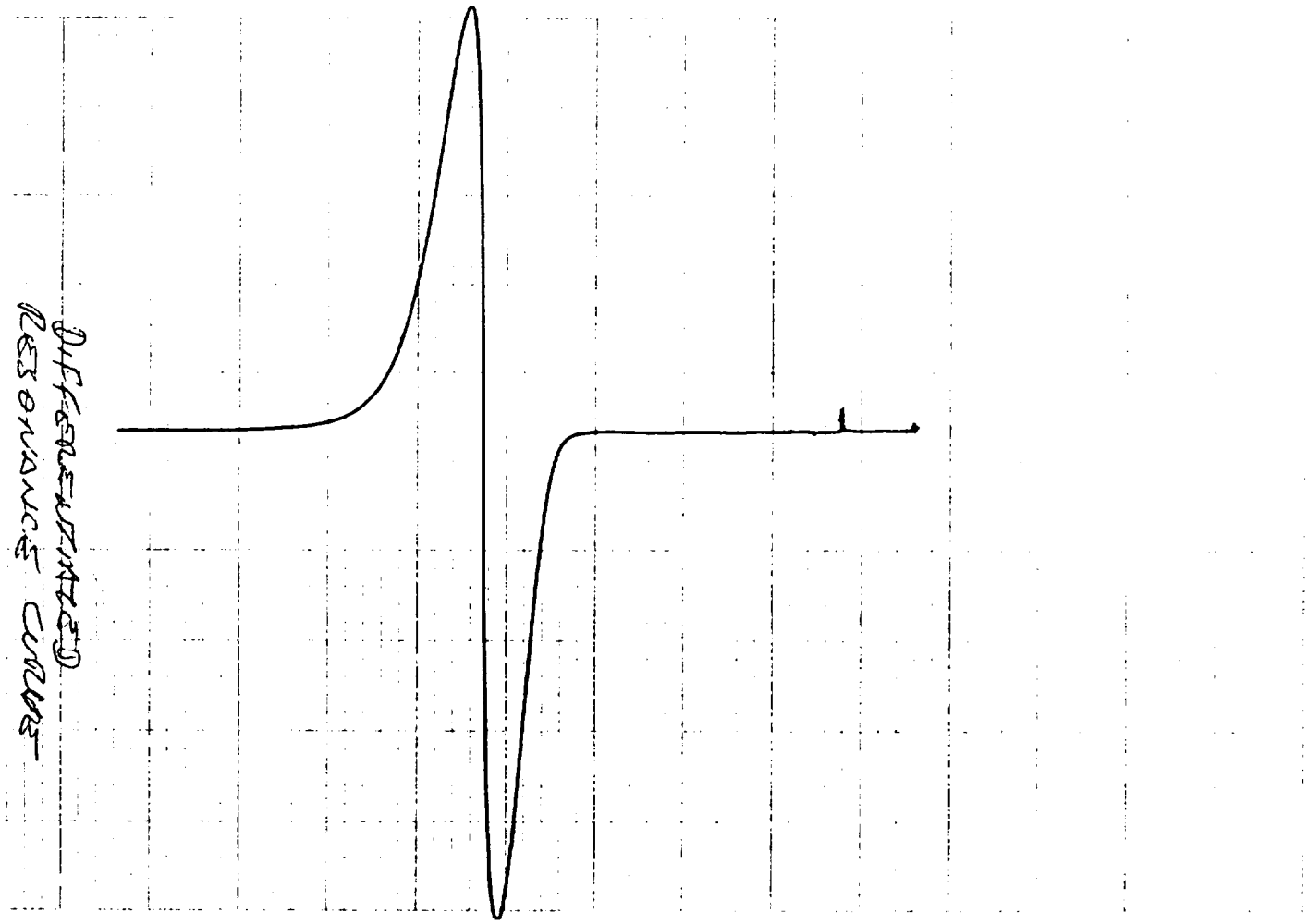

FIGURE 5.5 - DIFFERENTIATED SIMULATED RESONANCE LINE

noise in a 1 Hz bandpass. The associated signal-to-noise ratio for the simulated helium resonance was 56,700. A minimum detectable pk-pk signal of 0.0053 Hz is predicted. This predicts a magnetic sensitivity of 2.0 x 10^{-4} nT r.m.s. Closed-loop error signal measurements were done using an ITHACO lock-in amplifier to lock the central loop in a 100 Hz bandpass. A second ITHACO lock-in amplifier was used to measure the error voltage with a 1 sec time constant output filter (~ 1 Hz bandpass). The error signal was measured to be 5.0 x 10^{-4} nT rms. A favorable assumption is that the digital oscillator and the helium resonance simulator contribute equally to the resulting random noise. This assumption results in an estimate of 3.5 x 10^{-4} nT rms contribution from each source. This is in good agreement with predicted results. While inadequate to establish the digital oscillator stability, the dummy resonance was useful in proving the DRS system concept.

5.5 OPERATING PROCEDURES FOR THE DIGITAL RESONANCE SPECTROMETER

In order to characterize a magnetometer system and evaluate specific magnetometer components, certain measurement procedures were developed for the digital resonance spectrometer. The block diagram of the DRS (digital resonance spectrometer) operated as a magnetometer is shown in Figure 5.1. The DRS consists of the following components:

- Helium resonance sensor unit
- Optical pumping source at 1083 nm
- Photodetector and amplifier assembly
- Oscilloscope
- Lock-in amplifier
- Digital oscillator and coil driver
- A/D converter
- Strip chart recorder

5.5.1 INPUT/OUTPUT SYSTEM CALIBRATION

The first procedure consists of an input-to-output system calibration using the HP 680 strip chart recorder as a display. The zero input response on the strip chart recorder was established by connecting a shorting plug to the input of the ITHACO lock-in amplifier. The known input for the calibrated strip chart response was provided by a 100 millivolt pk-pk sine wave signal synchronized to the lock-in reference frequency and phase adjusted for maximum response. The system response calculation requires the lock-in sensitivity setting and bandpass, the strip chart gain and the number of minor divisions of strip chart response. It is noted that the lock-in produces $\pm$ 10 volts of full scale output at any sensitivity setting. The formula for the input level for a given strip chart response of x divisions, a strip chart setting of SCALE volts, and a lock-in sensitivity of SENS.

$$v = (x / 50 \text{ div}) (\text{SCALE}/10 \text{ volts}) (\text{SENS}), \quad (3)$$

The next procedure consists of noise level measurements. When the noise to be measured is attached to the input of the lock-in amplifier, SENS and/or SCALE are adjusted until the noise is readily measurable. The peak-to-peak response is recorded from at least five minutes of data. The rms noise level, assuming gaussian distribution, is estimated to be

$$N(\text{rms}) = v \text{ in (pk-pk)} \times B^{1/2}/5 \quad (4)$$

where v is given by Equation (3) and B is the bandpass in Hertz. The strip chart recorder acts as a low pass filter whose response is down 3 db at 2.2 Hz.

When the noise measurement procedure is used to measure system noise, the lock-in amplifier is first connected to the photodetector and amplifier assembly under dark conditions. The reference frequency is provided at the system rate and the noise is recorded. By using the nominal specification values for the transimpedance gain of the preamp and the responsitivity of the photodetector, an equivalent input optical noise power may be measured.

5.5.2 OPTICAL POWER CONSIDERATIONS

Our experiments required that we operate the optical-pumping tunable laser source at maximum available power. Experiments must eventually be performed to characterize the magnetometer as a function of optical power. The photodetector assembly, however, has limited by dynamic range. An initial adjustment is made following the helium cell to adjust the light level on the photodetector. The output is 1.0 volts for dark conditions at the photodetector. The transimpedance amplifier saturates at 3 volts d.c. output. The nominal incident power will produce an output of approximately 2 volts d.c. A means for easily inserting neutral density optical filters just before the photodetector is provided. This permits independent selection of optical power at the cell and at the photodetector.

The photodetector output signal is d.c. coupled to an r.f. filter near the signal observation equipment. This filter removes cell excitation r.f. pickup. Connectors are provided for d.c. coupling to an oscilloscope for the purpose of measuring the optical power of the laser. If the laser line wavelength varies, less absorption will occur and the d.c. level increases; if the laser quits entirely the d.c. will return to the dark level.

5.6 TRANSVERSE FIELD (HELMHOLTZ COIL) EXPERIMENT

The purpose of the transverse Helmholtz coil experiment is to observe the laser pumped signal without applying an r.f. field to the helium cell. This experiment is based on the cosine-squared dependence of the optically pumped helium signal amplitude on the angle between the optical axis and the ambient magnetic field direction. A pair of Helmholtz coils (See Figure 5.2) was assembled into the sensor head assembly either in the transverse or longitudinal orientation. The paramagnetic resonance signal amplitude is measured while applying a 400 Hz transverse magnetic field to the helium cell by means of these Helmholtz coils while the magnetometer optical axis is aligned along the earth's magnetic field. The transverse field amplitude with 430 milliamp rms current is sufficient to produce a magnetic vector which swings approximately 70° on either side of

the earth's field. This produces a second harmonic field modulation having an amplitude proportional to $g = (1-\cos^2\phi)$. For $\phi = 70°$, g=0.88. The absorption cell excitation level is adjusted to produce maximum optical pumping signal amplitude before performing other resonance experiments. The electrical hook-up is shown in Figure 5.1 with Helmholtz coils activated. Signal amplitude stability will depend upon the stability of the Helmholtz coil calibration constant and upon the coil driver amplitude stability.

5.7 PARAMAGNETIC RESONANCE EXPERIMENTS

Figure 5.1 presents a hook-up diagram for paramagnetic resonance experiments with resonance coils activated. It should be noted that the 800 Hz source is now used as a system phase clock and the reference frequency is a 400 Hz pulse train derived from the phase clock. The digital oscillator (D.O.) receives a new (or repeated) frequency command from the P.C. for each cycle of the phase clock. This frequency command is a 32-bit digital word which is proportional to the desired frequency. In the P.C. a square wave frequency modulation is produced by alternately adding and subtracting a pre-selected number from the frequency command each cycle of the phase clock. This process produces a frequency modulation at one-half the phase clock frequency or 400 Hz. The D.O. output is a stream of digital values at a 10 MHz rate to the D/A converter. The D/A converter output is analog r.f. directed to a low frequency filter followed by the r.f. field coil driver amplifier.

The D.O. is operated through an operator interface. The applications program is resident on the hard disk in the DOS subdirectory C:\EXECUTE\ The applications program is named CONFIX for fixed center frequency operation. The "CON" is mnemonic for "control program" and the "FIX" is mnemonic for obvious reasons. When CONFIX is executed the operator interface requires responses to a series of questions. Listed below in are the questions, typical responses, and comments.

PC Operator Interface Question-Response List for DO Operation

Question	Response	Comment
DATA LOG?	LOG.1	A Dos File Path Name
DELTA?	$4ABDB405	Frequency Command for 1,451,862 Hz (52,093 nT)
SWEEP?	$000758A8	Sweep Increment: ±208 Hz
UPDATE?	0.01	Frequency Command Update Interval Time in Seconds

A push-button run-stop switch is provided which when not depressed is in the run position. Therefore, when the update response is entered, the D.O. is activated and the selected frequency is applied to the resonance field coils.

When the resonance frequency is not known another application program is available with the name CONSTEP. This program is operated exactly the same as CONFIX except that at each frequency command update the frequency command is incremented so that the effective frequency ramp is generated. This effect is used when searching for the resonance line. Since an internal computation is derived from the input update interval time as a number of system phase clock cycles and is therefore not entirely accurate. Also the system phase clock is set with an oscilloscope measurement and is not known with high precision. Consequently a frequency rate calibration is required for each set-up including the selection of an update interval time. The method used is to read the frequency as the strip chart crosses major divisions and mark the chart. With the strip chart running at 1 inch per minute, ten major divisions are crossed and the average frequency difference between divisions is computed. This run is then retained with other frequency dependent runs from that set up. When an experimental run is started, if the recorder pen is lowered simultaneously with the entry of the update interval time, the start frequency will correspond to the DELTA response given via the operator

interface. Other frequencies are computable from recorder speed and number of chart divisions transversed.

To record a differentiated resonance line one can execute CONSTEP with a frequency calibrated strip chart recorder and with the peak signal amplitude adjusted near plus and minus full scale. The sweep width should be optimized to obtain the maximum pk-pk amplitude of the differentiated resonance line without producing line broadening.

To measure signal to noise ratio execute CONFIX with the center frequency set at one of the peaks of the differentiated line and the sweep set at the optimized value. The r.f. drive is adjusted to reduce its amplitude until the signal amplitude is just beginning to decrease.

On a magnetically quiet day at the test range, large signal-to-noise measurements should be possible because the field fluctuations relative to the resonance linewidth are small and because of the low sensitivity of a signal peak to minor frequency deviations. The noise level is obtained following a signal level run by disconnecting the r.f. field coils and having them open circuit during the run. Noise data runs of 5 minutes were made. All signal-to-noise ratios are obtained following the computation of equivalent input signals for each run.

These operating procedures allow the digital resonance spectrometer to perform a variety of experiments. These include measurement of linewidth and signal-to-noise dependency on laser power at the cell. Laser powers are estimated from the dc level measured at the output of the transimpedance amplifier, specification parameters, and measured optical attenuations due to polarizer, cell and neutral density filters. A laser power meter is used to confirm power levels.

5.8 MEASUREMENT OF SIMULATED HELIUM RESONANCE

The noise measurement procedures were used to measure the noise level of the simulated helium resonance. For this test the simulated helium resonance is excited with a frequency modulated resonance signal at the level required for the actual helium magnetic resonance. A stable frequency with appropriate fm sweep from the D.O. is applied at the previously determined resonance point and the noise is observed. The control loop is then closed and a second noise run is made. Figure 5.6 presents an open-loop noise run. Figure 5.7 shows a closed-loop noise run. The closed loop residual noise was 4.4×10^{-4} nT rms, which is consistent with the 3.5×10^{-4} nT rms predicted above. Because of the nature of the D.O. low frequency drift does not accumulate and the error voltage shows only periodic or gaussian noise in the bandpass. This occurs because the D.O. set-point is reestablished each cycle of the system phase clock.

5.9 PRELIMINARY CHECK-OUT OF DRS AND SENSOR COMPONENTS

Prior to the availability of a 1083 nm laser the optical unit of the magnetometer was fitted with a helium lamp optical pumping source provided by JPL. Preliminary testing was performed while placing the detector unit on the lawn of Polatomic's office building. This permitted evaluation of components including matching networks, electronic noise, light level, Helmholtz coils, and magnetometer assembly alignment. An optical pumping signal was initially obtained using transverse Helmholtz coil method. A resonance signal was observed which had a linewidth measured at 13,089 Hz (467 nT). After this preliminary check-out the D.O. was locked and magnetometer operation was observed. The center resonance frequency was found to be 1,459,656 Hz.

The linewidth is approximately two to five times broader than was expected for a helium 4 resonance. At this point only cursory magnetics checking had been done. Following this experiment the magnetometer was disassembled and each part tested on sensitive production magnetic inclusion testing apparatus. General construction was magnetic free, however, a few hot magnetic parts were identified and removed. After

6.9

5/24/89
J. Rice

DUMMY HELIUM RESONANCE
(WITH LAMBDA POWER SUPPLY)
(OPEN LOOP)

FIGURE 5.6 - SIMULATED RESONANCE/OPEN LOOP NOISE

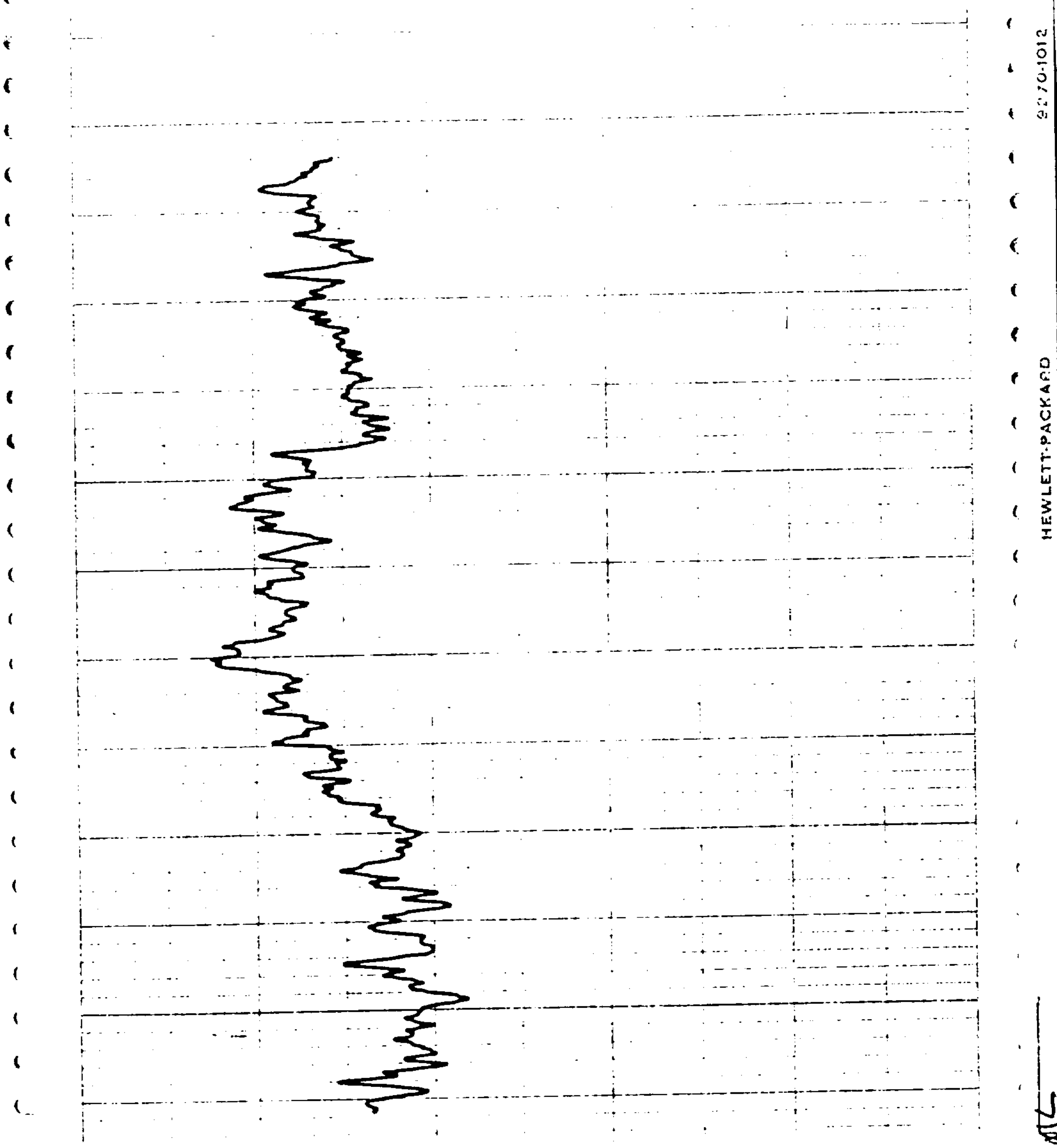

EQUIVALENT INPUT = 8.7 μ volt pk-pk ⇒ 1.74 μ volts r.m.s.

CALCULATED SENSITIVITY: $\frac{21{,}488}{(56{,}700/8.7)} \cong$ 3 milli-δ pk-pk

10^{12} watts pk-pk

10^{12} watts r.m.s.

ITHACO 3921 LOCK-IN AMPLIFIER

SENS = 1 mV × 3

TC = 0.1

POST FILTER = ON

PHASE = AUTO

STRIP CHART = SCALE = 100 m volt

EQUIVALENT INPUT: $\frac{14.6\ \text{div}}{50\ \text{div}} \times \frac{100 \times 10^{-3}\ \text{volt}}{10\ \text{volt}} \times 3 \times 10^{-3}$ volt (pk-pk)

5110

DUMMY HELIUM RESONANCE
(WITH LAMBDA POWER SUPPLY)
(CLOSED LOOP)

FIGURE 5.7 - SIMULATED RESONANCE/CLOSED LOOP NOISE

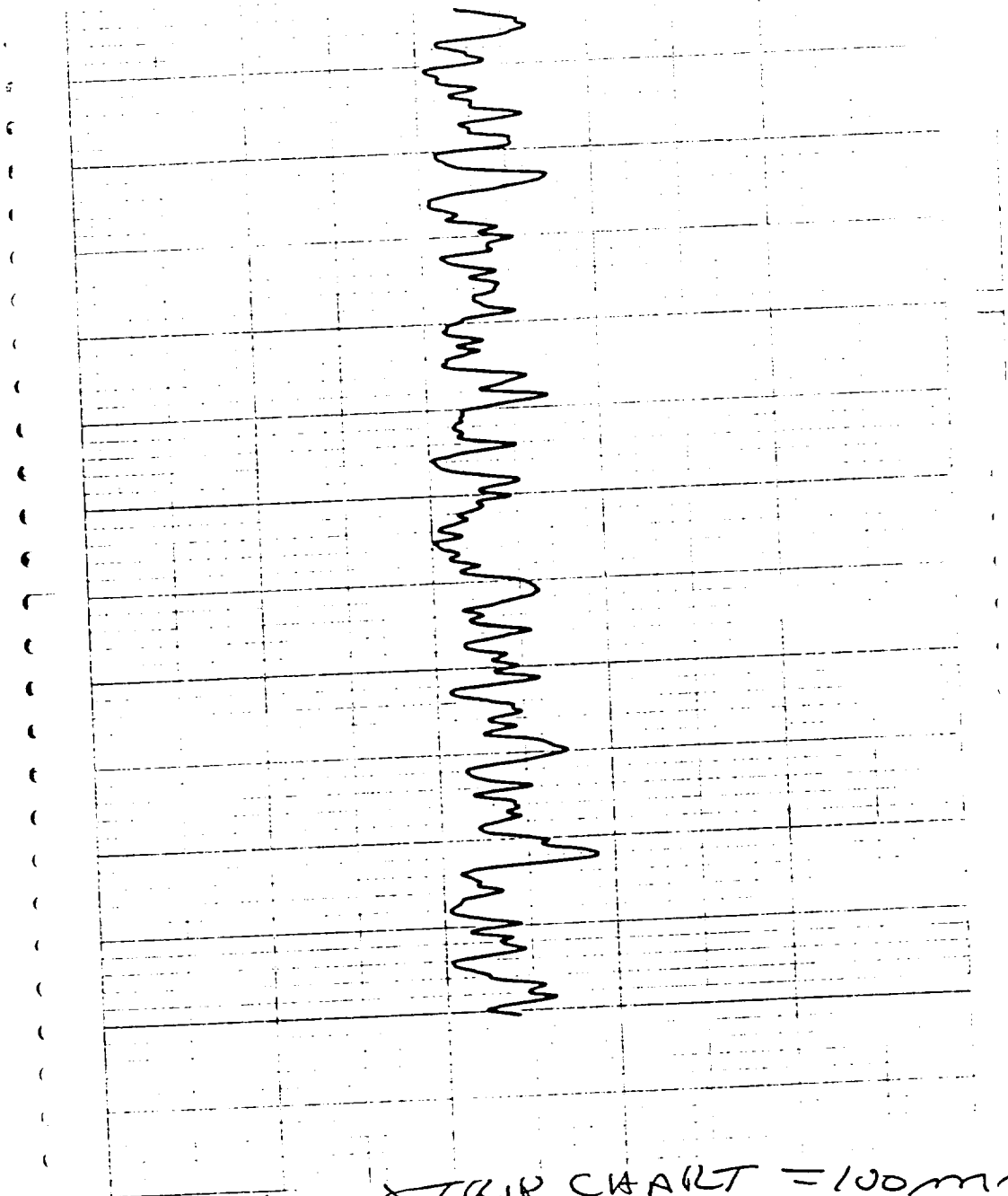

ERROR SIGNAL is equivalent to 2.2 millivolts (p-p) or 0.44 millivolts (r.m.s)

392/:

STRIP CHART = 100 mvolts
SENS = 1 mv x 3
TC = 0.1 sec
POST FILTER = ON
DIFFUSE = AUTO

EQUIVALENT INPUT: $\frac{9\ div}{500\ div} \times \frac{100 \times 10^{-3}}{10} \times 3 \times 10^{-3}$

$= 5.4\ \mu volts \Rightarrow \frac{5.4\ \mu v/6}{2.64\ mv/3\ mille} = 0.4$

this check-out the magnetometer was moved to the Polatomic Magnetics Laboratory. The LNA laser was integrated into the magnetometer in the instrument building which was used during preliminary testing. Light from the horizontally mounted LNA laser was directed down the center of the PVC tubing and through the cell (along the earth's field) by means of a gimballed minor as shown in Figure 5.1.

6.0 LASER PUMPED SCALAR MAGNETOMETER EVALUATION

6.1 EXPERIMENT DESCRIPTION

Evaluation of the laser pumped helium magnetometer was carried out using the LNA optical bench laser described in Section 4.0 as the optical pumping source and the digital resonance spectrometer. A simplified block diagram of the experimental equipment used during Polatomic's evaluation of the breadboard LNA laser pumped magnetometer is presented as Figure 6.1.

The set-up procedure included preliminary tuning of the LNA optical bench laser, adjusting and measuring the laser power and fine tuning the laser wavelength to produce fluorescence. A separate helium cell operated at relatively high discharge level by an independent r.f. transmitter was used to make the preliminary bench test for fluorescence. An additional procedure was developed to prove effective fine tuning of the laser. The ultra stable digital oscillator (DO) was set to the known magnetic resonance frequency minus or plus half of the resonance linewidth. An error signal was observable on the oscilloscope as the frequency alternated about the resonance line center at a 400 Hz rate. Fine tuning of the LNA laser with the etalon maximized the signal to noise ratio visually by peaking the resonance line for improved results after tuning with the fluorescence method. Although the laser was not rechecked for power or retuned for wavelength after each experiment, the dc level at the output of the photodetector amplifier was used as a rough monitor of laser power. The resonance signal could be observed to provide noise and magnitude clues to deterioration of the laser tuning. When deterioration was detected, the laser was readjusted and its power remeasured. Periodically the laser power was rechecked and/or readjusted to restore confidence in its condition regardless of indications.

Software designed into the digital resonance spectrometer permitted scanning over a wide range of resonance frequencies to perform an initial search for the magnetic resonance line. The presence of optical pumping signals was previously established by

FIGURE 6.1 - BLOCK DIAGRAM OF LAB MAGNETOMETER AND DIGITAL RESONANCE SPECTROMETER

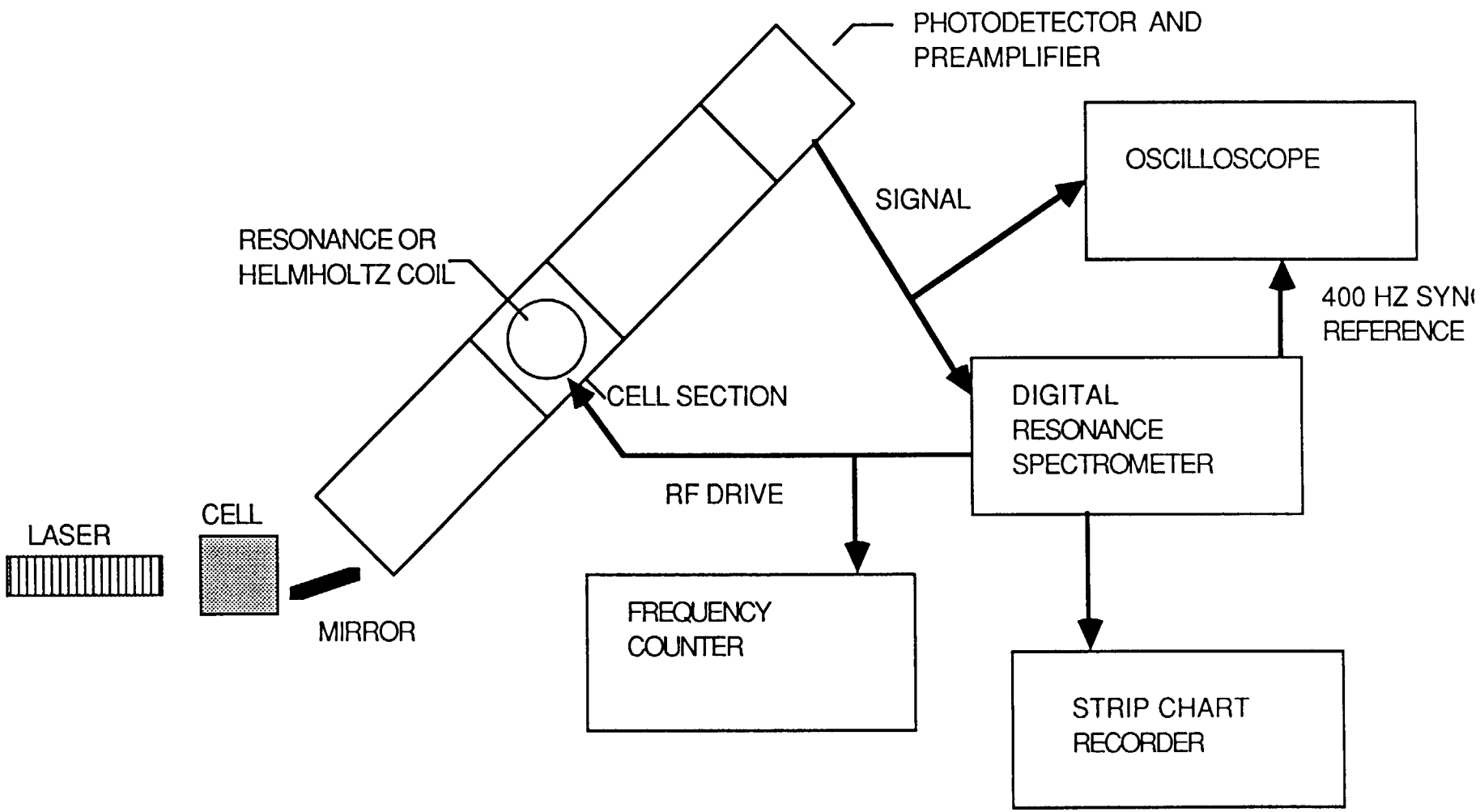

an experiment using built-in transverse Helmholtz coils. However, the magnetic resonance line must be found experimentally to allow optimization of the r.f. drive level.

The digital resonance spectrometer permits keyboard control of the frequency sweep range and starting frequency. If an appropriate fm offset much greater than the resonance linewidth is programmed into the digital oscillator during search, an undifferentiated resonance line can be plotted by connecting the lock-in amplifier (tuned to the fm frequency) output to a strip chart recorder. Gain adjustments were made by fixing the strip chart gain to 10 volts pk-pk and adjusting the overall gain at the lock-in amplifier sensitivity setting. The lock-in amplifier provides 10 volts output for each sensitivity setting.

Figure 6.2 shows a typical example of the resonance line measured by an fm scan by the digital oscillator. Similarly by setting the fm sweep width to a value small compared to the linewidth a strip chart of the differentiated resonance curve could be produced. Figure 6.3 presents a typical example of the differentiated resonance line.

Optimization of the cell level, resonance drive r.f. level, and sweep width level were attempted using both the resonance line and the differentiated resonance line. The laser was operated with no closed loop control for either laser power or laser wavelength. Periods of relative laser stability allowed a single experiment to be performed, however, difficulty was usually encountered when attempting to repeat the experiment to verify an observed difference in response to an increment of change in a parameter being optimized.

6.2 EXPERIMENTAL RESULTS

We used this setup to observe the resonance line during periods of best laser stability. The "best effort" resonance line with optimized cell r.f. level was differentiated. Figure 6.4 presents a "best effort" result of the differentiated resonance line. Evaluation of the LNA laser pumped magnetometer included the noise measurements necessary to prepare a summary noise audit on the total digital resonance

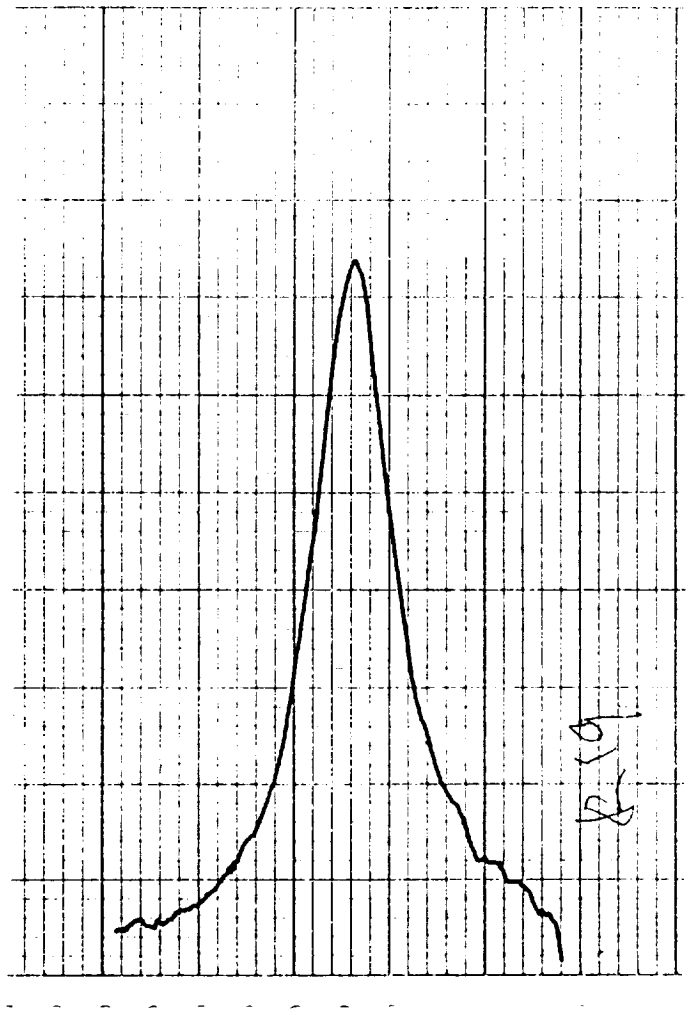

FIGURE 6.2 - TYPICAL LASER PUMPED MAGNETOMETER RESONANCE LINE OBSERVED BY FM SCAN OF DIGITAL OSCILLATOR

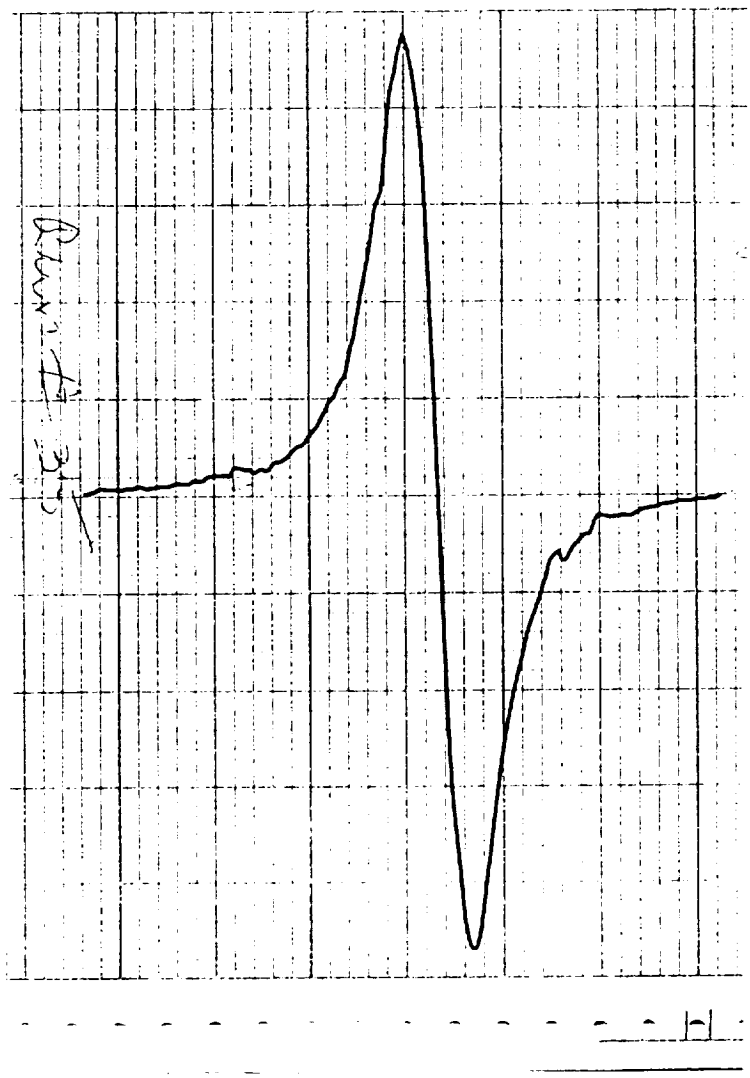

FIGURE 6.3 - TYPICAL DIFFERENTIATED LASER PUMPED MAGNETIC RESONANCE LINE BY NARROW FM SCAN OF DIGITAL OSCILLATOR

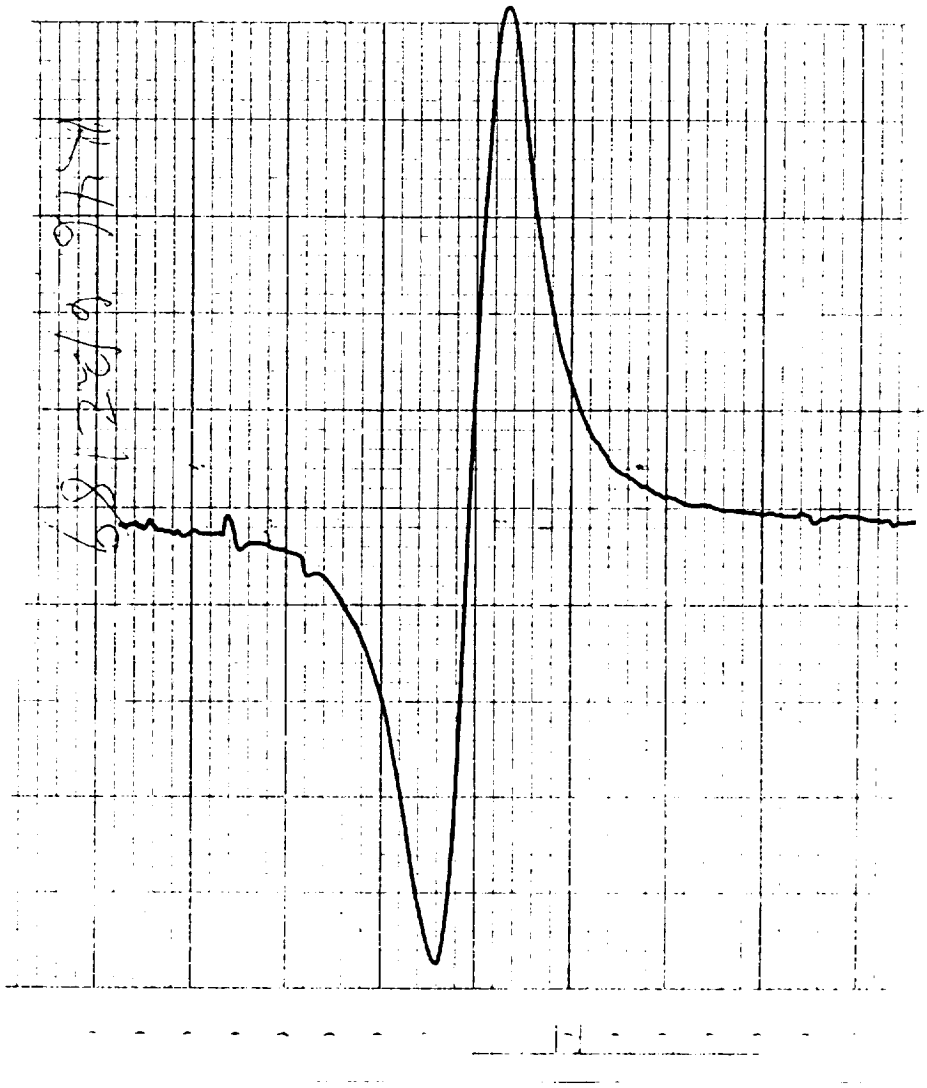

FIGURE 6.4 - OPTIMIZED LASER PUMPED DIFFERENTIATED MAGNETIC RESONANCE LINE

spectrometer. The technique involved making a five minute noise run for each of the following conditions:

- Shorted lock-in amplifier input (system noise floor)

  SEE 6/23/89,

  RUN #11: 0.053 picoampl/√Hz

- Dark current noise (photodetector noise floor)

  SEE 6/23/89,

  RUN #14: 6.65 picoamps/√Hz

  RUN #15: 5.32 picoamps/√Hz

  RUN #17: 3.19 picoamps/√Hz

- Adjusted cell only (resonance spectrometer noise floor)

  SEE 6/23/89,

  RUN #16: 5.06 picoamps/√Hz

  RUN #39: 7.98 picoamps/√Hz

- LNA laser plus cell

  SEE 6/23/89,

  RUN #12: 1165 picoamps/√Hz

  RUN #36: 279 picoamps/√Hz

- LNA laser plus adjusted cell (laser magnetometer noise floor)

  SEE 6/23/89,

  RUN #13: 1029 picoamps/√Hz

  RUN #38: 1117 picoamps/√Hz

- O Locked-loop magnetometer (laser pumped magnetometer noise including response to ambient magnetic changes)

  SEE 6/22/89, RUN #52

The results from the above cited measurements are presented in Figure 6.5.

6.3 SCALAR MAGNETOMETER

One run was made using the DO set at a fixed center frequency at the nominal center of the helium resonance as measured by the locked-loop frequency and confirmed by observation of the error signal on the oscilloscope, i.e. a second harmonic of the 400 Hz square wave sweep. An uncalibrated bar magnetic was placed at a distance from the helium cell with its center approximately on a horizontal east-west line from the center of the cell and rotating at 2 rpm in the north-south plane. The magnet has been calibrated to be 2324 cgs in magnet moment. The magnitude of the signal observed with this magnet rotating at 91 inches is 18.8 nT pk to pk as shown in Figure 6.6.

Signal amplitude and linewidth were measured using the data of 6/22/89, RUN #46. The signal amplitude was found to be 541,125 picoamps pk-pk, or 1.2 milliwatts pk-pk input optical power. The linewidth was found to be 795 nT. The tests were done in the instrumentation building of the Polatomic Magnetics Laboratory at the University of Texas at Dallas in order to accommodate the breadboard laser. Gradients sufficiently large to broaden the resonance line were expected and observed. Plans to move a remote head shack with the magnetometer head and a separate one for the laser failed to be implemented before the contract completion date.

Based upon the observed signal amplitude, resonance linewidth, and the noise audit the following sensitivity calculations were made:

- O Actual (measured linewidth and noise)

  $S/N = 1.94\ 10^3$ $\qquad$ $SENS = 4.10\ 10^{-1}\ nT/\sqrt{Hz}$

- O Noiseless light source (100 nT linewidth and cell only noise)

  $S/N = 1.07\ 10^5$ $\qquad$ $SENS = 9.35\ 10^{-4}\ nT/\sqrt{Hz}$

FIGURE 6.5 - MEASUREMENT DATA

LASER POWER AND ABSORPTION DATA

COMPUTATION OF OPTICAL POWER AND ABSORPTION

DARK DC VOLTS: 1

DATE	RUN	CELL OFF DC VOLTS	CELL MAX DC VOLTS	MAX ABSORPTION	CELL ADJUSTED DC VOLTS	ADJ ABSORPTION	I1/I2	IN WATTS
6/22	1	2.1	N/A	N/A	1.9	18.2%	81.8%	2.06×10^{-3}
6/22	9	2.7	N/A	N/A	2.5	11.8%	88.2%	2.65×10^{-3}
6/22	10	2.7	N/A	N/A	2.3	23.5%	76.5%	2.65×10^{-3}
6/22	15	2.0	N/A	N/A	1.8	20.0%	80.0%	1.96×10^{-3}
6/22	20	2.3	N/A	N/A	1.9	30.8%	69.2%	2.26×10^{-3}
6/22	24	2.3	N/A	N/A	2.0	23.1%	76.9%	2.26×10^{-3}
6/23	4	2.2	1.3	75.0%	2.0	16.7%	83.3%	2.16×10^{-3}
6/23	18	2.9	1.9	52.6%	2.5	21.1%	78.9%	2.85×10^{-3}

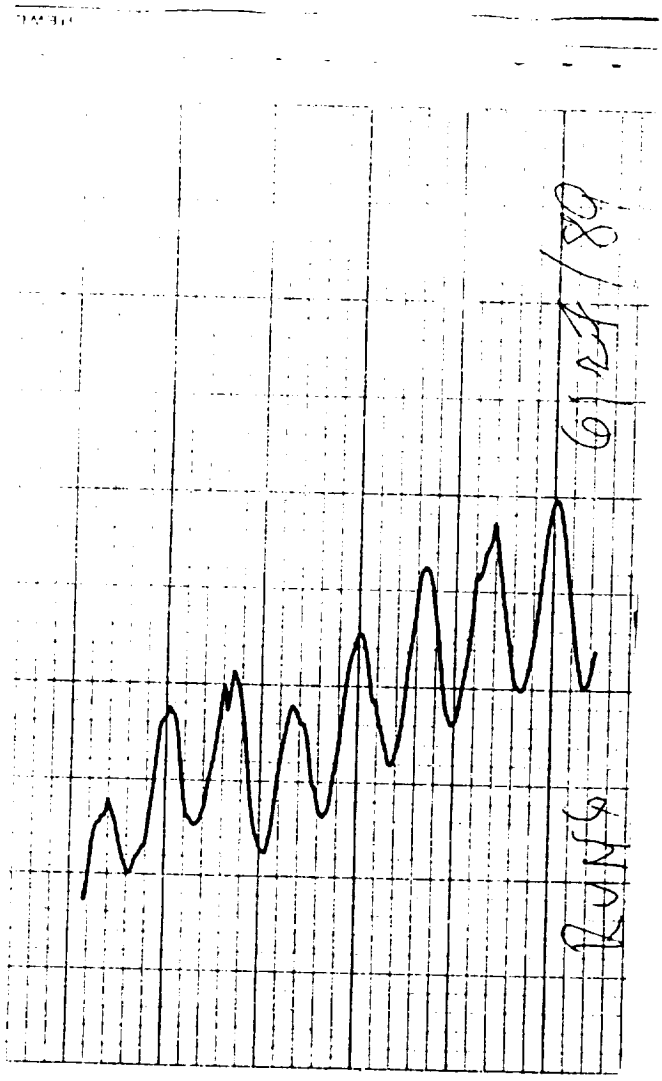

FIGURE 6.6 - Calibration Signal

- Dark noise limit (100 nT linewidth and photodiode blocked)

  S/N = 1.70 10^5 SENS = 5.90 10^{-4} nT/$\sqrt{Hz}$

- Photodiode limit (100 nT linewidth and photodiode dark noise specification)

  S/N = 2.71 10^6 SENS = 3.70 10^{-5} nT/$\sqrt{Hz}$

A summary of equivalent input optical power and absorption measurements are listed in Figure 6.5 based on transmission characteristics of the circular polarizer, the unexcited cell, and a neutral density filter used following the cell to bring the post cell intensity into the linear operating range of the detector. These attenuations were measured and were found to be: polarizer = 0.5, cell = 0.817, neutral density filter = 0.462. The cell-on optical power divided by the cell-off optical power was computed to give the I1/I2 result in the Figure 6.5. The quantity measured was the dc volts at the output of a transimpedance amplifier coupled to the photodiode. The specification values of transimpedance (12000 ohms) and responsivity (0.45 amps/watt) were used in the equivalent input power computations. The dc level with the photodetector dark is 1.0 volts. Actual optical levels were determined by subtracting this value from the measured dc volts. Neutral density filters were used to modify the input optical power to observe effects of power on the linewidth. No hole-burning or line broadening effects were observed, indicating that higher levels of laser power at 1083 nm could be effectively used to improve signal size.

6.4 CONCLUSIONS

An LNA laser emitting at 1083 nm was used to optically pump a helium absorption cell and observe the helium magnetic resonance used in scalar helium magnetometers. The optical power of the lamp exceeds 1 mW at 1083 nm and is greater than that of a typical helium lamp. The LNA laser has noise in excess of the next lower limit, i.e. the adjusted absorption cell, by a factor of 50.7. It is considered that three orders of magnitude or more improvement in laser noise may be possible with closed-

loop control of optical power and wavelength. To meet the 1.0 nT design goal, laser noise must be reduced to approximately 2 picoamps/$\sqrt{Hz}$. This would produce a S/N of approximately 10^5 and would produce a sensitivity of 10^{-3} nT/$\sqrt{Hz}$. The improvement in optical power and in pumping efficiency in the current evaluation is offset by the excessive laser noise. The noise contributions from wavelength variation and from laser optical power variations were not separable during this evaluation.

7.0 ADVANCED TECHNIQUES USING LASER PUMPING: OPTOGALVANIC EFFECT

7.1 INTRODUCTION

In Section 7.0 we describe the investigation of a newly observed phenomena, the optogalvanic effect in laser pumped helium. It was our stated objective to investigate the AMOP (amplitude modulated optical pumping) effect as a possible new technique for monitoring magnetic resonance signals in optically pumped helium. The AMOP phenomena was observed using the optogalvanic effect which was investigated at the University of Missouri-Rolla under this contract. Initially it was anticipated that the AMOP drive signal could be generated by modulating the laser in some direct manner in order to produce a laser output modulated at the Larmor frequency (the order of 1.5 MHz). It was observed that the diode laser could be modulated at these frequencies, but the LNA relaxation times were too long to allow modulation of the output beam at this high a frequency. The AMOP beam was instead chopped with an electro-optic modulator.

7.2 OPTOGALVANIC SIGNALS

The optogalvanic effect is the name applied to impedance changes in a discharge plasma produced by a modification of the equilibrium populations. It has been effectively used in the determination of spectroscopic constants and plasma properties.[1,2,3] Typically it involves the interaction of a light beam containing resonant photons with the atoms in one or more excited states of the plasma. As the level population is modified by the optical excitation, the effective ionization potential of the plasma is modified, and the discharge current changes.

The effect is most easily described when metastable levels in the system are involved. For example, if resonant photons from a discharge helium lamp at 2μ are incident on a helium discharge cell, the singlet metastable 2^1S_0 density is quenched:

$$He(2^1S_0) + h\nu \rightarrow He(2^1P_1) \rightarrow He(1^1S_0) + h\nu' \qquad (1)$$

The effective ionization potential is changed and the electron density in the plasma is reduced. Thus, the discharge impedance increases. If the triplet metastable atom (2^3S_1) is excited with radiation at 1083 nm, a transition to the ground state cannot occur, and the ionization potential is reduced: the discharge current increases.

This effect can be sufficiently summarized by the reaction

$$He^* + e \rightarrow He^+ + 2e \qquad (2)$$

If the He^* density is modified as a consequence of optical excitation, the electron density changers along with the cell impedance. For the purposes of this report we will call this mechanism an intensity modulated optogalvanic effect (IMOGE).

An important contribution to the electron density in a weak helium discharge is the collisional quenching of the helium metastable atoms in Penning ionization:

$$He^m + A \rightarrow He + A^+ + e \qquad (3)$$

where A is some atom or molecule whose ionization potential is less than the 19.8 eV internal energy of the $He(2^3S_1)$. Of particular interest is the case in which the $He(2^3S_1)$ also plays the role of species A. This penning ionization process has a particularly large cross-section, 10^{-14} cm^2 and under appropriate discharge conditions may be the primary source of electrons in the discharge.[4]

In the following sections we consider the special case of the Penning process:

$$He(2^3S_1\uparrow\uparrow) + He(2^3S_1\uparrow\uparrow) \rightarrow He(1^1S_0\uparrow\uparrow) + He^+(1^2S_{1/2}\uparrow) + e\downarrow \qquad (4)$$

which is forbidden as shown since it does not conserve spin angular momentum.[5] It should thus be possible to modulate the electron density, hence cell impedance, by modulating the orientation of the helium metastable atom spins in the discharge cell, or (SMOGE). In this experiment the spin orientation of the $He(2^3S_1)$ state is prepared by optical pumping with a tunable IR laser.[6]

7.3 EXPERIMENTAL SETUP

The schematic representation of the experimental apparatus is shown in Figure 7.1. The cell impedance is monitored by measuring the discharge current indirectly. A

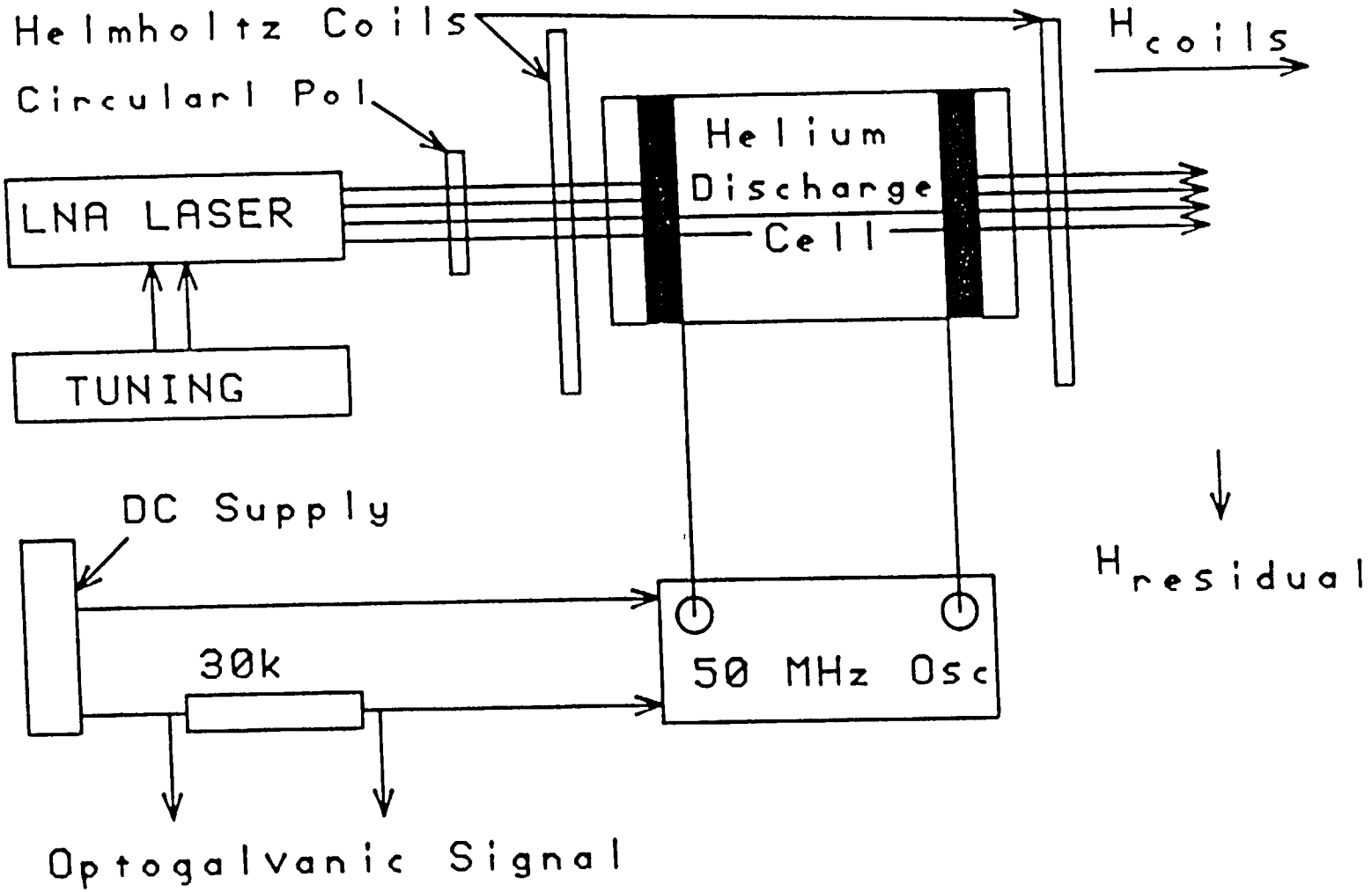

FIGURE 7.1 - Optical Pumping Apparatus for Helium 4 Optogalvanic Signal

dc voltage powers the 50 MHz oscillator through a 30Ω resistor. As the cell impedance varies, the drive current is modified inducing a voltage change across the resistor. The tunable laser used is our Nd-doped $LaMgAl_{11}O_{19}$ crystal (LNA) which is end-pumped by a 500 mw GaAlAs diode laser. Several milliwatts of laser emission at the 1083 nm helium wavelength are available in a single longitudinal mode. When this radiation is incident on the discharge cell and tuned to the resonance wavelength of helium both of the two types of optogalvanic signals IMOGE and SMOGE can be observed.

The conventional optogalvanic signal, (IMOGE) is obtained by intensity modulating the laser beam. The helium metastable density is thus modified and according to reaction (2), the cell impedance is modulated synchronously with the laser intensity.

In order to observe the spin-modulated signals, the laser output is circularly polarized and directed into the helium discharge cell, along the axis of an externally applied magnetic field. The magnetic field of several gauss is generated by a Helmholtz pair. A residual magnetic field of approximately 0.5 gauss is applied along an axis orthogonal to the laser pump beam. When the Helmholtz coils are energized, the resultant field is along the pump beam direction. When the coil current is zero, the resultant magnetic field is perpendicular to the laser pump beam. Thus, alternately activating the Helmholtz coil, alternately polarizes then depolarizes the $He(2^3S_1)$ atom ensemble. The reaction rate for reaction (3) is then modulated synchronously with the current in the field coils. The cell impedance is modulated accordingly.

7.4 EXPERIMENTAL RESULTS

With approximately 1 mw cm^{-2} of tunable laser power near 1083 nm intensity modulated at 200 Hz, the IMOGE signals of Figure 7.2 are obtained as the laser is tuned through the $D_0(2^3S_1 - 2^3P_0)$, $D_1(2^3S_1 - 2^3P_1)$, and $D_2(2^3S_1 - 2^3P_2)$ transition at 1082.908 nm, 1083.025 nm and 1083.034 nm respectively. The fractional change in the supply current is a 3.5×10^{-5}. The single mode laser bandwidth is approximately 10 MHz. The

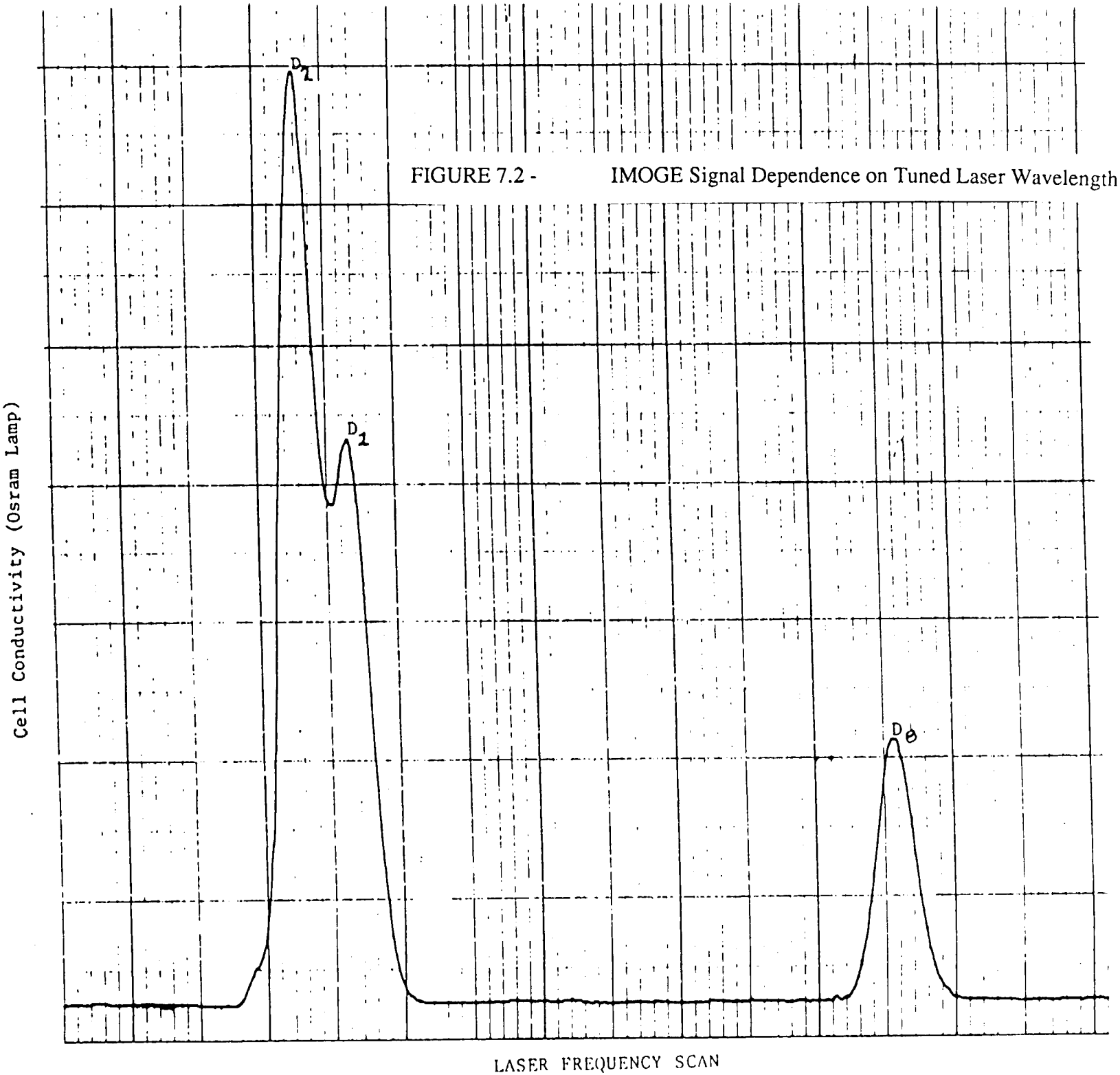

FIGURE 7.2 - IMOGE Signal Dependence on Tuned Laser Wavelength

separation between the D_1 and D_2 transition is about the Doppler width of the helium absorption line and is thus incompletely resolved.

When the laser emission is now circularly polarized and directed onto the helium discharge cell with the applied field parallel to the pump axis, the metastable atoms are oriented with their electronic spins along the field direction. The coil current is now modulated and the magnetic field switches between the H_{coil} and the $H_{residual}$ shown in Figure 7.1. The effect of this modulation is to alternately polarize and then depolarize the helium spins. There is no intensity modulation of the laser pump beam. The process of Eq. (4) is now active. The impedance change, SMOGE, accompanying this spin modulation as the laser is tuned as described above is shown in Figure 7.3. The fractional change in the supply current is approximately 5.0×10^{-3}, a factor of 100 times larger than the IMOGE signals. The metastable polarization, defined as $(N\uparrow - N\downarrow)/(N\uparrow + N\downarrow)$ is approximately 0.1. It is clear from these observations that $He^* - He^*$ collisions dominate the ionization mechanism under weak discharge conditions.

An interesting variation of the SMOGE signals can be obtained by forcing the helium magnetization to coherently precess at the Larmor frequency. This can be accomplished with a technique introduced by Bell and Bloom.[7] If the laser pump beam is circularly polarized and incident on the discharge cell along a direction perpendicular to the magnetic field, no metastable polarization occurs. If, however, the laser beam is intensity or polarization modulated at the Larmor frequency of the $He(2^3S_1)$ atoms, corresponding to 2.8 MHz $Gauss^{-1}$, the magnetization is driven coherently to precess about magnetic field direction. The metastable atoms are polarized as before but now they are coherently precessing. The reaction of Eq. (4) remains operative and SMOGE signals may be observed as the modulation frequency is changed from the Larmor frequency.

A Bragg acousto-optic modulator was used to intensity modulate the laser pump beam at 1.4 MHz, the resonance frequency in the 0.5 Gauss residual magnetic

FIGURE 7.3 - SMOGE Signal Dependence on Tuned Laser Wavelength

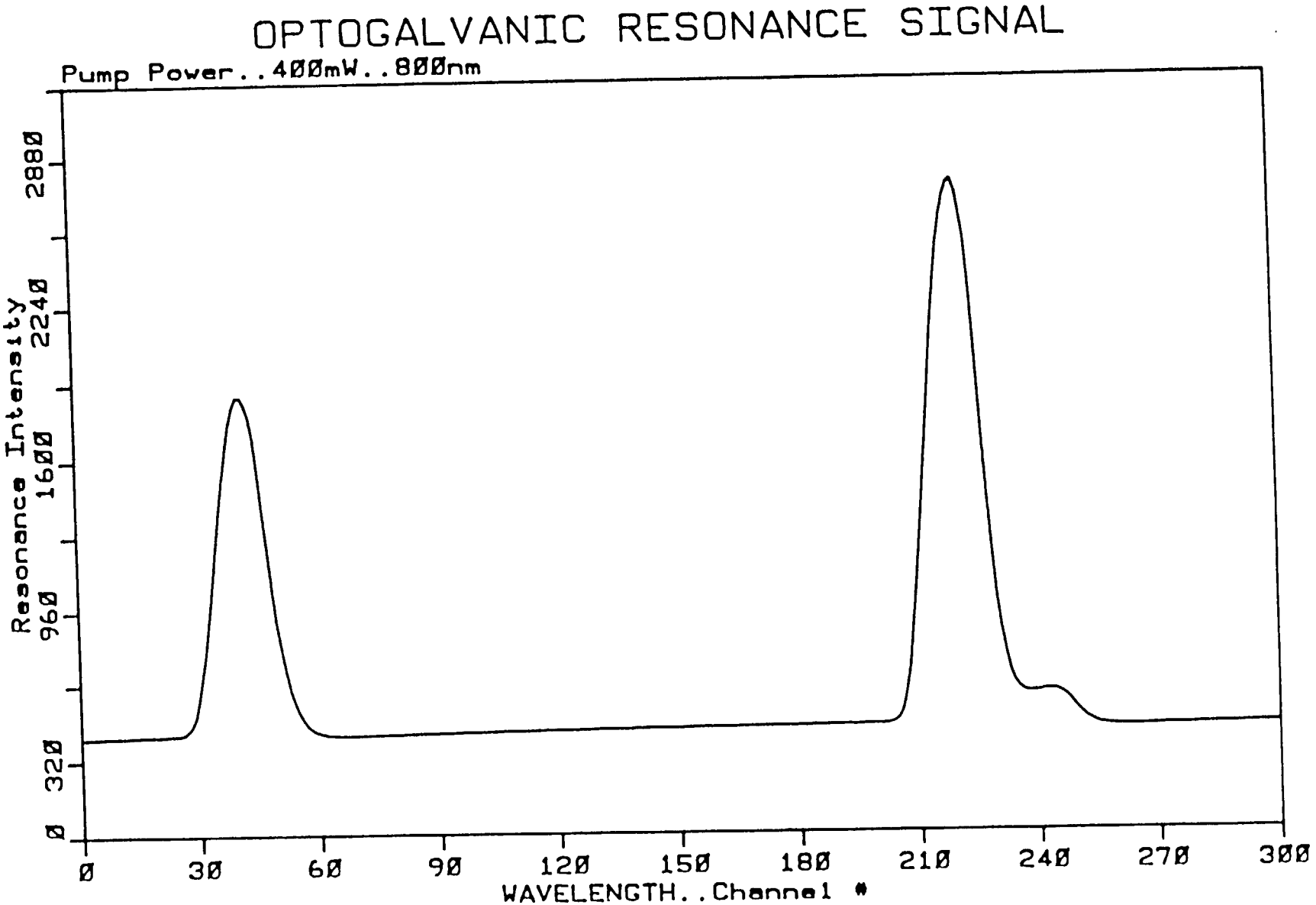

field. As the frequency of the Bragg modulator is scanned through the resonance condition, changes in the cell impedance are observed as shown in Figure 7.4. No impedance changes at this frequency are observed due to the intensity modulation of resonance. These signals were comparable in strength to the spin modulation signals.

It should be mentioned that the transverse modulation pumping signals may be observed optically as well. Comparable signals are observed. The transverse pumping scheme has much to recommend it since an rf resonance coil with its attendant broadening of the resonance signal is absent.

7.5 APPLICATIONS

One of the important applications of spin polarized ensembles of metastable He^4 is in magnetometry.[8,9,10] Extremely sensitive magnetic field measuring devices can be constructed, typically having sensitivities at 1 part in 10 million level. Such optically pumped helium magnetometers have been used to indicate the presence of submarines when towed in a drone above the sea and to measure planetary and interplanetary magnetic fields when installed in space probes.

Typically the magnetometers monitor the intensity of the pump light beam after it traverses the cell. Contributions to the noise can thus arise from intensity fluctuations in the light beam. The laser pump sources are considerably more efficient in the optical pumping process, offering the potential of 100-fold improvements in sensitivity; however, they are intrinsically noisier than discharge sources. At the present time the major obstacle to fully exploiting the potential of laser pumped magnetometers is this noise problem.

If, instead of observing magnetic resonance signals with the transmitted light intensity, one monitors the cell impedance as described herein, the contribution to the noise spectrum of the resonance signal due to amplitude fluctuations of the laser pump source is significantly diminished. As a practical matter, the optical diodes used to monitor the optical pumping signal are no longer necessary. We also observe that useful

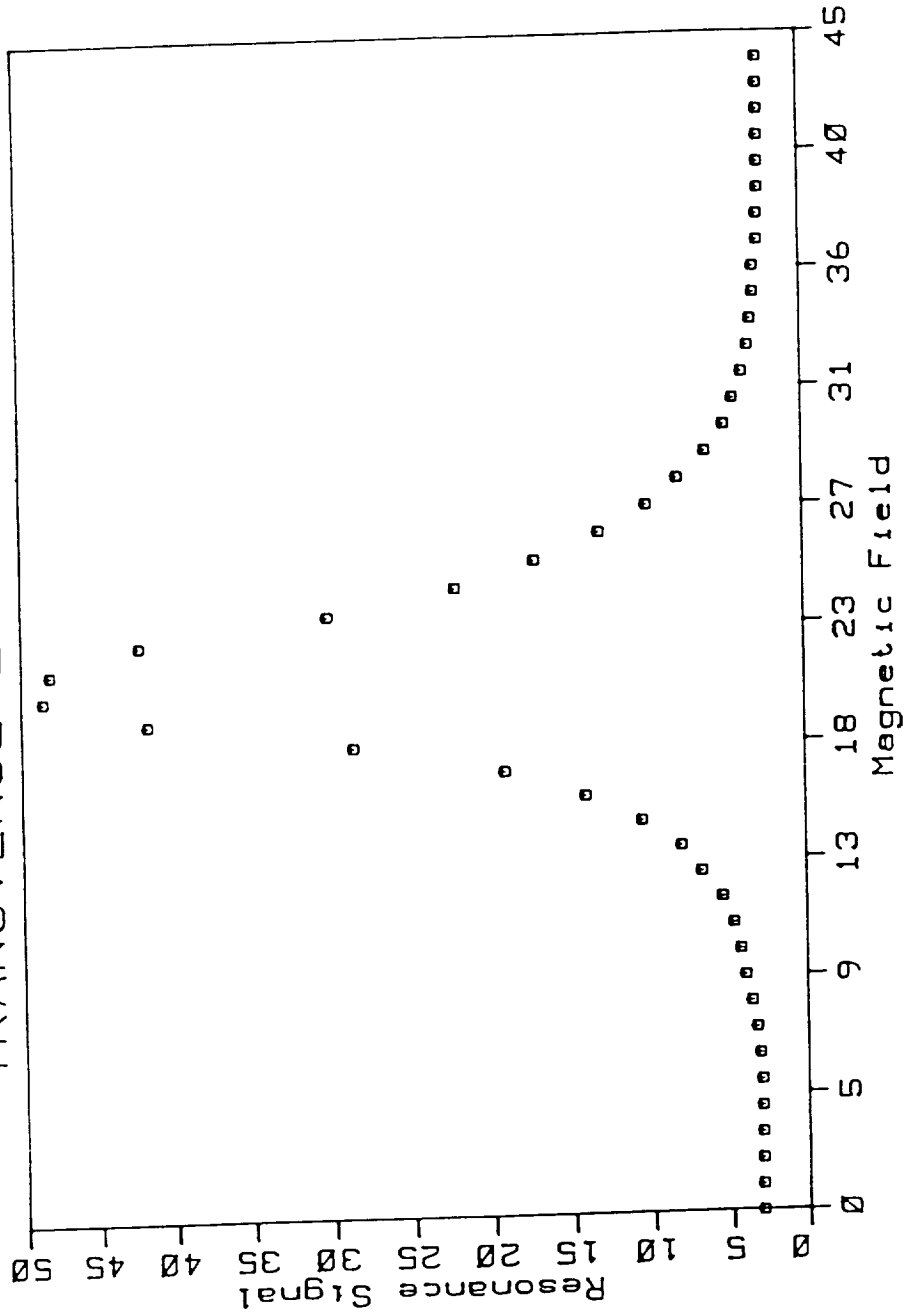

FIGURE 7.4 - Optogalvanic Signal for Transverse Laser Optical Pump with Amplitude Modulated Laser Beam

magnetic resonance signals with this method are obtained down to the threshold level of the LNA laser. At this point the conventional transmitted magnetic resonance signals are not observable. Further, if the transverse pumping scheme described above is also utilized, the resonance magnetic field coil with its attendant line broadening is also eliminated, providing further simplification. Such demonstrations are currently being evaluated.

REFERENCES -SECTION 7

1 R. B. Green, R. A. Keller, G. G. Luther, P. K. Schenk, and J. C. Travis, Appl. Phys. Lett. 29, 727 (1976).

2 J. E. Lawler, Phys. Rev. A22, 1025 (1980).

3 L. Julien and M. Pinard, J. Phys. B; At. Mol. Phys. 15, 2881 (1982).

4 L. D. Schearer and L. A. Riseberg, Phys. Lett. 33A, 325 (1970).

5 J. C. Hill, L. L. Hatfield, N. D. Stockwell, and G. K. Walters, Phys. Rev. A5, 189 (1972).

6 J. Hamel, A. Cassimi, H. Abu-Safia, M. Leduc, and L. D. Schearer, Opt. Commun. 63, 114 (1987).

7 W. E. Bell and A. L. Bloom, Phys. Rev. Letters 6, 280 (1961).

8 J. A. Rice, A. Keyser and L. D. Schearer, J. Geophys. Res. 66, 4163 (1961).

9 A. M. A. Fransden, B. V. Conner, J. Van Amersfoort, and E. J. Smith, Trans. Geo. Electron. GE-16, 195 (1978).

10 R. E. Slocum, L. D. Schearer, P. Tin and R. Marquedant, J. Appl. 64, 6613 (1988).

CONCLUSIONS

SUMMARY

We have successfully demonstrated single line optical pumping of helium 4 magnetometer cells. Laser pumped helium has been examined in both the parametric resonance mode used in the Vector Helium Magnetometer (VHM) and the paramagnetic resonance mode used in the Scalar Helium Magnetometer (SHM). A digital resonance spectrometer was designed and built. This instrument can be used as a rf spectrometer to investigate optically pumped magnetic resonances in helium. It was also used to observe magnetometer operation in both the open-loop and the closed-loop mode. Finally, the DRS can be used in the future to operate as a dual cell gradiometer for investigating light shifts and offsets.

A solid-state laser tunable at 1083 nm was developed as a light source for single line pumping experiments. The choice of Nd-doped LNA crystals pumped by a high brightness diode laser was made after a thorough investigation of laser crystals and pumping sources. Our investigation of laser pumped signals in helium 4 revealed signal strength that was 45 times that achieved with a conventional electrodeless discharge helium lamp used to pump space magnetometers. However, the laboratory LNA laser has a noise level which is considerably greater than the noise level of the helium lamp. If the noise level can be reduced by a factor of 50, it appears feasible to construct a laser pumped magnetometer with a minimum detectable signal of 1 pT or better. This noise reduction task would be approached by modular packaging of the laser components in a rigid optical mount free from microphonics.

We have demonstrated amplitude modulated optical pumping (AMOP) where the laser beam is modulated at the Larmor frequency to drive the magnetic resonance. This would allow removal of the rf drive coils at the sensor. We also demonstrated the optogalvanic effect in laser pumped helium which would do away with the need for optical detectors. A laboratory LNA diode pumped laser was developed and assembled

for delivery to JPL. This laser is intended for continued investigation and demonstration of laser pumped magnetometers. The laboratory laser must be manually tuned, but has sufficient stability to observe laser pumping and magnetometer operation.

PHASE III PROJECT TECHNICAL OBJECTIVES

Based on the progress of the Phase II Project in demonstrating the concept and feasibility of laser pumped helium magnetometers, the following technical objectives must be met in Phase III to produce a prototype laser pumped magnetometer with improved sensitivity and accuracy as well as reduced power requirements.

1. Low Noise Tunable Solid-State Laser for 1083 nm - The tunable solid-state laser must be developed to the point where the noise is reduced by packaging improvements and by feedback controls. The design goal is a minimum detectable signal of 1 pT or better and should be readily achievable based on the observed laser pumped resonance signal strength.

2. Light Shift Reductions - Techniques must be identified for using the single line pumping characteristics of the laser to reduce both real and virtual light shifts in order to improve the overall accuracy of the helium magnetometer. Theory predicts that both shifts can be eliminated by selective line tuning. These light shifts can be observed using the DRS.

3. Closed-Loop Wavelength Control - A servo control unit must be developed which will tune the wavelength of the laser to the helium resonance at 1083 nm. The tuning accuracy requirement is set by the results of the light shift measurements and the requirement to maintain maximum signal size. Tuning technique using etalon rotation and piezoelectric modulation has been demonstrated in the laboratory.

4. Optimization of Magnetic Field Data Extraction - The unique properties of laser pumping must be utilized to devise the optimum design for both the VHM mode and SHM mode of operation as well as the hybrid mode which combines the two in a single instrument.

5. Digital Electronics Package - The laser magnetometer electronics must be a digital design based on the digital oscillator included in the DRS. A digital design is required to exploit the potential sensitivity of the laser pumped sensor.

Nd:LNA laser optical pumping of ^{4}He: Application to space magnetometers

R. E. Slocum
Polatomic, Inc., Dallas, Texas 75248

L. D. Schearer and P. Tin
University of Missouri-Rolla, Physics Department, Rolla, Missouri 65401

R. Marquedant
Jet Propulsion Laboratory, Pasadena, California 91109

(Received 31 May 1988; accepted for publication 7 September 1988)

We have observed Hanle signals and $n = 0, p = 1$ parametric resonances of 2^3S_1 metastable helium atoms in a discharge cell by optically pumping the helium atoms with a tunable Nd:LNA laser. These resonances were used to construct a sensitive magnetometer for the measurement of very small magnetic fields. Since magnetometer sensitivity is proportional to the slope of the parametric resonance signal (signal amplitude divided by linewidth), the slopes for single-line laser pumping were compared with similar quantities obtained from conventional helium lamp pumping. Laser pumping yielded 45 times greater slopes with comparable power requirements, thus establishing the potential for developing ultrasensitive resonance magnetometers using single-line laser pumping.

I. INTRODUCTION

Optically pumped helium magnetometers have been used since the early 1960s to measure interplanetary, planetary, and cometary magnetic fields.[1-3] These instruments use 1083-nm radiation from an rf electrodeless discharge helium lamp to optically pump a sample of 2^3S metastable helium atoms. The pumping radiation consists of the three spectral lines D_0, D_1, and D_2 around 1083 nm corresponding to the 2^3S-$2^3P_{0,1,2}$ transitions. The pumping beam both optically polarizes the sample and monitors the ensemble polarization.[4]

A rate equation analysis of the optical pumping process predicts the inefficiencies resulting when the ensemble is pumped by the natural output from a helium discharge lamp. The optical pumping signal, defined as the change in the transmitted light that occurs when the sample goes from the pumped to the unpumped condition, consists of the contributions from each of the three spectral components present in the lamp, D_0, D_1, and D_2. The D_1 and D_2 components produce signals of opposite polarity and nearly equal intensity so that their contribution to the total signal is negligible.[5] Thus, the fractional change in the transmitted light signal as the sample is pumped by a discharge lamp is typically 0.1%.

An obvious solution is to use a tunable emission-line source to avoid this cancellation. However, until recently there were no lasers available that matched the helium absorption lines at 1083 nm and could be used to test this solution. We have used the recently developed Nd-doped, $La_{1-x}Nd_xMgAl_{11}O_{19}$ crystals pumped by a high-power, cw diode laser to produce tunable emission at 1083 nm[6] in order to evaluate single-line optical pumping for use in high-sensitivity helium magnetometers. Zero-field parametric resonance techniques[7] were used to observe single-line laser pumping and compare the resonance signals with those obtained using conventional helium lamps.

We report here the initial results obtained from laser pumping in a helium magnetometer sensor using the Nd:LNA laser pumped with a high-power diode laser.

II. EXPERIMENT DESCRIPTION

It is more convenient to use parametric resonances rather than paramagnetic resonances to compare resonance signals generated by optical pumping since no rf fields perturb the optically pumped sample.[8] It does, however, require that the experiment be conducted in a region of low magnetic fields. The low-field region found inside a μ-metal room at the magnetic Test Facility at the Jet Propulsion Laboratory was used for our experiments. The shield eliminated the major part of the earth's field and residual fields can be controlled or eliminated using Helmholtz coils within the shield.

The optical pumping apparatus is shown in Fig. 1 and has been described in detail in Ref. 8. The amplitude of the resonance signal for the optically pumped metastable level was measured using the Hanle effect. With the optical pumping apparatus loctated in zero field inside the JPL Magnetic Shield a field H_0 is applied perpendicular to the beam direction. The signal along the pumping beam direction is proportional to M_x, where

$$M_x = M_0/[1 + (\omega_0\tau)^2], \tag{1}$$

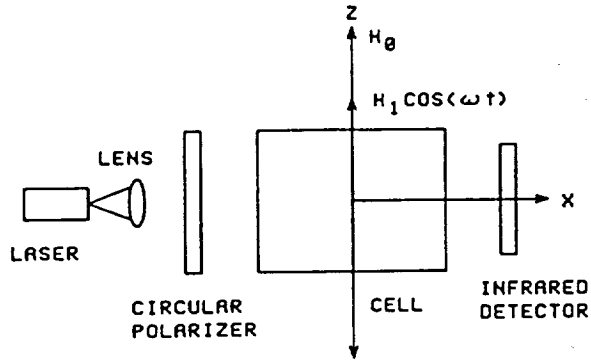

FIG. 1. Schematic representation of the helium magnetometer. The cell containing the helium gas is placed in a nominally zero magnetic field. H_0 and $H_1 \cos \omega t$ are fixed and oscillating magnetic bias fields produced by Helmholtz coils.

 0021-8979/88/246615-03$02.40

and M_0 is the optically induced magnetic moment in the gas, τ is the decay time of M_x, and ω_0 is the Larmor precession frequency.

Since our primary interest in the tunable solid-state laser is a radiation source for single-line optical pumping, a direct comparison of laser-pumped resonance signals and resonance signals produced by radiation from a typical rf electrodeless helium lamp of the type commonly used in helium magnetometers is desirable. The key parameter is the slope of the resonance curve at the inflection points which is proportional to the resonance amplitude divided by the linewidth. This quantity has been shown[8] to be proportional to the slope of the dispersion-shaped curve at zero field for the $n = 0$, $p = 1$ parametric resonance that is observed on the transmitted light beam as a signal proportional to

$$M_x = M_0 J_0\left(\frac{\gamma H_1}{\omega}\right) Jp\left(\frac{\gamma H_1}{\omega}\right) \frac{\omega_0 \tau}{1 + (\omega_0 \tau)^2} \sin p\omega t. \quad (2)$$

The term H_1 is the parametric drive field, which in the present H_1 experiment is a 30-kHz field, was applied perpendicular to the direction of the optical pumping beam. The resonance signal described by Eq. (2) is monitored by the infrared detector with its output directed to a lock-in amplifier tuned to 30 kHz. The lock-in output is displayed on an X-Y recorder. We have demonstrated in an earlier paper that the slope of the dispersion signal is proportional to the minimum detectable signal for a magnetometer operating on this resonance.[7,8] Maximum signal size can be obtained when the amplitude of the 30-kHz drive field is adjusted to the optimum value as determined by the Bessel function solutions to the phenomenological Block-type equation describing the $n = 0, p = 1$ parametric resonance [Eq. (2)].

III. TUNABLE SOLID-STATE LNA LASER

The essential features of the diode-pumped LNA laser are described in Ref. 9. The principal changes in the laser cavity described there and the device used in this experiment are the use of a single 1-W GaAlAs diode, model 304W from SONY Corp., a special coating on the output coupler, which obviated the need for the Lyot filter, and the use of a 50%, 0.25-mm-thick etalon for tuning. With the diode providing a pump power of about 550 mW (1.6 V, 890 mA) the LNA laser output at 1083 nm is typically several mW. The scattered light from a helium cell registered as the laser wavelength is tuned through the resonance lines as shown in Fig. 2. The resolution of the D_1 and D_2 lines shown suggests that the laser linewidth is less than the Doppler width (1.8 GHz).

The laser is easily tuned to each of the three desired transitions and is stable for long periods of time without operator intervention. With the SONY diode operating at maximum output, the laser power at the helium transition exceeded 10 mW. For the experiments described below, the diode was operated with a power input of approximately 1.5 W.

IV. EXPERIMENTAL RESULTS

We were able to observe both the Hanle signals and the $n = 0, p = 1$ parametric resonance by monitoring the pumping radiation passing through the cell. Distinct resonance curves were observed for each of the three lines D_0, D_1, and D_2 even though the D_1 and D_2 absorption line is barely resolved spectroscopically. For comparison of the laser curves with the resonance curves produced by a standard rf electrodeless discharge helium lamp used in space magnetometers, the sample of helium atoms in the standard helium cell was further restricted to a column 42 mm long and 16 mm in diameter. The sample length was set by the cell length and the sample diameter was set by the diameter of the infrared detector.

When the pumping light intensity increases, the resonance line is slightly broadened. It is therefore important to measure not only the amplitude of the resonance of the parametric resonance signal but also the slope at zero field that is effectively the resonance line amplitude divided by the linewidth.

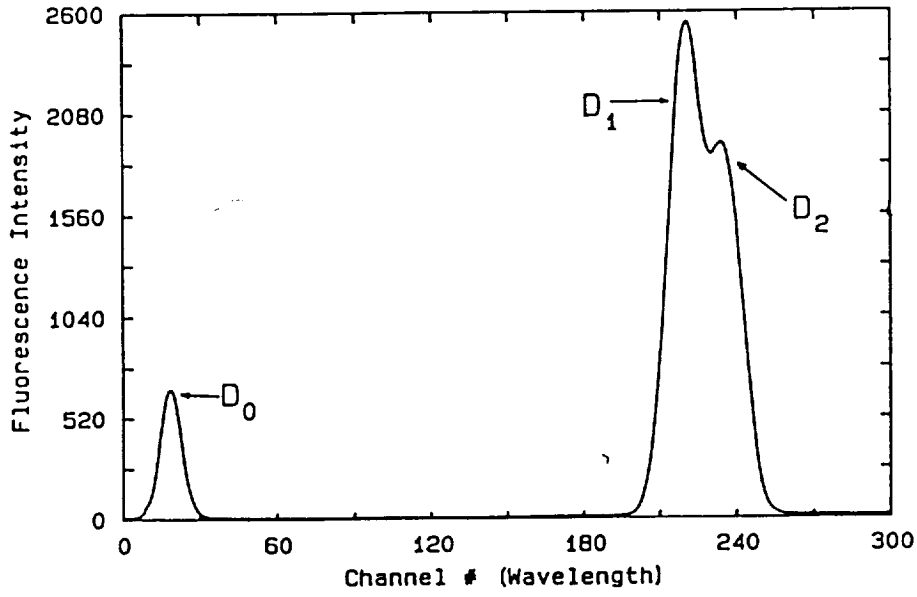

FIG. 2. Shown is the fluorescence spectrum from the He^4 metastable atoms as the laser is scanned through the 2^3S-2^3P transitions. The D_0 to D_1 separation is about 1 Å. The laser frequency is changed by tilt tuning the etalon.

A. Single-line pumping resonance signal amplitude

The amplitude of the resonance signal for the optically pumped metastable level was measured using the Hanle effect. With the optical pumping apparatus located in zero field inside the JPL Magnetic Shield, a field H_0 was applied perpendicular to the beam direction. The oscillating field at 400 Hz has a period greater than the relaxation time of the optically pumped helium. Maximum amplitude must be greater than the half-width of the resonance curve, which is 150 nT. As the field sweeps through zero field, a signal is produced at 800 Hz, which is proportional to the amplitude of the resonance curve. The optical resonance signal was detected by monitoring both the intensity of the pumping beam transmitted through the cell and by monitoring light scattered from the absorption cell in a direction parallel to the direction of the applied magnetic field.

The resonance signal was examined for each of the three helium lines generated by $2P$-$2S$ transition by etalon tuning the laser through lines at 1082.908 nm (D_0), 1083.025 nm (D_1), and 1083.034 nm (D_2). Lines D_1 and D_2 are barely resolved in the absorption cell; however, two separate resonance signals clearly separated by a null were observed. The laser linewidth is estimated to be less than 100 MHz.

For a laser power level of 1.39 mW the relative amplitudes of the Hanle signal measured in the transmission mode are: $D_0 = 0.71$, $D_1 = 1.00$, and $D_2 = 0.16$.

The same resonance was observed by monitoring resonance radiation scattered from the cell normal to the pumping beam direction along the direction of the sweep field. The resonance signal amplitudes have the following ratios: $D_0 = 0.41$, $D_1 = 1.00$, and $D_2 = 0.06$.

The D_1 line is clearly the choice for producing optical pumping signals. In this initial evaluation the D_1 signal for scattered light detection was a factor of 2.3 times larger than the signal for transmitted light detection.

B. Relative resonance slope for magnetic-field measurements

Using the parametric resonance method with a 30-KHz drive field swept about zero field, the slope for a helium lamp pumped signal was compared with the slope for the D_1 laser line, which generated the largest resonance signal. The comparison was made for a volume of the cell defined by the cell length (42 mm) and the diameter of the large-area silicon infrared detector (16 mm), which is approximately 15% of the 32-mm-diam cell's volume. The laser pumped resonance exhibited an observable light broadening; however, the signal amplitude resulted in a slope increase of 45.

V. CONCLUSIONS

We were able to experimentally demonstrate single-line pumping in the 2^3S level of helium 4 and obtain resonance signals more than an order of magnitude greater in strength than those produced by conventional helium discharge lamps. As the diode laser-pumped Nd:LNA laser was tuned through the D_0, D_1, and D_2 transitions, three distinct resonance signals were produced.

Optical broadening of the resonance line as well as the resonance signal amplitude must be taken into account in predicting potential improvements in magnetometers using laser pumping. A direct comparison of the slope of lamp-pumped signals and laser-pumped D_1 signals was made using the $n = 1, p = 1$ parametric resonance. Under otherwise identical conditions, we found the slope of the D_1 laser signal to be 45 times greater than the lamp-pumped signal.

No attempt was made to minimize the noise contributed by the solid-state laser. It can be concluded, however, that for the case of laser noise that is equal to that of current rf discharge helium lamps, laser-pumped magnetometers can be built that have sensitivities at least two orders of magnitude greater than the current instruments. Since the present day helium space magnetometers have a sensitivity of 0.01 nT, our current effort will proceed toward achieving sensitivities of 0.1 pT.

ACKNOWLEDGMENTS

This work was performed under NASA Contract No. NAS7-993 and sponsored by the Jet Propulsion Laboratory.

[1] R. E. Slocum and F. N. Reilly, IEEE Trans. Nucl. Sci. NS-10, 165 (1963).
[2] B. V. Conner, IEEE Trans. Magn. MAG-4, 391 (1986).
[3] A. M. A. Frandsen, B. V. Conner, J. Van Amersfoort, and E. J. Smith, Trans. Geo. Electron. GE-16, 195 (1978).
[4] L. D. Schearer, *Advances in Quantum Electronics*, edited by J. R. Singer (Columbia University Press, New York, 1961), pp. 239–251.
[5] L. D. Schearer, Phys. Rev. 160, 76 (1967).
[6] L. D. Schearer, M. Leduc, D. Vivien, A. M. Lejus, and J. Thery, IEEE J. Quantum. Electron. QE-22, 713 (1986).
[7] R. E. Slocum, Phys. Rev. Lett. 29, 1642 (1972).
[8] R. E. Slocum and B. I. Marton, IEEE Trans. Magn. MAG-9, 221 (1973).
[9] J. Hamel, A. Cassimi, H. Abu-Safia, M. Leduc, and L. D. Schearer, Opt. Commun. 63, 114 (1987).